THERMOMECHANICAL MODELING AND ANALYSIS OF PRECISION GLASS MOLDING PROCESS

by

Dhanooj Bobba

A dissertation submitted to the faculty of
The University of North Carolina at Charlotte
in partial fulfillment of the requirements
for the degree of Doctor of Philosophy in
Mechanical Engineering

Charlotte

2023

Approved by:

Dr. Harish P. Cherukuri

Dr. Christopher J. Morgan

Dr. Ronald E. Smelser

Dr. Konstantinos Falaggis

Dr. Youxing Chen

Dr. Thomas J. Suleski

ABSTRACT

DHANOOJ BOBBA. Thermomechanical Modeling and Analysis of Precision Glass Molding Process. (Under the direction of DR. HARISH P. CHERUKURI)

The tremendous development in digital technology in the last few decades has increased the demand for ultra-precision optical components with enhanced optical performance, such as aspherical or freeform lenses. Typically, lenses made of polymers have been widely used in the industry. But due to the superior optical properties of glass, there is a steady increase in demand for glass-based optical components. However, conventional manufacturing processes become time-consuming and expensive when used for manufacturing aspherical glass components. Precision glass molding (PGM) technology offers an alternate method of production for aspherical glass lenses and irregular optical products. Compared to the conventional manufacturing process, it has the advantages of high forming accuracy, short manufacturing cycles, low cost, and high-volume production. However, the process has a few drawbacks, such as lens profile deviations, stress birefringence. These drawbacks must be addressed before the glass molding process can be a viable option for mass-producing optical components.

As such, in this dissertation, a coupled thermo-mechanical finite element model is established to simulate the precision glass molding process on two different glass types, D-ZK3 (CDGM) and P-SK57 (Schott). The glass is modeled as a thermo-viscoelastic material by defining the stress and structural relaxation parameters. A new testing technique based on the cylinder compression test is developed in this study to extract the viscoelastic parameters at different temperatures. The obtained material parameters, when used in the numerical simulations, showed a good agreement with the experimental data throughout the testing temperature range. Further, the viscosity of the glass (a highly sought-after property of glass in precision molding) is obtained as a by-product of the proposed material calibration test. Finally,

the structural relaxation parameters are obtained from the impulse excitation test based on ASTM standard E1876. All the experiments required for fully calibrating the viscoelastic response of the glass are performed on a precision glass molding machine, Moore Nanotech GPM170 machine. The obtained material parameters are used in the finite element model to predict the lens deviations and the stresses in the molded lens. A mold compensation technique is used to correct the mold profiles for any deviations. The lens molded using the corrected molds is shown to fall within the designer's specifications. However, it was observed that the process parameters used during the molding process have an influence on the deviations and the stresses in the molded lens. Therefore, it is essential to optimize the molding process prior to implementing mold compensation techniques. The developed numerical model is used to analyze the impact of various process stages and parameters on the optical quality of molded lenses. Based on the observations, a modified molding process was developed, which is shown to minimize the influence of the molding parameters on the deviations and the residual stress. In addition, it was demonstrated that the modified manufacturing process reduces the total cycle time for producing a glass lens of comparable optical quality by more than 50%, reducing the manufacturing cost of a molded glass lens.

ACKNOWLEDGEMENTS

I express my sincere gratitude to my advisor Dr. Harish Cherukuri for his continuous support, guidance, and mentoring throughout my stay at UNC Charlotte. His continuous encouragement and confidence in me motivated me throughout my work. I sincerely acknowledge his constant support and guidance. I am extremely grateful to Dr. Christopher Morgan for his support, guidance, and valuable insights throughout the work presented in this study. I would like to thank Dr. Ronald E. Smelser, Dr. Konstantinos Falaggis, Dr. Youxing Chen, and Dr. Thomas J. Suleski for being a part of my dissertation committee and providing valuable inputs.

I am extremely grateful to Paul Vermette and Mark Boomgarden at Moore Nanotechsystems for providing me with an opportunity to work on this project. I would also like to thank Peter J. LaPerriere and Zachary Timothy for helping me with the experiments done during the course of this study. Finally, I would like to thank my family, friends, and colleagues for their support and for making my stay at UNC Charlotte memorable.

TABLE OF CONTENTS

LIST OF TABLES ix

LIST OF FIGURES x

CHAPTER 1: INTRODUCTION 1

1.1. Precision Glass Molding 3

1.2. Motivation 6

1.3. Dissertation Organization 7

CHAPTER 2: GLASS TRANSITION AND TERMINOLOGY 9

2.1. Glass transition and viscosity 9

2.2. Viscoelasticity 12

2.3. Thermorheological simplicity 16

2.4. Structural relaxation 17

CHAPTER 3: VISCOELASTIC MATERIAL CHARACTERIZATION USING CONSTANT STRAIN RATE TEST 22

3.1. Introduction 22

3.2. Experimental setup 26

3.3. Linear Thermo-viscoelasticity Theory 29

3.4. Estimation of viscoelastic parameters 33

3.5. Numerical Verification of the viscoelastic parameters 38

3.6. Temperature Dependence of the viscoelastic parameters 40

3.6.1. TRS assumption 40

3.6.2. Temperature dependent Burgers parameters 43

3.7. Numerical Validation 45

3.8. Conclusions 48

CHAPTER 4: EVALUATION OF STRUCTURAL RELAXATION PARAMETERS USING IMPULSE EXCITATION TEST 50

4.1. Theory 51

4.1.1. Impulse excitation test 51

4.1.2. TNM model 52

4.2. Experimental setup 53

4.3. Estimation of structural relaxation parameters 56

4.4. Implementation of structural relaxation behavior in FE model 58

4.5. Conclusions 62

CHAPTER 5: FINITE ELEMENT MODEL OF PRECISION GLASS MOLDING PROCESS AND MOLD COMPENSATION 64

5.1. Introduction 64

5.2. Molding Process details and the molding machine 65

5.3. Finite Element Model 68

5.4. Experimental vs. Numerical lens profile 71

5.5. Double Aspheric Lens 72

5.6. Mold compensation 73

5.7. Conclusions 76

CHAPTER 6: SELECTION OF PROCESS PARAMETERS IN PRECISION GLASS MOLDING PROCESS 78

6.1. Introduction 78

6.2. Overview of the Molding Process 80

6.3. Issues with Hold-up Force 81

6.4. Influence of Molding Step Parameters 82

6.4.1. Effect of viscoelastic material properties 82

6.4.2. Effect of molding viscosity 84

6.4.3. Effect of molding velocity 85

6.5. Stress Relaxation in Molded Lens 86

6.6. Influence of Gradual Cooling Parameters 90

6.6.1. Effect of Release Velocity 91

6.6.2. Effect of Gradual Cooling rate 91

6.7. Effect of Friction Coefficient 93

6.8. Conventional vs Modified Molding Process 94

6.9. Conclusion 95

CHAPTER 7: CONCLUSIONS AND FUTURE WORK 97

7.1. Conclusions 97

7.2. Future Work 100

REFERENCES 101

APPENDIX A: Equivalency between the Burgers model and the two-term generalized Maxwell model 107

LIST OF TABLES

TABLE 1.1: Comparison of glass and plastic properties [1]. 2

TABLE 3.1: Mechanical and thermal properties of the molds and the glass. 28

TABLE 3.2: P-SK57 relaxation parameters at different temperatures. 37

TABLE 3.3: Temperature dependent viscoelastic parameters. 45

TABLE 4.1: Structural relaxation parameters used in the numerical model. 63

TABLE 5.1: Asphere lens profile parameters. 73

TABLE 5.2: Aspherical coefficients of compensated bottom mold. 75

TABLE 5.3: Aspherical coefficients of compensated top mold. 76

TABLE 6.1: Temperature of different materials at similar viscosity. 83

LIST OF FIGURES

FIGURE 1.1: A schematic showing spherical aberration. 2

FIGURE 1.2: A schematic showing the precision glass molding process. 4

FIGURE 1.3: The temperature and force profiles during different steps of the molding process. 5

FIGURE 2.1: Change in volume with temperature in a glass vs crystalline solid. 10

FIGURE 2.2: Change in slope of $\frac{dV}{dT}$ during cooling of a glass forming liquid. 11

FIGURE 2.3: Change in viscosity with respect to temperature [12]. 12

FIGURE 2.4: Viscoelastic response of a material subjected to constant stress. 13

FIGURE 2.5: Viscoelastic models of glass a) Maxwell model, b) Kelvin model, and c) Burgers model. 14

FIGURE 2.6: Thermorheological simple behavior of glass. 17

FIGURE 2.7: Structural relaxation behavior of glass. 18

FIGURE 2.8: Temperature-dependent nonlinear behavior of glass. 19

FIGURE 3.1: Cylindrical glass samples before and after the compression test. 25

FIGURE 3.2: Precision glass molding machine (Moore Nanotech GPM170). 27

FIGURE 3.3: Cylindrical compression test. 27

FIGURE 3.4: The displacement and the force profiles during the compression test. 29

FIGURE 3.5: Cylindrical glass samples before and after the compression test. 30

FIGURE 3.6: Curve fit of the Burgers model to the constant strain rate test. 34

FIGURE 3.7: The relaxation function from experiments vs calculated. 35

FIGURE 3.8: The stress profiles at different temperatures under constant strain rate and stress relaxation. 36

FIGURE 3.9: The viscosity values obtained from the constant strain rate test at different temperatures compared to the manufactures data. 37

FIGURE 3.10: Axisymmetric finite element model to verify the viscoelastic parameters. 38

FIGURE 3.11: Experimental vs simulated force profiles at different temperatures. 39

FIGURE 3.12: Normalized shear modulus at different temperatures. 40

FIGURE 3.13: WLF shift factor with respect to temperature. 41

FIGURE 3.14: Experimental vs simulated force profiles at 560°C using the TRS assumption. 42

FIGURE 3.15: The master curve and the shifted functions at different temperatures. 43

FIGURE 3.16: Temperature dependent Burgers model parameters, P-SK57. 44

FIGURE 3.17: Validation of the temperature dependency of the Burgers model. 46

FIGURE 3.18: Stress profiles of D-ZK3 at different temperatures and the corresponding curve fit of Burgers model. 47

FIGURE 3.19: Numerical verification of the force profiles at different temperatures, D-ZK3. 48

FIGURE 3.20: Temperature dependent Burgers model parameters, D-ZK3. 48

FIGURE 3.21: Validation of the temperature dependency of the Burgers model, D-ZK3. 49

FIGURE 4.1: IET specimen setup for measuring Young's modulus [30]. 52

FIGURE 4.2: Glass sample suspended at the two nodes of their first vibration mode. 54

FIGURE 4.3: Impulse excitation test setup in Moore Nanotech GPM170. 55

FIGURE 4.4: Audio sample and the resulting resonant frequency obtained using IET. 55

FIGURE 4.5: Change in Young's modulus with respect to temperature during the crawl test. 56

FIGURE 4.6: Change in Young's modulus with respect to time and the corresponding TNM model fit at a temperature jump from 480°C to 525°C. 58

FIGURE 4.7: Change in Young's modulus with respect to time and the corresponding TNM model fit at a temperature jump from 510°C to 525°C. 59

FIGURE 4.8: Change in Young's modulus with respect to time and the corresponding TNM model fit at a temperature jump from 525°C to 525°C. 59

FIGURE 4.9: Change in Young's modulus with respect to time and the corresponding TNM model fit at a temperature jump from 510 °C and 540°C to 525°C. 60

FIGURE 4.10: Coefficient of thermal expansion of glass cooled through transition region. 60

FIGURE 5.1: Process data from GPM170 molding machine (Nanotech), for a lens made of D-ZK3 at 570°C. 66

FIGURE 5.2: Molding process with a) only IR lamps, and b) IR lamps and platen heaters 67

FIGURE 5.3: The biconvex molds used in the experiment. 68

FIGURE 5.4: Finite element model 69

FIGURE 5.5: Finite element mesh 70

FIGURE 5.6: Experimental vs Numerical profile deviation. 72

FIGURE 5.7: Double aspheric lens profile deviation a) Bottom profile, and b) Top profile. 74

FIGURE 5.8: Profile deviations before and after mold compensation a) Bottom profile, and b) Top profile. 77

FIGURE 6.1: Process parameters in precision glass molding process. 80

FIGURE 6.2: The final profile of the lens when molded with a) appropriate hold-up force, b) low hold-up force, and c) excessive hold-up force. 82

FIGURE 6.3: Maximum force at the end of the pressing cycle. 83

FIGURE 6.4: Effect of molding viscosity on profile deviation a) Bottom profile, and b) Top profile. 85

FIGURE 6.5: Form error of the molded lens at different viscosities. 85

FIGURE 6.6: Effect of molding velocity on profile deviation a) Bottom profile, and b) Top profile. 86

FIGURE 6.7: Form error of the molded lens at different molding velocities. 87

FIGURE 6.8: Stress distribution in the molded lens at the end of pressing and gradual cooling step a) at a viscosity of 10^8 Pa.s and b) at a viscosity of $10^{6.8}$ Pa.s. 88

FIGURE 6.9: Maximum Mises stress in the molded lens at different viscosities a) Pressing step b) Gradual cooling step. 89

FIGURE 6.10: Maximum Mises stress in the molded lens at different velocities a) Pressing step b) Gradual cooling step. 89

FIGURE 6.11: Form error (PV) vs molding viscosity in the top and bottom lens profile with and without relaxation. 90

FIGURE 6.12: Form error (PV) vs molding velocity in the top and bottom lens profile with and without relaxation. 91

FIGURE 6.13: Form error (PV) of the molded lens at different release velocities. 92

FIGURE 6.14: Form error (PV) of the molded lens at different gradual cooling rates. 92

FIGURE 6.15: Maximum residual stress in the molded lens at different gradual cooling rates. 93

FIGURE 6.16: Form error (PV) vs friction coefficient in the top and bottom lens profile with and without relaxation. 94

FIGURE 6.17: Temperature profile with respect to cycle time in a conventional vs modified molding process. 95

FIGURE 6.18: Profile deviation in different glass materials under similar molding conditions a) bottom profile and b) top profile 96

CHAPTER 1: INTRODUCTION

The tremendous development in digital technology in the last few decades increased the demand for ultra-precision optical components. Additionally, there has been a corresponding increase in the need to enhance optical performance while reducing the size of the optical modules. These requirements can only be satisfied by using highly precise optical components with complex profiles, such as aspheric lenses. The surface of the aspheric lens does not conform to the surface of the sphere, which allows them to correct for distortions and aberrations in an image that would otherwise be present in a spherical lens, as shown in Fig. 1.1. Additionally, one of the main benefits of the aspheric lenses is that they can be designed to have a much flatter surface than a spherical lens of the same focal length. This enables them to be much thinner and lighter, which is particularly important in applications where weight and size are important considerations, i.e., for example, phone camera modules, eyeglasses, etc.

There are many applications for aspherical optical elements, ranging from astronomical applications, life systems, machine vision, and metrology, digital cameras, etc. Most of these applications currently use polymer-based lenses as they are simple to manufacture on a large scale and have low cost. Different polymers, including acrylic, polystyrene, and polycarbonate, have been used for years to produce consumer-level semi-precision optical systems. But when compared with glass, polymers have inferior optical properties. Some of the relevant properties of glass and plastics as lens materials are shown in the Table 1.1.

As shown in Table 1.1, glass has high abrasion resistance and higher transparency. Also, the thermal expansion coefficient of glass is about 10 times lower than that of polymers, which is a highly sought property for designing high-precision optical

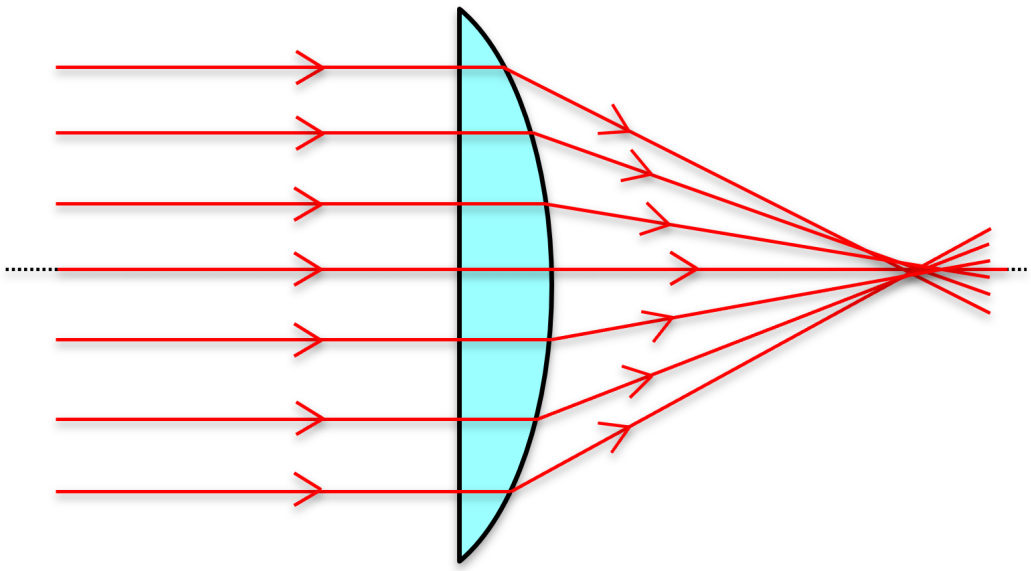

Figure 1.1: A schematic showing spherical aberration.

Table 1.1: Comparison of glass and plastic properties [1].

Property	Glass	Polymers
Moisture resistance	high	low
Scratch resistance	high	low
Transparency	high	moderate
Thermal stability	high	low
Impact strength	brittle	moderate
Specific gravity	high	low
Manufacturability	hard	easy

assemblies. Furthermore, plastics offer a limited range of refractive indices, have a large variation in the refractive index with temperature, have coating instabilities, and may have excessive surface irregularities, which make them unsuitable for precision applications. Despite these disadvantages, polymer-based lenses have been used

extensively as they are light in weight and are simple to manufacture/mass produce.

However, the exponential growth in the consumer electronics industry (cameras, telecommunications, projectors, AR/VR, etc) and the desire for high-performance and high-precision products has led to increasing demand for aspherical glass lenses. It is estimated that the aspherical lens market will grow at a rate of 6.5% for the forecast period of 2021 to 2028. In fact, a report published by BIS Research [2] highlights that the market was estimated at 19.50 billion units in 2019 and is projected to reach 28.47 billion units by 2025. The glass segment contributed 68.58 % in terms of volume in 2019 and dominated the high precision asphere market over the plastic counterparts. However, complicated production processes and design-related issues with the aspherical lens are the main factors that are restraining the further growth of the aspheric lens market.

Conventionally, the optical surfaces in brittle materials like glass are generated by an abrasive procedure followed by surface polishing. During the abrasive process, a rough aspherical shape is generated on the surface of the glass by grinding with abrasives. In the second step, the rough surface generated during the grinding process is polished to obtain the desired roughness and shape accuracy. These techniques provide satisfactory curve conformation in the case of spherical lenses but become very time-consuming and costly when used for fabricating aspherical components with complex profiles. The production of aspheric lenses necessitates more sophisticated polishing techniques such as Magneto-rheological finishing (MRF), the Precision polishing method, or ion beam finishing. While these techniques can produce high-quality surfaces, the cost involved in the production is significant and the by-products such as the polishing slurries are not environmentally friendly [3].

1.1 Precision Glass Molding

Precision glass molding (PGM) was devised as an alternative technique to manufacture aspherical optical components. It has the advantages of high forming accuracy,

a short manufacturing cycle, and low cost compared to the traditional process. Over the past three decades some work has been done towards developing the molding method for fabricating glass lenses [4–6]. A schematic of the steps involved in the precision glass molding process is shown in the Fig. 1.2.

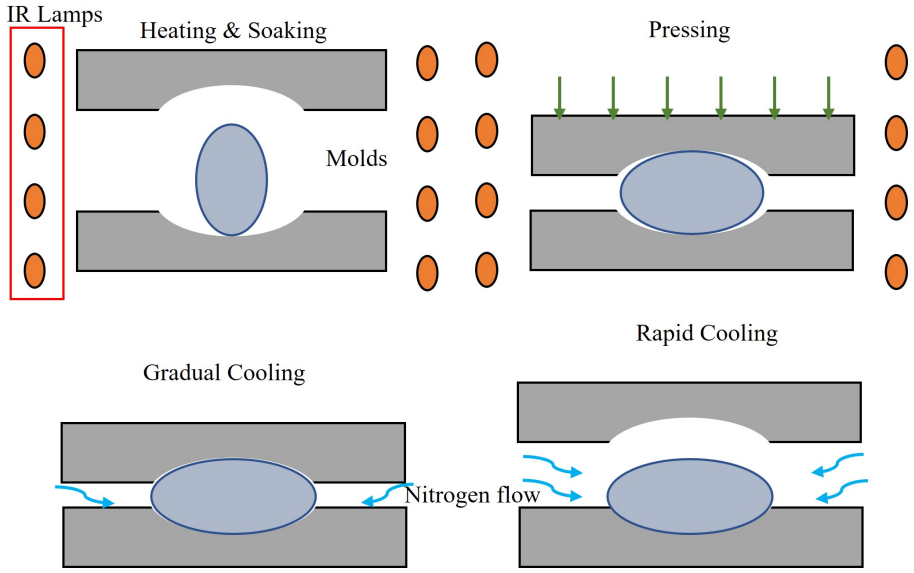

Figure 1.2: A schematic showing the precision glass molding process.

The process commences by loading a glass gob onto the lower mold. Generally, glass gobs in the form of a cylinder, sphere, ellipse, or even a pre-machined lens are used in the molding process to obtain the desired lens shape. The glass and the mold assembly are then heated to a specific temperature above the glass transition temperature. The objective is to heat the glass to a temperature just above its softening point, so the glass viscosity lies in the range of 10^7 to 10^9 Pa-s. Typically, infrared lamps are used as a heat source during the precision glass molding process. Once the molding temperature is attained, the system is held at this temperature for several minutes to obtain a uniform temperature distribution in the glass.

Once the system has attained a steady state molding temperature, the gap between the top and bottom molds is reduced by applying a force or displacement to the top mold. This deforms the glass into the shape of the molds. The molding temperature

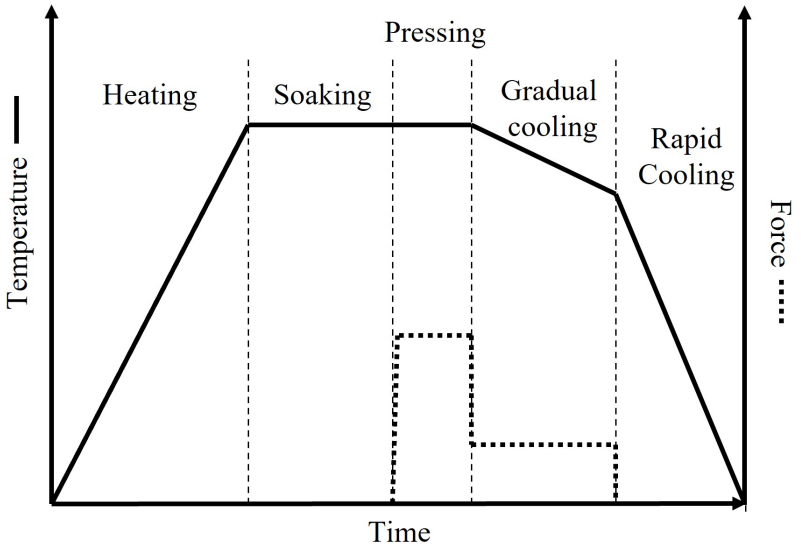

Figure 1.3: The temperature and force profiles during different steps of the molding process.

is maintained constant during the pressing process. All the molding steps mentioned so far are either carried out in a vacuum or nitrogen environment to prevent any oxidation of the mold tooling. Next, the formed lens is gradually cooled by controlled nitrogen flow with molds still in the closed position with a constant force. During the annealing step, the temperature is slowly reduced from the molding temperature to a temperature just below the transition point. And finally, the force is removed and the lens is rapidly cooled and released from the mold below oxidation temperature, or approximately 250°C.

The lens fabricated through the molding process is a near-net shape and requires either no follow-up operations or a simple finishing operation. Compared to the conventional lens manufacturing process, the part-to-part variation in glass lens molding can be controlled to a higher precision and by having multiple cavity designs the process can be customized for higher volume production. Apart from that, precision glass molding is also an environmently-friendly procedure since it does not require the use of any coolants and does not generate debris. In addition to fabricating aspherical components, glass press molding can be used to manufacture microlens arrays

as well as free-form lenses that are used in digital displays, for data storage, optical communication, printing, scanning, etc.

1.2 Motivation

Despite being a better alternative to conventional manufacturing techniques, the precision glass molding operation suffers from a few shortcomings that need to be addressed before the process can be used economically to mass-produce glass lenses. Some of the challenges that have prevented the process from extensively being used for the production of glass lenses are as stated below.

One of the major issues in precision glass molding is the deviation of the lens profile from the mold geometry after the molding process. Typically, in precision glass molding the mold surfaces are machined to be exact negatives of the required lens profile, assuming the lens would take the shape of the molds. But in reality, the complex mechanical behavior of the glass and its high-temperature dependence affects the final lens profile at room temperature. The molded lens profile might deviate from the required profile by as much as 20 microns which is considered to be much higher than the allowable deviation [7]. To address this issue, the often-used approach is to correct the mold profile for deviations, commonly referred to as mold compensation. In mold compensation, the deviations on the lens profile are subtracted from the mold surface to satisfy the required specs. Typically, the molds are compensated by trial and error, which is a time-intensive and costly process. Empirically compensating the mold may take up to a few months to meet the required product specifications. Whereas, numerical simulations have proved to be more efficient compared to trial and error techniques. As such, one of the primary goals of this study is to develop a reliable numerical model to simulate the precision glass molding process. The developed model will then be used to predict the profile deviations at the end of the molding process and to pre-compensate the molds. However, a reliable numerical model necessitates a proper characterization of the viscoelastic response of the glass

material used in the precision glass molding process. To that extent, a significant portion of the literature is focused on the viscoelastic material characterization of a few moldable glasses. Due to the ambiguity of commonly used material testing experiments and the non-uniqueness of constitutive model parameters, various sets of parameters for the same glass type have been reported in the literature [8, 9]. As a consequence, one of the primary objectives of this study is to establish a more reliable procedure for characterizing materials in order to obtain a unique set of material parameters. In addition, the various material testing experiments required for completely characterizing the glass will be consolidated so that they can be readily implemented on any glass molding machine.

The precision glass molding process involves several process parameters, and the appropriate selection of these parameters plays a vital role in achieving the required profile accuracy as well as the optical quality of the molded lens. Typically, the process parameters are adjusted by trial and error until the desired dimensional requirements of the glass lens are achieved. But due to the complex and obscure nature of the molding process, it often takes weeks or months to establish a process that satisfies the required dimensional specifications. However, satisfying the required dimensional specifications does not necessarily indicate an excellent optical quality, i.e., change in refractive index [10] or high birefringence. As such, the developed numerical model will be used to analyze the effect of different process steps and their corresponding process parameters on the profile deviations and the residual stresses in the molded lens. The observations and comments made in this study can be used as a reference to expedite the manufacturing process of glass lenses.

1.3 Dissertation Organization

The contents of this dissertation are organized as follows: this chapter discusses the advantages of glass lenses over polymer-based lenses and provides an introduction to

precision glass molding and its limitations. The next chapter discusses glass rheology and the general terminology used in glass press molding. It also introduces the constitutive models used to characterize stress relaxation and the structural relaxation phenomenon of glass materials. In Chapter 3, the current literature on obtaining viscoelastic material properties is discussed, and a new reliable technique is proposed to extract a unique set of material parameters at different temperatures. Chapter 4 discusses the implementation of the impulse excitation test to obtain the structural relaxation parameters using the TNM model. The obtained material parameters are used in the developed finite element model to analyze the profile deviation of a biconvex lens in Chapter 5. The experimental and numerical deviations are shown to be in a similar range. Further, the developed model is used to analyze the curve deviation in a double aspheric lens, and a mold compensation technique is used to minimize the deviations in the molded lens. In Chapter 6, the influence of different process parameters on the curve deviation and residual stresses is fully analyzed. Based on the observations, a new molding process is proposed to minimize the influence of process parameters on the deviations and residual stresses. Further, it is shown that the proposed technique reduces the total molding time significantly.

CHAPTER 2: GLASS TRANSITION AND TERMINOLOGY

When compared to crystalline solids, glasses behave as amorphous solids at room temperature. Crystalline solids tend to have a stable equilibrium state at room temperature. In contrast, glass tends to be in a non-equilibrium form at room temperature, also commonly referred to as a frozen liquid state or glassy state. Figure 2.1 shows the change in volume in a glass versus crystalline solid when cooled from a temperature greater than the melting point (T_m) to the room temperature. At higher temperatures, the glass and the crystalline solids behave as viscous liquids. However, when cooled below the melting temperature, their paths deviate. The crystalline solids exhibit elastic behavior below the melting point and immediately crystallize into a solid state. But the glasses exhibit three distinct states: the super-cooled liquid region, the transition region, and the glassy or frozen liquid region. And when a mechanical load is applied, the glass behaves as a viscous liquid in the liquid region, a viscoelastic solid in the glass transition region, and an elastic solid in the glassy region. The viscoelastic nature of the glass in the transition region is used for forming the glass into the desired shape in precision glass molding.

2.1 Glass transition and viscosity

The glass transition state is defined as the region of temperature at which the equilibrium state is attained by molecular rearrangement on a scale ranging from a few minutes or hours. The glass transition region is revealed by a shift in the temperature dependency of a liquid's property, such as volume, enthalpy, or entropy, as it cools to room temperature [11]. Figure 2.1 shows the change in volume of the glassy liquid as it cools through the transition region. At temperatures above T_U, in the liquid state, the

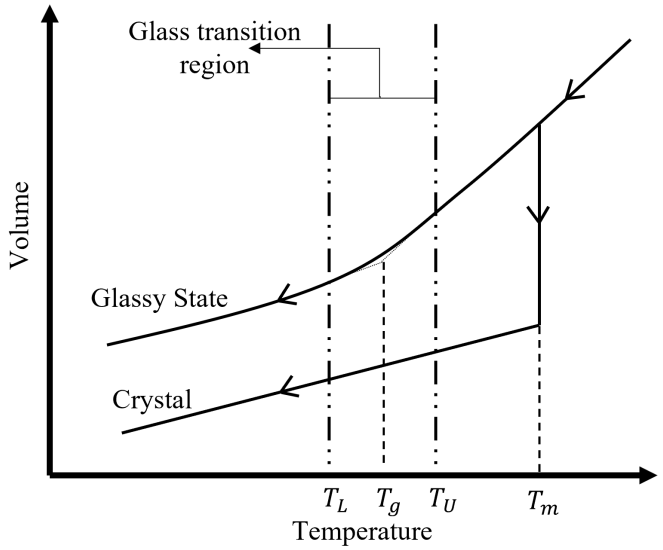

Figure 2.1: Change in volume with temperature in a glass vs crystalline solid.

viscosity is so low that any step change in temperature will result in an instantaneous equilibrium state. But as the temperature decreases below T_U, the viscosity increases, increasing the time required to attain equilibrium. And as the temperature reaches T_L, the viscosity is so high that the liquid's internal structure is essentially frozen, resulting in a glassy state. The region that corresponds to the temperatures above T_L and below T_U is the glass transition region. In the transition region, the slope dV/dT (which corresponds to the coefficient of linear thermal expansion) from a high-value characteristic of a liquid (α_l) to a low-value characteristic of a glassy state (α_g) as shown in Fig. 2.2. The glass transition temperature T_g is arbitrarily defined as the center of the transition region.

In precision glass molding, the viscosity of the glass being molded plays an important role in determining the quality of the manufactured lens. Figure 2.3 shows the change in viscosity of soda-lime-silicate glass as it is cooled through the transition region [12]. Given the importance of the property, five standard viscosity reference points are defined at different temperatures. At high temperatures, i.e., above the melting point (T_m), the viscosity is very low (10 dPa.s), and the glass essentially

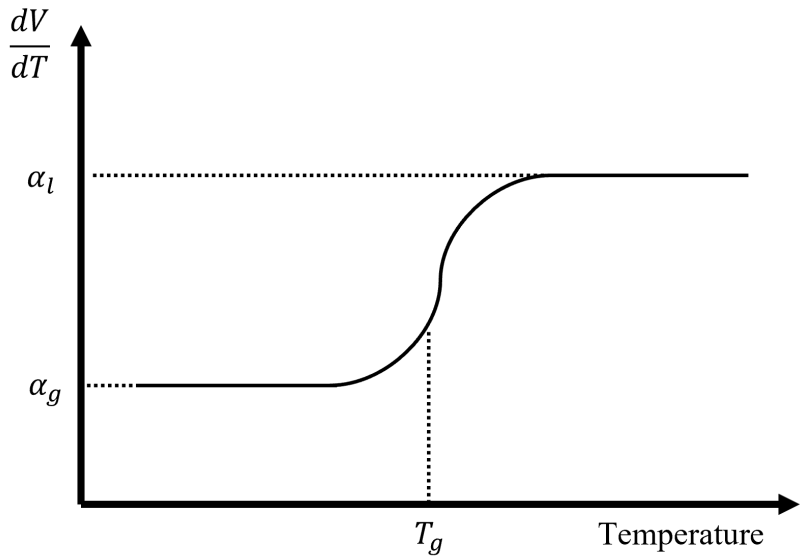

Figure 2.2: Change in slope of $\frac{dV}{dT}$ during cooling of a glass forming liquid.

behaves as a liquid. As the temperature is decreased, the viscosity of the glass increases as shown in Fig. 2.3. At a viscosity of 10^4 dPa.s (working point), the glass transitions from a liquid-like state to a more viscoelastic state. The interval between the 10^4 dPa.s (working point) and $10^{7.6}$ dPa.s (Littleton softening point) is known as the working range of the glass, which is used for glass forming operations. The Littleton softening point is defined as the viscosity at which the glass deforms at a rate of 1mm/min under its own weight. In precision glass molding, the temperatures that correspond to viscosity above the softening point are used. At these temperatures, the viscosity of the glass is low enough to dissipate the stresses in order of a few seconds. With the further increase in viscosity to about 10^{13} dPa.s (Annealing point), the time required to relieve stresses will be in the order of a few seconds to a few minutes. During the gradual cooling stage of PGM, the molded glass is cooled to a temperature just below the annealing point to relieve any internal stresses formed during the molding process. With any further increase in viscosity, the time required to attain equilibrium is so large that the glass can be deemed as solidified.

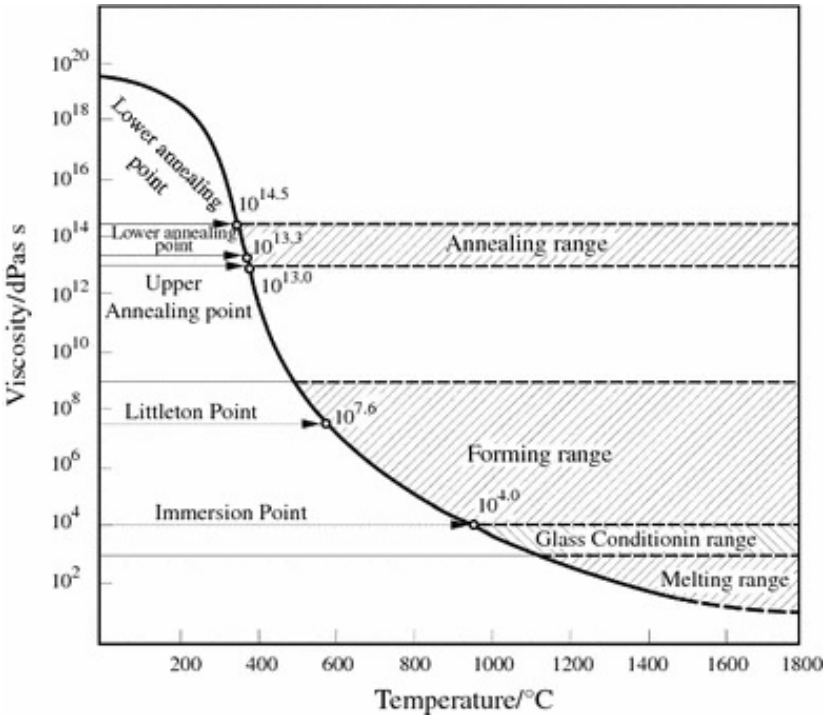

Figure 2.3: Change in viscosity with respect to temperature [12].

2.2 Viscoelasticity

If a glass is subjected to a mechanical load in the transition region, a time-dependent change in the dimension is observed. This time-dependent behavior is known as viscoelasticity. Figure 2.4 shows the typical behavior of a linear viscoelastic material under constant load. Unlike elastic materials, which show an instantaneous strain response to the applied stress, viscoelastic materials exhibit three distinct strain components; the instantaneous elastic strain ϵ_E, the delayed elastic strain ϵ_D that appears over a period of time, and the viscous flow strain ϵ_v. When the load is removed, the instantaneous strain is immediately recovered, followed by a gradual recovery of the delayed elastic strain. But the strain produced by viscous flow does not recover, resulting in a permanent change in the shape of the viscoelastic material. For an accurate representation of the viscoelastic material, the constitutive model should be able to model the three strain components.

Historically, viscoelastic material behavior has been represented by rheological

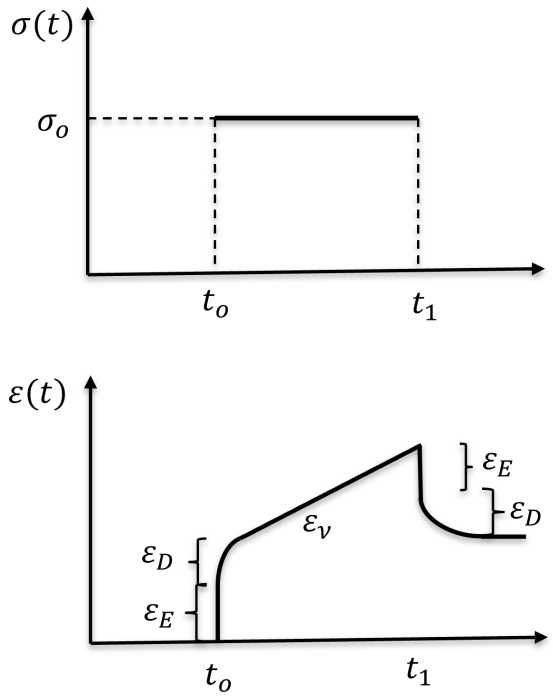

Figure 2.4: Viscoelastic response of a material subjected to constant stress.

models consisting of different combinations of linear springs (elastic element) and dashpots (viscous element). The stress-strain relation of a spring and a dashpot are as given in Eqs. 2.1 and 2.2, respectively.

$$\sigma = E\epsilon \tag{2.1}$$

$$\sigma = \eta\dot{\epsilon} \tag{2.2}$$

where E is the spring constant or Young's modulus and η is the coefficient of viscosity. When subject to a step of constant stress, the spring element will exhibit an instantaneous strain response. In comparison, a dashpot will deform continuously at a constant rate when subject to constant stress.

Figure 2.5 shows some of the rheological models used to represent the glass material behavior during molding. The Maxwell model, shown in Fig. 2.5a, consists of a

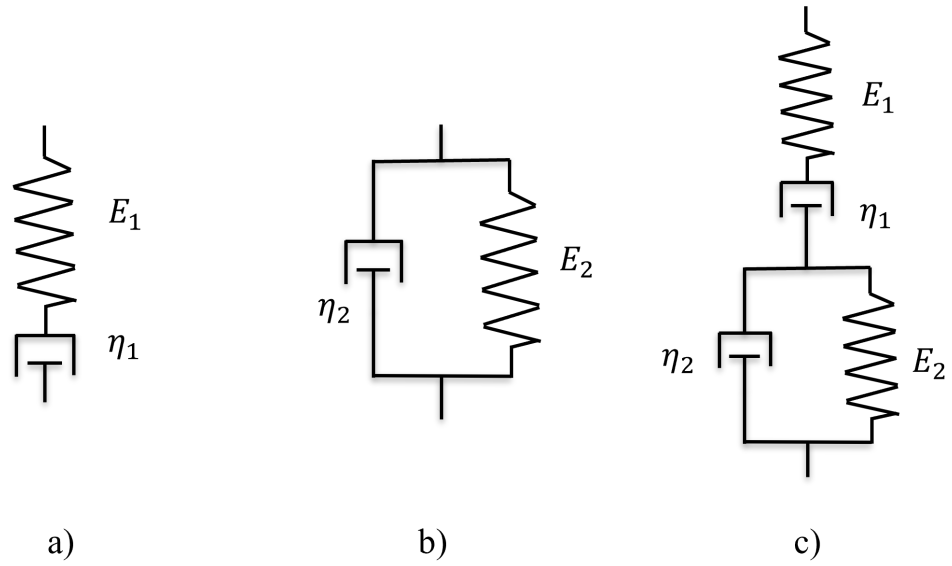

Figure 2.5: Viscoelastic models of glass a) Maxwell model, b) Kelvin model, and c) Burgers model.

spring and dashpot connected in series. When subjected to constant stress, the stress-strain relation of the Maxwell model is given by Eq. 2.3. Figure 2.5b shows the Kelvin model where a spring and a dashpot are connected in parallel. When subjected to constant stress, the stress-strain relationship of a Kelvin model is given by Eq. 2.4. It was observed that neither the Maxwell model nor the Kelvin model described the viscoelastic response accurately [13]. While the Maxwell model shows no time-dependent elastic response, the Kelvin model does not exhibit the instantaneous elastic and the viscous response of a viscoelastic material.

$$\epsilon = \frac{\sigma}{E} + \frac{\sigma t}{\eta} \tag{2.3}$$

$$\epsilon = \frac{\sigma}{E}\left(1 - e^{\frac{-Et}{\eta}}\right) \tag{2.4}$$

Evidently, the simplest model that can represent all the components of the viscoelastic model is obtained by connecting a Maxwell model in series with the Kelvin model. Figure 2.5c shows the Burger model which is the combination of Maxwell

and Kelvin models connected in series. The stress-strain relation of a Burgers model when subjected to constant stress is given by Eq. 2.5.

$$\epsilon = \left[\frac{1}{E_1} + \frac{1}{E_2}\left(1 - e^{\frac{-E_2 t}{\eta_2}}\right) + \frac{t}{\eta_1}\right]\sigma \tag{2.5}$$

where E_1 and η_1 are the spring constant and the viscosity coefficient of the Maxwell element and E_2 and η_2, are the spring constant and the viscosity of the Kelvin element. The first term in Eq. 2.5 represents the instantaneous elastic response followed by the delayed elastic response, and the final term represents the permanent viscous response of the viscoelastic material.

The constitutive equations of linear viscoelasticity are given as follows,

$$S_{ij}(t) = \int_0^t G_1(t - t')\frac{\partial e_{ij}(t')}{\partial t'}dt' \tag{2.6}$$

$$\sigma(t) = \int_0^t G_2(t - t')\frac{\partial \epsilon(t')}{\partial t'}dt' \tag{2.7}$$

where S_{ij} and σ are the deviatoric and dilatational stresses, e_{ij} and ϵ are the corresponding strains. $G_1(t)$ and $G_2(t)$ are the relaxation moduli that correspond to the deviatoric and the dilatational responses, respectively. The total stress in the viscoelastic element can be obtained by combining the deviatoric and dilatational responses as shown in Eq. 2.8

$$\sigma_{ij} = S_{ij} + \frac{1}{3}\delta_{ij}\sigma \tag{2.8}$$

The relaxation moduli in Eqs. 2.6 and 2.7 are obtained from the rheological models [11]. In the literature, the Generalized Maxwell model is the most widely used to describe the linear viscoelastic behavior of the materials. It consists of several Maxwell elements connected in parallel, and the relaxation moduli have the form,

$$G_1 = 2G_o \sum_{i=1}^{n} w_i e^{-t/\tau_i} \tag{2.9}$$

$$G_2 = 3K_\infty - 3(K_\infty - K_o) \sum_{j=1}^{n} w_i e^{-t/\lambda_i} \tag{2.10}$$

where G_o and K_o are the instantaneous shear and bulk modulus, respectively. K_∞ is the equilibrium bulk modulus, τ_i and λ_i are the deviatoric and dilatational relaxation times, and w_i are the corresponding weight functions. The series of weighted exponential terms in Eqs. 2.9 and 2.10 are called the Prony series, and the weights and relaxation times of the series are known as the Prony coefficients. The Prony series coefficients are obtained by curve fitting the experimentally obtained stress-strain curve.

2.3 Thermorheological simplicity

In a viscoelastic material, the rate of relaxation varies significantly with a change in temperature. It was observed that the rate of relaxation is slow at low temperatures and increases rapidly with an increase in temperature. That is, if a constant strain is applied to a glass, the uniaxial stress relaxation function ψ_u will vary with temperature, as shown in Fig. 2.6. If the relaxation moduli at different temperatures are plotted with respect to time in log scale, the curves are identical in shape but are only shifted by a factor $(A(T))$ in time scale, as shown in Fig. 2.6. This behavior of the viscoelastic materials is called thermorheological simple material.

The shift factor in a TRS material is given by,

$$A(T) = \frac{\tau(T)}{\tau(T_R)} \tag{2.11}$$

where $\tau(T)$ is the relaxation time at a temperature T, and $\tau(T_R)$ is the relaxation time at a reference temperature, T_R. The temperature dependence of the shift factor

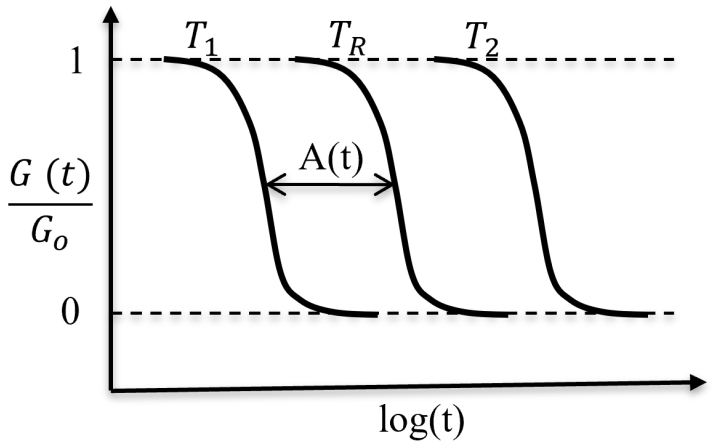

Figure 2.6: Thermorheological simple behavior of glass.

is approximated by the Williams-Landel-Ferry (WLF) equation given by

$$\log(A(T)) = -\frac{C_1(T - T_R)}{C_2 + (T - T_R)} \tag{2.12}$$

where T is the temperature at which the shift factor is being calculated, T_R is the reference temperature, and C_1 and C_2 are constants.

2.4 Structural relaxation

When glass in the transition region is subjected to a sudden change in temperature, a time-dependent property change is observed. This time-dependent behavior of glass to a temperature jump is referred to as structural relaxation. Figure 2.7 shows the response of the volume of a glass subjected to a sudden change in temperature. Similar to stress relaxation, the structural relaxation response exhibits an instantaneous change in the property and then a time-dependent change. That is when a glass equilibrated at a temperature T_1 with volume $V(\infty, T_1)$ is suddenly subjected to a temperature T_2 at time t_o, will see an instantaneously change in volume to $V(0, T_2)$ at time t_o and then a slow time-dependent change to a final value of $V(\infty, T_2)$ when equilibrated at temperature T_2, as shown in Fig. 2.7. Different properties of glass, such as specific heat, viscosity, Young's modulus, etc., show a similar time-dependent

response in the transition region [7].

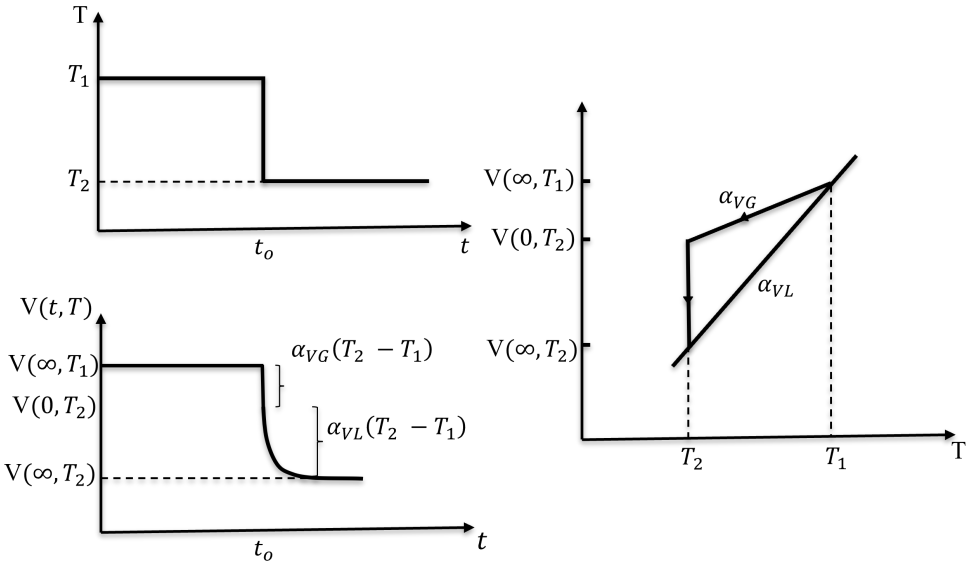

Figure 2.7: Structural relaxation behavior of glass.

In Fig. 2.7, the instantaneous change in property is characterized by α_{VG}, the glassy thermal expansion coefficient of the material, and the total change after equilibration is characterized by α_{VL}, the liquid thermal expansion coefficient. As shown in Fig. 2.7, the instantaneous response of the property follows the slope α_{VG}, and the time-dependent response of the property occurs in the vertical direction towards the equilibrium.

An important aspect of structural relaxation is that the rate of relaxation depends on the thermal history [11]. That is, if one sample is equilibrated at a temperature $T_1 = T_2 + \Delta T$ and the other sample at a temperature $T_3 = T_2 - \Delta T$ and then suddenly subjected to a temperature T_2 which is in between T_1 and T_3. The sample at a higher temperature (T_1) relaxes faster than the sample at a lower temperature (T_3), as shown in Fig. 2.8. In the sample that is equilibrated at a higher temperature, the atoms have more mobility than those in the sample at a lower temperature.

One of the most important concepts in the theory of structural relaxation is the introduction of the concept of fictive temperature by A. Q. Tool [14]. The fictive

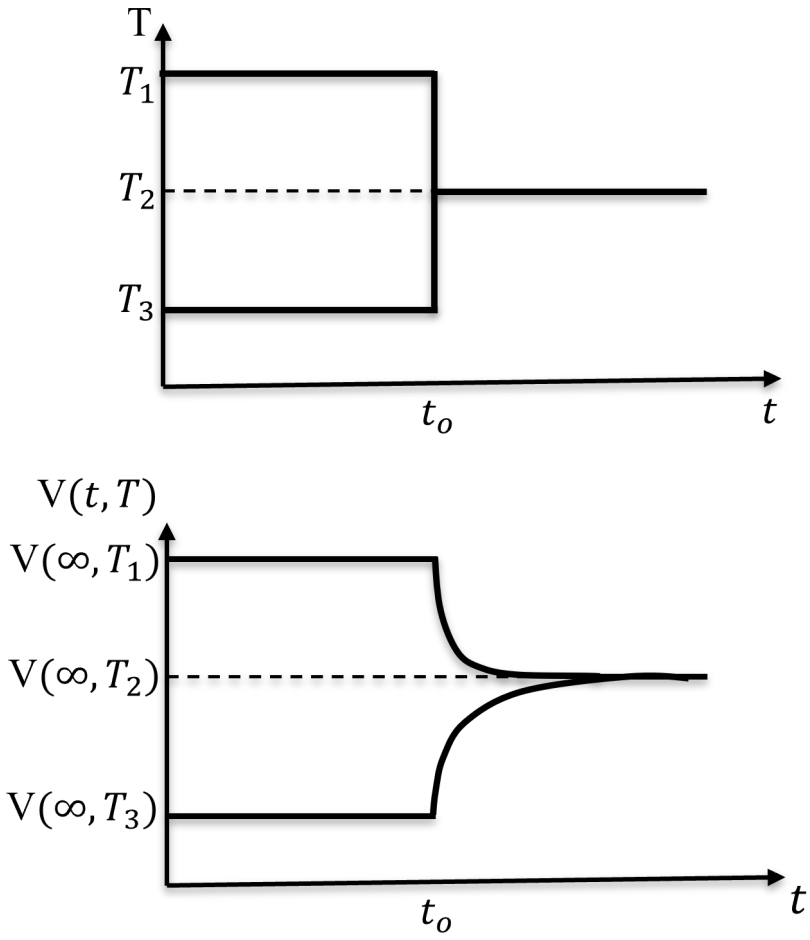

Figure 2.8: Temperature-dependent nonlinear behavior of glass.

temperature is a theoretical concept that determines the amount of structural relaxation in a glass. It is a hypothetical temperature at which a glass would need to be equilibrated for a sufficient time to reach it's current state of internal structural relaxation. Based on the concept of fictive temperature, Tool described the structural relaxation in glass using Eq. 2.13.

$$\frac{dT_f}{dt} = \frac{T - T_f}{\tau_p} \tag{2.13}$$

T_f is the fictive temperature, T the actual temperature of the glass and τ_p the structural relaxation time. Using the analogy to viscoelasticity, Tool initially defined the relaxation time as a function of the actual temperature, Eq. 2.14, which he found to

be inadequate to describe the experimental data. He modified Eq. 2.14 to include the influence of changing structure of the glass and developed the Eq. 2.15

$$\tau_p = \tau_o * exp(-AT) \tag{2.14}$$

$$\tau_p = \tau_o * exp(-A_1T - A_2T_f) \tag{2.15}$$

where τ_o, and A_i are constants. The inclusion of the dependence on the fictive temperature in Eq. 2.15 made Tool's equation non-linear. It was later realized that the Tool's equation is not adequate to describe structural relaxation [11].

A successful theory of the structural relaxation was introduced by Narayanaswamy [15], where the differential equation given by Tool is replaced with an integral equation given below

$$T_f(t) = T(t) - \int_0^t M_p(t-t')\frac{dT}{dt'}dt' \tag{2.16}$$

Where M_p is the relaxation function for the property p and is given by equation 2.17

$$M_p(t) = exp\left[-\left(\frac{t}{\tau_p}\right)^b\right] \tag{2.17}$$

Where b is a constant such that $0 \leq b \leq 1$, and τ_p is the relaxation time defined by Eq. 2.18

$$\tau_p = \tau_0\left(\frac{x\Delta h}{RT} + \frac{(1-x)\Delta h}{RT_f}\right) \tag{2.18}$$

Where τ_o is a constant; Δh is an activation energy constant; x is a constant such that $0 \leq x \leq 1$; and R is the ideal gas constant. To remove the non-linearity due to the time dependence of the relaxation time, he used the concept of reduced time, $\xi = \tau_{pr}\int_0^t dt'/\tau_p$, where τ_{pr} is the relaxation time at an arbitrary reference temperature

T_r which is generally taken to be 50 to 100 $^{\circ}C$ above the glass transition temperature.

Later, Moynihan [16] replaced the single relaxation time in Eq. 2.17 with a series of relaxation times and modified the single nonlinear differential equation in Narayanaswamy's model with a series of linear differential equations as shown below,

$$T_{f_i} = T - \int_0^t M_p(t - t')\frac{dT}{dt'}dt' \tag{2.19}$$

Where the structural relaxation function M_p is given by the Prony series as shown in Eq. 2.20

$$M_p = \sum_{i=1}^{n} w_i exp(-\frac{t}{\tau_i}) \tag{2.20}$$

Where w_i are the weights such that the sum of the weights is equal to 1. They defined the effective fictive temperature of the glass as the weighted average of the fictive temperatures.

$$T_f = \sum_{i=1}^{n} w_i T_{f_i} \tag{2.21}$$

Equations 2.18 to 2.21 are referred to as the TNM model and are widely used in the literature to describe the structural relaxation process of glass during glass press molding.

CHAPTER 3: VISCOELASTIC MATERIAL CHARACTERIZATION USING CONSTANT STRAIN RATE TEST

3.1 Introduction

The precision glass molding process involves a glass blank deformed into a desired lens shape by applying pressure at high temperatures. Typically, the molding temperatures range from about 40 to 50°C above the glass transition temperature. As stated in the previous chapter, glass when subjected to mechanical and thermal loads above the transition temperature, behaves as a viscoelastic material, i.e., it exhibits stress relaxation and structural relaxation when subjected to mechanical and thermal loads, respectively. As such, the viscoelastic material properties play a crucial role in determining the final form of the molded lens [17, 18]. The numerical modeling of the precision glass molding process requires a coupled thermo-mechanical constitutive model to understand the response of the glass deformation throughout the molding process.

The early numerical studies on the PGM process are limited due to the lack of experimental data available on the viscoelastic parameters. Initially, the behavior of the glass is assumed to be purely Newtonian, where the stress is considered to be directly proportional to the strain rate [17,19]. While few studies used simple Maxwell or Kelvin models to approximate the stress relaxation or creep responses, respectively [8,10]. Zhou et al. [20] studied different mechanical models and reported that neither the Maxwell nor the Kelvin models were able to accurately describe the experimental data. But they showed that the Burgers model, which is a combination of the Maxwell and Kelvin models, could describe the experimental data. The generalized Maxwell model is extensively used in the literature for modeling the viscoelastic behavior of

glass during the molding process. Anathasayanam et al. [21] used the ring compression test to characterize the linear viscoelastic behavior of the L-BAL35 glass. They used a hybrid approach where the parameters, i.e., the weights and the relaxation times, of the generalized viscoelastic model, were varied manually until the displacement curves from the simulations matched the experiments. Arai et al. [22] used creep experiments on cylindrical glass samples to characterize the properties of BK7 and TaF-3 glass. They used a generalized Voigt model to fit the creep data and used Laplace transforms to convert the creep compliance into a relaxation modulus in the form of a generalized Maxwell model. Although the generalized Maxwell model is able to accurately model the viscoelastic response, it is emphasized that the number of parameters to be estimated varies depending on the temperature chosen during the experimental characterization. In contrast, the Burgers model has the fewest fitting parameters and can represent the complete viscoelastic material behavior [13].

For characterizing the thermo-viscoelastic material behavior of the glass, the experimental methods used in the literature can be divided into two categories: the dynamic method and the static method. In the dynamic method, usually called dynamic thermo-mechanical analysis (DMA), a sinusoidal load or stress is applied to the specimen, and the resulting displacement or strain is measured, which is used to quantify the material properties. The major drawback of the DMA method is that the testing equipment used to measure the viscoelastic properties is unsuitable for evaluating glasses with transition temperatures above 500°C [22]. The static methods, which consist of either the stress relaxation experiments or creep experiments, are commonly used test methods to calibrate the viscoelastic material properties of the glass used in precision glass molding. Of these, the stress relaxation experiment is more favorable because the viscoelastic model parameters can be directly obtained by fitting the relaxation data [23,24]. However, the major limitation of the relaxation experiment is the instantaneous application of strain on the glass specimen at different

temperatures. This limits the experiments to the temperatures in the vicinity of the transition temperature, which are different from the typical temperatures used during glass molding. In contrast, the creep experiments, which require the application of constant load/stress, are more suitable for characterizing the viscoelastic properties at the molding temperatures.

Jain et al. [25] used cylindrical compression tests on two different types of glass to determine the viscosity data at high temperatures. They used custom-built equipment to perform the experiments and found that the viscosity values obtained from the compression test are similar to the values obtained from traditional methods. Zhou et al. [13] were the first to use a precision molding machine to perform the creep compression test to evaluate the viscoelastic material properties. Joshi et al. [26] used the creep compression test and reported that the friction between the glass specimen and the molds has a significant effect on the measurement of the viscoelastic material properties of glass. In a later paper [9], the same authors developed a no-slip compression test where they used a fused silica disc between the glass and the molds creating a no-slip condition. Zhou et al. [27] used the creep compression test and modified the obtained stress relaxation function to compensate for the influence of friction. They numerically analyzed the change in thickness of the glass sample at different friction conditions and compared it to the thickness change in experiments. Yu et al. [28] used different substrates between the glass sample and the molds during the compression test to reduce the effect of friction on the viscoelastic data and showed that by diminishing the effects of friction on the experimental data, more accurate viscoelastic properties can be obtained from the creep tests.

One of the major drawbacks of the creep compression test is the application of instantaneous initial stress which has to be maintained constant throughout the experiment. However, when a cylindrical glass sample is compressed with a constant load, the sample expands in the radial direction which results in a decrease in com-

pressive stress. Typically to account for the change in load during the experiment, the true stress and true strain are calculated using the experimental data by considering the constant volume of the glass sample [29]. This is applicable if the cylindrical shape of the glass sample holds true during the entire compression test. However, due to the presence of friction, the sample bulges at the mid-section as shown in figure 3.1. To minimize the effect of the shape change, a few authors have restricted the maximum deformation of the sample or used a different substrate between the glass sample and the mold to reduce the effects of friction on the viscoelastic data [28, 30]. Zhang et al. [30] used a minimal uniaxial creep testing method, where the samples are compressed to only a few microns essentially preserving the cylindrical shape of the sample. While these techniques reduced the effect of friction on the compression tests, they require specialized equipment so that enough material data is captured to obtain the viscoelastic material parameters.

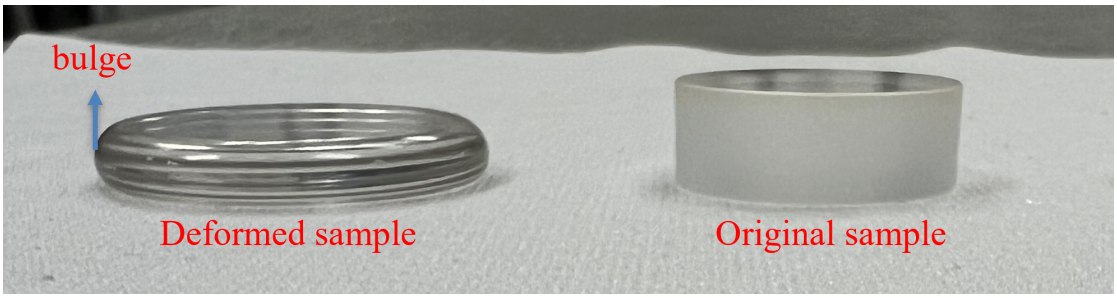

Figure 3.1: Cylindrical glass samples before and after the compression test.

In this study, a new testing method is developed to accurately characterize the viscoelastic material properties of the glass samples using the precision glass molding machine. The creep compression tests are replaced with constant strain rate tests where the bulging effect of the glass samples on the viscoelastic data is minimized. Apart from the viscoelastic material data, the constant strain rate tests are used to obtain the viscosity of the glass samples at different temperatures. The proposed method is used on two different glass types commonly used in compression glass molding.

3.2 Experimental setup

The experimental setup used for characterizing the viscoelastic material properties of the glass is similar to that of the parallel plate viscometer, as given in ASTM C1351M-96 [31]. The experiments are conducted in a precision glass molding machine, Moore Nanotech GPM170, shown in Fig. 3.2. The different types of glass used in this study and their thermal and mechanical properties are provided in table 1.1. It should be noted that, in this study, P-SK57 is used to establish the material model and D-ZK3 is used to verify the material model. For the compression tests, cylindrical glass samples with a diameter of 19.02 mm and a thickness of 6.35 mm are used for the compression test. As shown in Fig. 3.3, the glass is compressed between flat molds made of high-temperature resistant tungsten carbide material. The molds are fine polished with a roughness of $R_a = 2$ nm. Such an ultraprecision mold surface enables a small friction coefficient between the glass and the molds [29]. The molds are coated with DLC (diamond-like carbon) coating to prevent the glass from sticking to the mold surface at high temperatures.

To characterize the viscoelastic material properties two types of tests are performed using the cylinder compression method. In the first test, a cylindrical glass sample is compressed at a constant strain rate by applying a constant velocity to the top mold. It is shown in the literature, that for a given temperature, there exists a critical strain rate, which increases with increasing temperature. Exceeding the critical strain rate causes the glass to crack [32, 33]. Based on the data provided in [32], a strain rate of 5×10^{-4} to 5×10^{-3} are used which corresponds to a velocity of 0.2 mm/min to 2 mm/min, with higher velocities used at higher temperatures. A constant velocity is maintained on the top mold till a purely viscous deformation was reached, i.e., when the stress remained constant with further deformation. Once the viscous flow is attained, the velocity of the top mold is reduced to zero, i.e., it is held in its current position, to perform the relaxation test. The displacement profile and the resulting

Figure 3.2: Precision glass molding machine (Moore Nanotech GPM170).

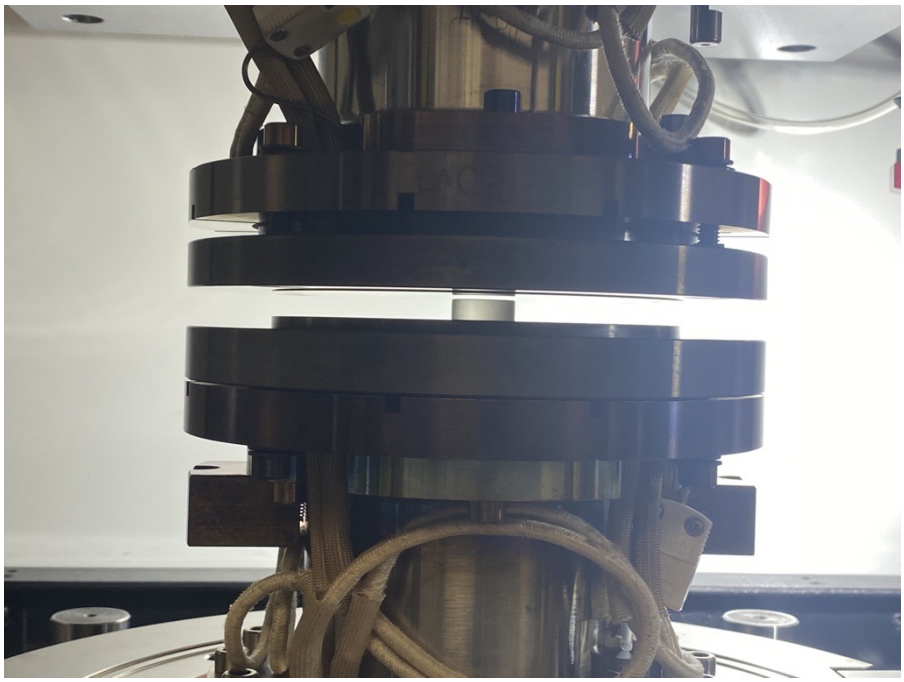

Figure 3.3: Cylindrical compression test.

force profile during the compression test are shown in Fig. 3.4. Initially, as the displacement increases with a constant velocity the force tends to increase and then converges to a maximum value with further increase in the displacement, i.e., a pure

Table 3.1: Mechanical and thermal properties of the molds and the glass.

Property	Tungsten carbide molds	P-SK57	D-ZK3
Young,s modulus, E (GPa)	570	93	97.67
Poissons ratio, ν	0.22	0.249	0.234
Density, ρ (Kg/m^3)	14650	3010	2830
Expansion coefficient, α (10^{-6}/K)	4.9	9.1	9.3
Specific heat, C_p (J/Kg-K)	314	760	1100
Conductivity, λ (W/m-K)	38	1.010	1.126
T_g (°C)	-	493	511
S_p (°C)	-	593	605

viscous deformation is achieved. At this moment, the top mold is fixed in its current position to start the relaxation test. During the relaxation test, the force tends to relax back to zero as the material tends to expand in the horizontal direction to relax the internal stresses induced during the compression as shown in Fig. 3.4.

One of the major concerns with the creep compression tests used in the literature is the effect of the bulge on the stress calculations used to evaluate the viscoelastic parameters. The advantage of the current testing procedure is that pure viscous deformation is achieved by inducing only a minimum amount of deformation to the glass sample as evident in Fig. 3.5. Figure 3.5 shows the glass sample before and after the compression test, showing that the cylindricity of the glass sample is preserved throughout the test.

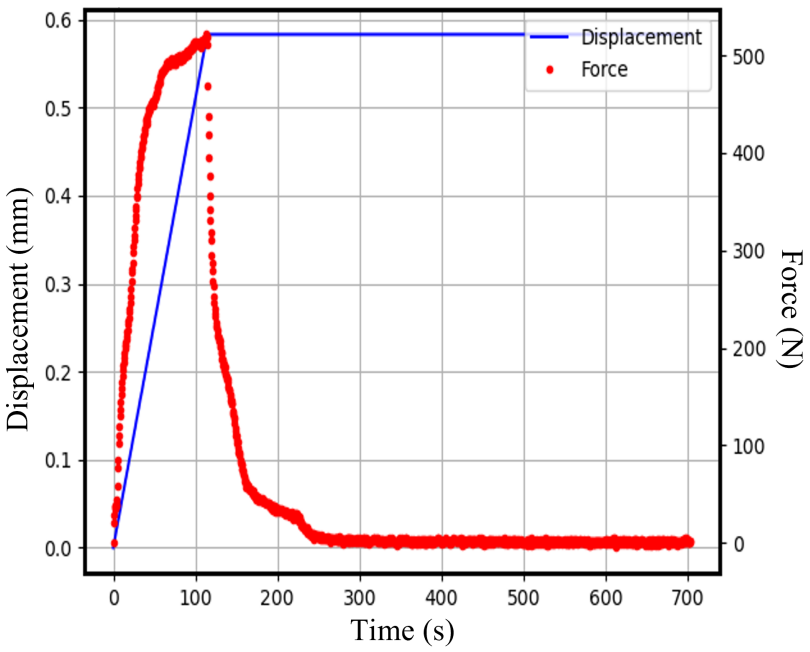

Figure 3.4: The displacement and the force profiles during the compression test.

The compression experiments are performed at five different temperatures around the softening point of the glass (S_p), which corresponds to a viscosity range of $10^{9.5}$ - $10^{6.6}$ Pas. This viscosity range is of interest because this corresponds to the typical temperatures used during the precision glass molding process. Initially, during the compression test, the cylindrical glass samples are placed on the bottom mold and slowly heated to the molding temperature at a rate of 10°C/min and then undergo a sufficient soak of approximately 15 minutes. This soaking time allows for the glass specimen to equilibrate at the molding temperature.

3.3 Linear Thermo-viscoelasticity Theory

The constitutive equations of the linear viscoelastic model in their integral form are:

$$\sigma(t) = \int_0^t G(t-t')\frac{\partial \varepsilon(t')}{\partial t'}dt' \tag{3.1}$$

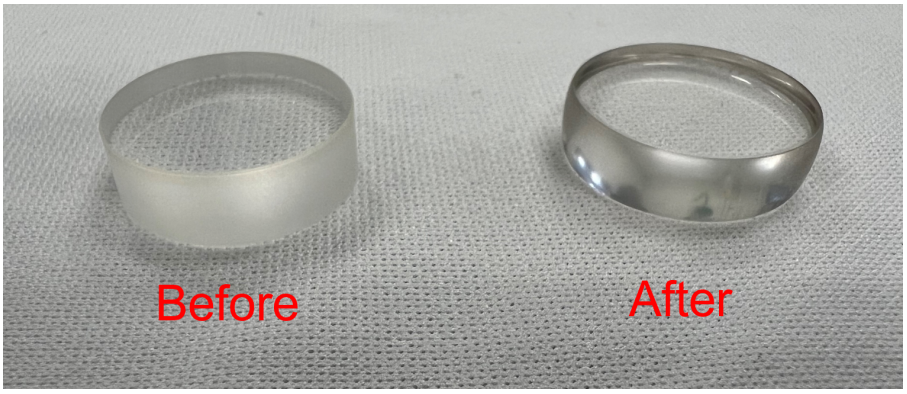

Figure 3.5: Cylindrical glass samples before and after the compression test.

$$\varepsilon(t) = \int_0^t J(t-t')\frac{\partial \sigma(t')}{\partial t'}dt' \tag{3.2}$$

where $G(t)$ and $J(t)$ are the relaxation modulus and the creep compliance function respectively. The relation between the creep compliance function and the relaxation modulus is given by Eq. 3.3.

$$\hat{J}(s)\hat{G}(s) = \frac{1}{s^2} \tag{3.3}$$

where $\hat{G}(s)$ and $\hat{J}(s)$ are the Laplace transforms of the relaxation modulus and the creep compliance function in the Laplace domain. In general, to obtain the viscoelastic material parameters, the experimental data from the creep compression test is used to obtain the creep compliance function by discretizing Eq. 3.2 using a finite difference scheme [34]. Then by using Eq. 3.3, the relaxation modulus is obtained through Laplace and inverse Laplace transforms. Finally, the viscoelastic parameters are obtained by performing a second fitting operation on the calculated relaxation modulus.

Typically, the generalized Kelvin and Maxwell models are used in the literature to describe the creep and stress relaxation behavior respectively. While the generalized models were able to well describe the viscoelastic behavior of the glass, the

number of parameters required to be estimated varies with the temperature (6 term Maxwell model is commonly used in literature which requires 12 material parameters to be estimated). Often, the fit parameters are chosen by trial and error methods [7]. In contrast, the Burgers model, also shown to well describe the glass behavior [13], consists of only four material parameters that are to be estimated at different temperatures. In addition, the Burgers model is shown to be equivalent to the two-term generalized Maxwell model, and the parameters from the Burgers model can be used to directly calculate the relaxation function thereby avoiding the second fitting procedure [35] and can be used in most of the commercial FEM software (Abaqus, Ansys etc.). The mathematical equivalency and the procedure to calculate the Prony series parameters from Burgers model parameters is given in Appendix A.

As such, to model the viscoelastic behavior of the glass, the Burgers model was used in this study. The constitutive equation of the Burgers model in the differential form is given in Eq. 3.4 [35].

$$\sigma + p_1\dot{\sigma} + p_2\ddot{\sigma} = q_1\dot{\epsilon} + q_2\ddot{\epsilon} \tag{3.4}$$

where

$$\begin{gathered} p_1 = \frac{\eta_1}{E_1} + \frac{\eta_1}{E_2} + \frac{\eta_2}{E_2}; p_2 = \frac{\eta_1\eta_2}{E_1E_2} \\ q_1 = \eta_1; q_2 = \frac{\eta_1\eta_2}{E_2} \end{gathered} \tag{3.5}$$

E_1, E_2, η_1, and η_2 are the material parameters of the Burgers model. The Laplace transform of Eq. 3.4 is given by Eq. 3.6.

$$\sigma(s) + p_1 s\sigma(s) + p_2 s^2\sigma(s) = q_1 s\epsilon(s) + q_2 s^2\epsilon(s) \tag{3.6}$$

The constant strain rate boundary condition used for the compression test is expressed by Eq. 3.7 and its Laplace transform is given by Eq. 3.6.

$$\dot{\epsilon}(t) = \epsilon_o = constant \tag{3.7}$$

$$\epsilon(s) = \epsilon_o / s^2 \tag{3.8}$$

Substituting Eq. 3.8 into Eq. 3.6, we obtain

$$\frac{\sigma(s)}{\epsilon_o} = \frac{q_1/s + q_2}{1 + p_1 s + p_2 s^2} \tag{3.9}$$

Equation 3.9 can be simplified as Eq. 3.10

$$\frac{\sigma(s)}{\epsilon_o} = \frac{A}{s} + \frac{B}{s + r_1} + \frac{C}{s + r_2} \tag{3.10}$$

where A, B, and C are introduced for the convenience of Laplace transform and are calculated by using partial fractions

$$\begin{aligned} A &= \frac{q_1}{r_1 r_2} \\ B &= \frac{q_1 - r_1 q_2}{r_1 \bar{A}} \\ C &= -\frac{q_1 - r_2 q_2}{r_2 \bar{A}} \end{aligned} \tag{3.11}$$

where r_1, r_2 are the roots of the denominator in Eq. 3.9, given by

$$\begin{aligned} r_{1,2} &= \frac{p_1 \pm \bar{A}}{2 p_2} \\ \bar{A} &= \sqrt{p_1^2 - 4 p_2} \end{aligned} \tag{3.12}$$

Substituting Eq. 3.11 into Eq. 3.10 and applying the inverse Laplace transform gives the final form of Burgers equation under constant strain rate:

$$\sigma(t) = \eta_1 \dot{\epsilon} \left[1 + \frac{1 - r_1 \eta_2 / E_2}{r_1 \bar{A}} e^{-r_1 t} - \frac{1 - r_2 \eta_2 / E_2}{r_2 \bar{A}} e^{-r_2 t} \right] \tag{3.13}$$

Here it should be noted that, as time goes to infinity, Eq. 3.13 reduces to 3.14, an equation representing a dashpot.

$$\sigma(t) = \eta_1 \dot{\epsilon} \tag{3.14}$$

where η_1 is the bulk viscosity of the material. Hence, by fitting Eq. 3.13 to the experimental data obtained from the constant strain rate tests, one should be able to determine the viscoelastic parameters as well as the viscosity of the material being tested.

The response of the Burgers model to constant strain (stress relaxation) is obtained by solving Eq. 3.4 using a constant strain condition. The derivation is similar to the constant strain rate test and can be found at [35]. The Burgers model equation to represent the stress relaxation test is given below

$$\sigma(t) = \frac{\epsilon}{\bar{A}} \left[(q_1 - r_2 q_2)\, e^{-r_2 t} - (q_1 - r_1 q_2)\, e^{-r_1 t} \right] \tag{3.15}$$

Equations 3.13 and 3.15 are used to represent the constant strain rate and the stress relaxation test respectively in this study.

3.4 Estimation of viscoelastic parameters

To characterize the viscoelastic response of the glass, the four parameters of the Burgers model (E_1, η_1, E_2, and η_2) are to be estimated by curve fitting the Eqs. 3.13 and 3.15 to the experimental data. As mentioned in the previous chapter, Burgers model is a combination of a single Maxwell element and a Kelvin element in a series. While the Kelvin element represents the delayed elastic response, the spring, E_1, and the dashpot, η_1, in the Maxwell element represent the instantaneous elastic response and the viscous response of the viscoelastic material, respectively. Young's modulus of the glass material accounts for the elastic response and is presumed to be constant, the value at room temperature. This reduces the number of fit parameters to three.

The computational procedure to estimate the viscoelastic parameters of the glass is as follows. First, the true stress, $\sigma(t)$, is calculated from the displacement $u(t)$ and the force $F(t)$ data obtained from the compression test, as given by Eq. 3.16.

$$\sigma(t) = \frac{F(t)}{A(t)} = \frac{F(t)L(t)}{A_o L_o} \tag{3.16}$$

where $A(t)$ and A_o are the current and initial cross-sectional area of the glass specimen, and $L(t)$ and L_o are the current and the initial thickness of the specimen. Equation 3.16 is typically used in the literature to calculate the true stress considering the incompressibility. However, the effects of bulging of glass samples due to interface friction are often neglected. This leads to an estimation error of the relaxation parameters [30]. However, with the testing procedure used in this study, and as shown in Fig. 3.5, the glass samples are shown to retain the original shape, thereby avoiding any errors in stress calculations. The strain rate used in the test is calculated by dividing the velocity by the original thickness of the sample.

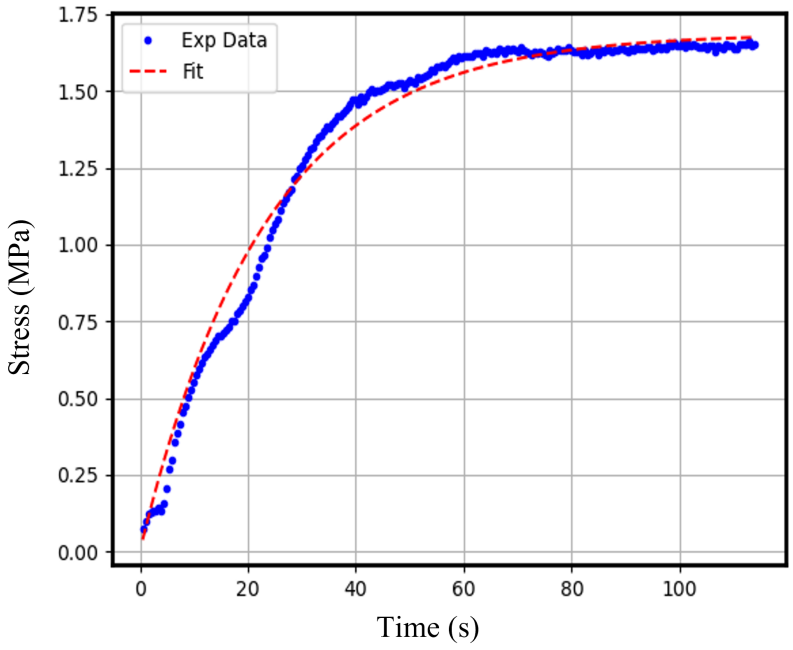

Figure 3.6: Curve fit of the Burgers model to the constant strain rate test.

Initially, to determine the Burgers parameters, Eq. 3.13 is fit to the stress data obtained from the constant strain rate tests. A non-linear curve fitting algorithm is used to obtain the fit parameters. Figure 3.6 shows the experimental data and the resulting curve fit from the constant strain rate test on a P-SK57 sample at a temperature of 550°C. As shown, the Burgers model derived for constant strain rate is able to describe the experimental data well. Next, to verify the model, the obtained fit parameters are used in Eq. 3.15 to model the stress relaxation and then compared to the experimental data from the stress relaxation test, as shown in Fig. 3.7. This shows that just the strain rate test data can be used to obtain the viscoelastic parameters that are able to describe the relaxation phenomenon as well. However, for better accuracy of the fit parameters, both the Eqs. 3.13 and 3.15 are fit simultaneously to the experimental data.

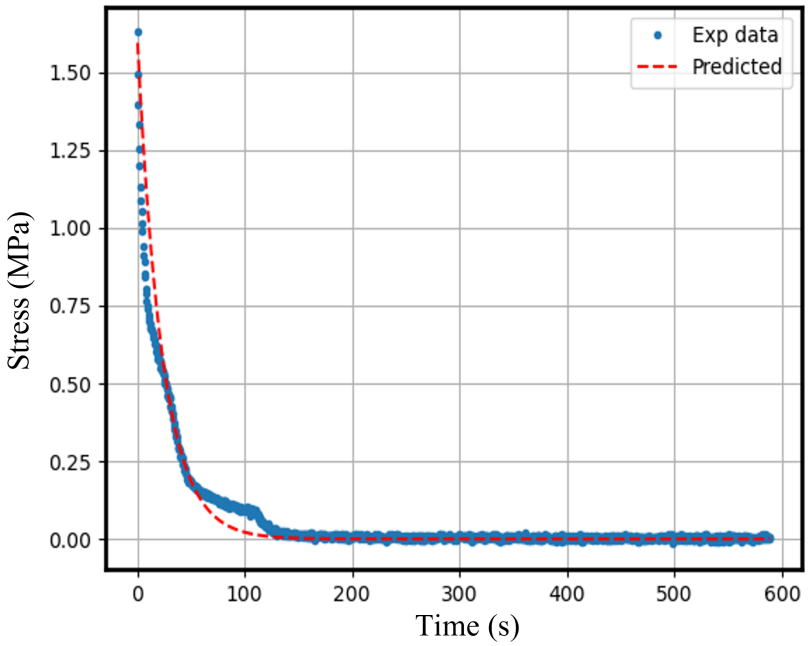

Figure 3.7: The relaxation function from experiments vs calculated.

To obtain the viscoelastic parameters at different temperatures, the Burgers model is fit to the experimental data acquired at different temperatures. Figure 3.8 shows that the Burgers model provides an accurate fit over different temperatures used in

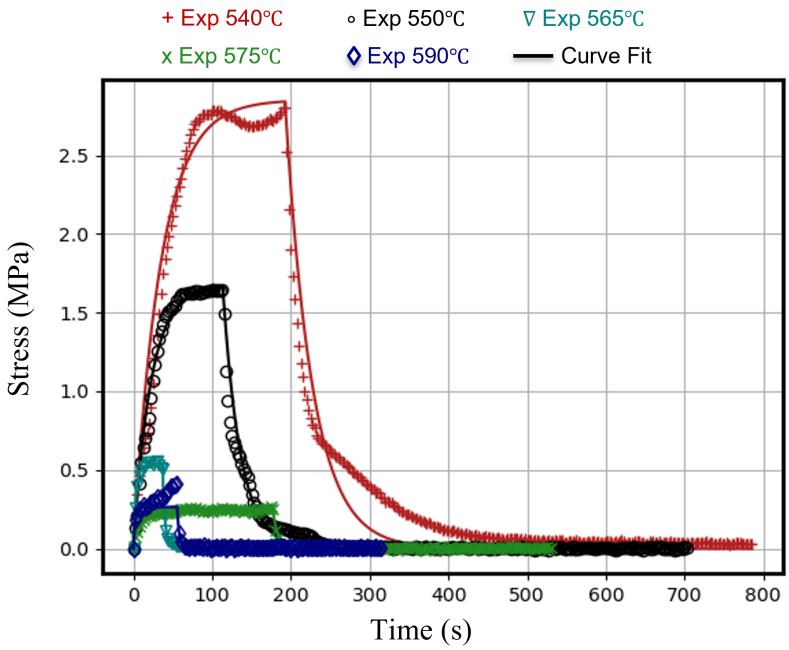

Figure 3.8: The stress profiles at different temperatures under constant strain rate and stress relaxation.

this study. Further, to verify the fit parameters, η_1, which corresponds to the bulk viscosity of the glass, is compared to the manufacturer's data. Figure 3.9 shows that the viscosity values obtained by the current testing method agree well with the Schott data [36].

As stated in Section 3.3, the Burgers model is mathematically equivalent to a two-term Prony series; therefore, the parameters obtained from the fitting function can be directly used to obtain the Prony series parameters, i.e., the weights w_i and the relaxation times, τ_i, as given in Eq. 2.9. Details of the mathematical equivalency between the Burgers model and the Prony series are given in Appendix A. The shear parameters of the Burgers model are readily obtained from the four fitting parameters as shown in Eq. 3.17.

$$\begin{aligned} G_1 &= \frac{E_1}{2(1+\nu)}, \ \mu_1 = \frac{\eta_1}{2(1+\nu)} \\ G_2 &= \frac{E_2}{2(1+\nu)}, \ \mu_2 = \frac{\eta_2}{2(1+\nu)} \end{aligned} \tag{3.17}$$

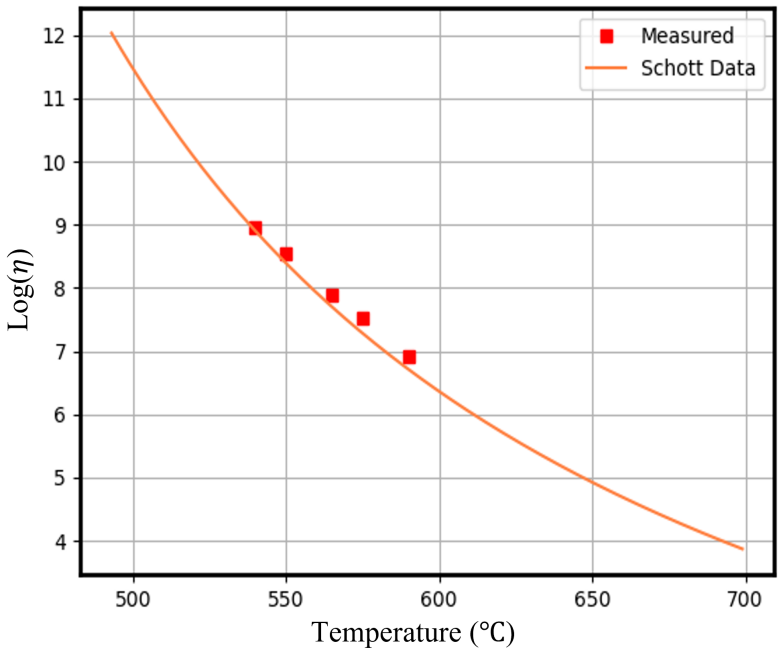

Figure 3.9: The viscosity values obtained from the constant strain rate test at different temperatures compared to the manufactures data.

where ν is the Poisson's ratio given in Table 3.1. Using the shear parameters, Prony series coefficients, the weights w_i, and the relaxation times τ_i are calculated as shown in Appendix A. Table 3.2 shows the computed Prony series parameters at the different temperatures used in this study.

Table 3.2: P-SK57 relaxation parameters at different temperatures.

Temperature (°C)	Weights		Relaxation time	
	w_1	w_2	τ_1	τ_2
540	9.42e-4	99.905e-2	33.09	9.43e-06
550	6.04e-4	99.939e-2	17.40	6.04e-06
565	3.30e-4	99.966e-2	7.29	3.31e-06
575	2.29e-4	99.977e-2	4.31	2.29e-06
590	1.38e-4	99.986e-2	2.10	1.39e-06

3.5 Numerical Verification of the viscoelastic parameters

A coupled temperature-displacement finite element model is developed in ABAQUS to verify the viscoelastic parameters obtained from the compression test. Figure 3.10 shows the axisymmetric model used in this study. The glass specimen is modeled as a deformable viscoelastic body, while the molds are defined as deformable elastic bodies. The material parameters of the molds and the glass are given in Tables 3.1 and 3.2. The displacement boundary conditions on the top and the bottom mold are applied by defining a coupling constraint on the bottom surface of the bottom mold and the top surface of the top mold, as shown in Fig. 3.10.

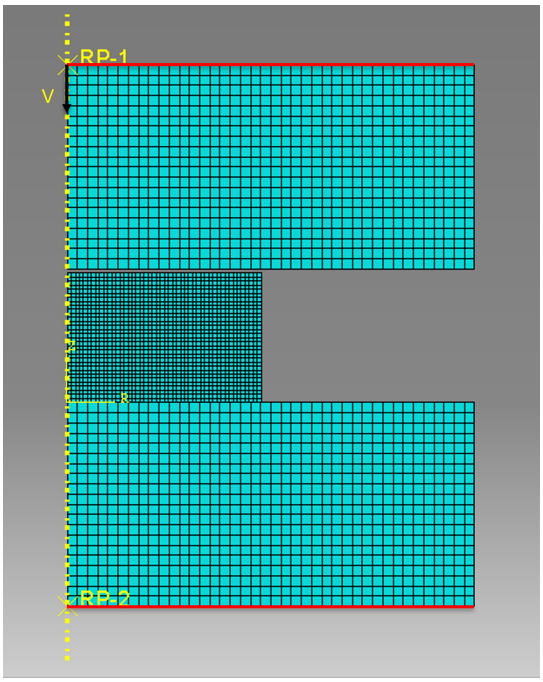

Figure 3.10: Axisymmetric finite element model to verify the viscoelastic parameters.

To verify the viscoelastic model, three steps of the experimental process are modeled in ABAQUS. Initially, the molds and the glass are heated to the molding temperature by applying a temperature boundary condition on the outer surface of the molds. Isothermal conditions are assumed in the model. In fact, as shown in [37], the current setup of GPM 170 is shown to hold the temperatures accurately throughout the mold-

ing process. The vertical displacement of the bottom mold is constrained throughout the simulation. To model the constant strain rate test, a velocity boundary condition is applied to the top mold for a duration similar to that of the experiments, and then, the top mold is fixed in its current position to simulate the relaxation test. The inputs provided to the simulations are set with respect to the same experimental temperatures.

To verify the material parameters, the force profiles obtained from the simulations at different temperatures are compared to the force profiles obtained from the experiments, Fig. 3.11. The simulated results show a good agreement with the experimental data. This validates the viscoelastic parameters derived from the compression test at individual testing temperatures. However, for the glass molding simulations, temperature-dependent viscoelastic properties are required. As stated in Chapter 2, the glass is considered to obey the TRS assumption widely used in the literature to model the thermo-viscoelastic response. The next section focuses on the temperature dependence of the viscoelastic parameters.

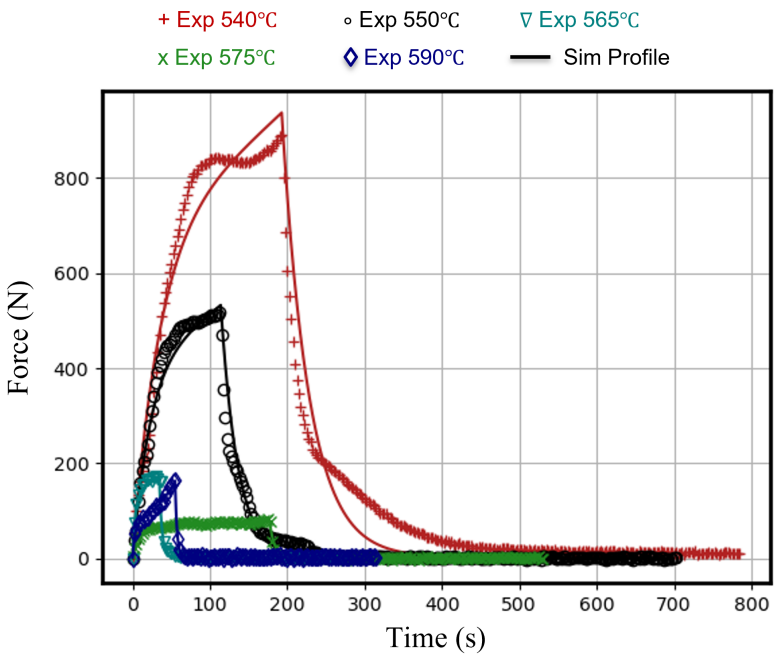

Figure 3.11: Experimental vs simulated force profiles at different temperatures.

3.6 Temperature Dependence of the viscoelastic parameters

3.6.1 TRS assumption

As stated in Chapter 2, in a viscoelastic material, the rate of relaxation varies significantly with a change in temperature. But when the relaxation moduli at different temperatures are plotted with respect to time in log scale, the curves tend to be in identical shape but are shifted horizontally by a scale factor (TRS behavior). Using the Prony series coefficient from Table 3.2, Fig. 3.12 plots the normalized shear relaxation moduli of the five testing temperatures.

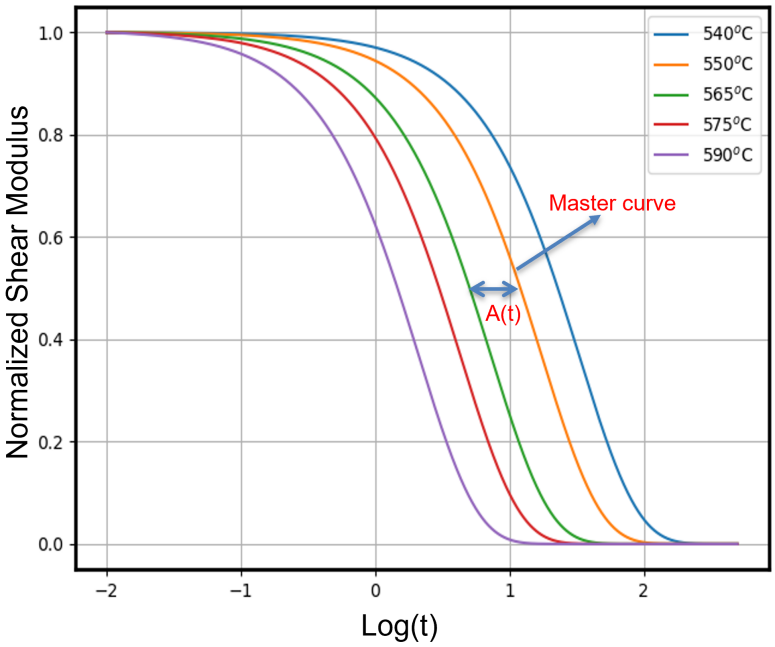

Figure 3.12: Normalized shear modulus at different temperatures.

To determine the shift factor (A(T)), first, a relaxation curve at an arbitrary experimental temperature, i.e., a reference temperature T_r, is selected as a master curve. In this study, the shear relaxation function at 550°C is considered the master curve. Next, the master curve is shifted in the horizontal direction to match the relaxation curves at other temperatures. The shift factor is given by the difference in abscissa between the two curves. The temperature dependence of the shift factor is defined

by the Williams-Landel-Ferry (WLF) equation,

$$\log(A(T)) = \frac{-C_1(T - T_r)}{C_2 + (T - T_r)} \tag{3.18}$$

where C_1 and C_2 are constants obtained by fitting the shift factor obtained from the master curve to each individual temperature. Figure 3.13 shows the shift factor at different temperatures and the corresponding curve fit by the WLF equation.

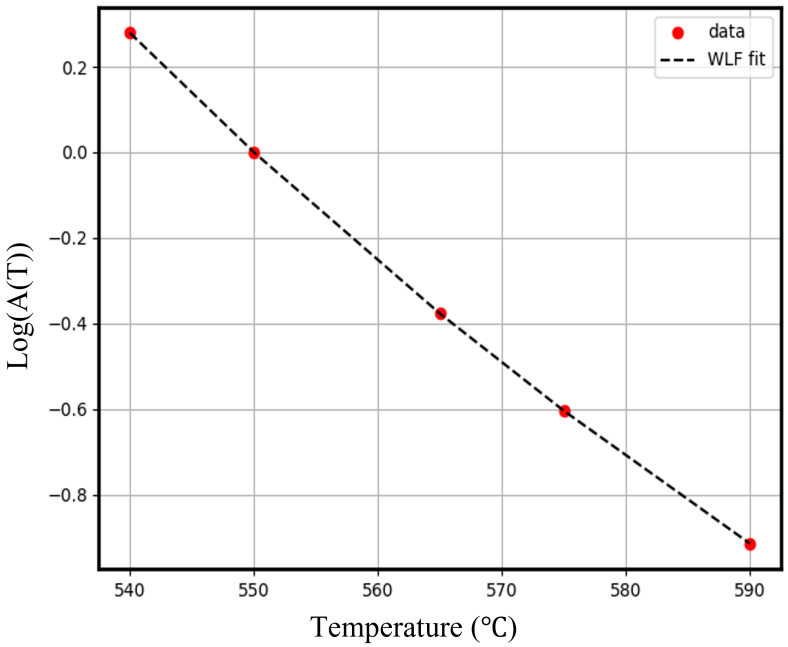

Figure 3.13: WLF shift factor with respect to temperature.

The TRS assumption can be readily implemented in the FEM model by defining the WLF constants in ABAQUS. To verify the temperature dependence, the simulations were rerun at five different temperatures. The temperature dependence is defined in the simulation by providing the viscoelastic material properties (Prony coefficients) at the reference temperature (T_r) and the constants of the WLF equation. Figure 3.14 shows the experimental force profiles at 560°C and the force profiles obtained from the simulations using the TRS assumption. As expected, the experimental and simulated results at the reference temperature (550 °C) are validated. However, at

other temperatures where the viscoelastic parameters are obtained from the TRS assumption, the simulated results deviate from the experimental results, especially at higher temperatures. This shows the inadequate implementation of the TRS behavior at a wide temperature range. In principle, the application of the TRS behavior is valid if and only if the master curve and the shifted curves are fully identical. To verify the TRS assumption, in Fig. 3.15 the master curve and the shifted curves at different temperatures are plotted on the log time scale. It shows the relaxation curves at different temperatures are not fully identical. Similar discrepancies were observed in the literature [27–29].

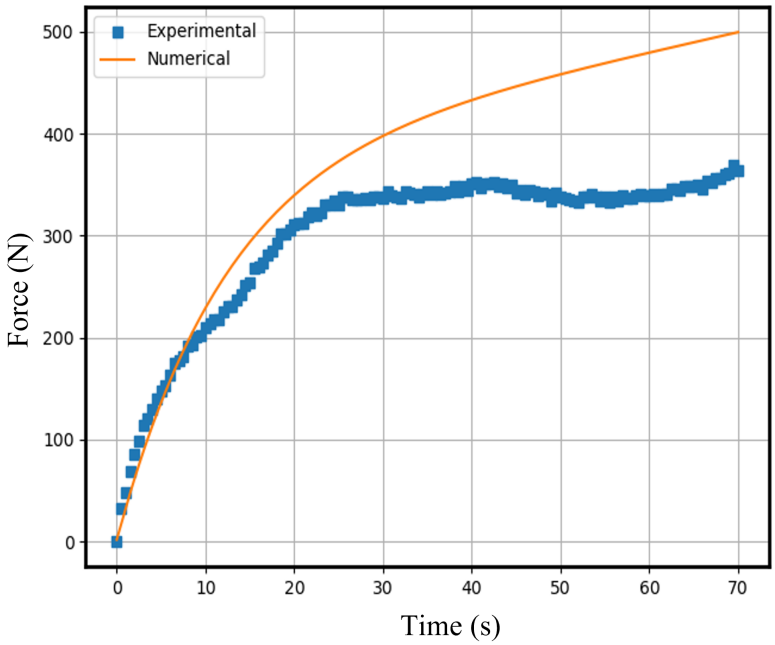

Figure 3.14: Experimental vs simulated force profiles at 560°C using the TRS assumption.

While different attempts have been made to enhance the TRS model predictions in the literature [38, 39] to reduce the differences between the master and the shifted curves, these are again assumptions that are only valid if the curves are fully identical. Considering the above drawbacks, in the following section, an alternative approach, similar to the one used by Vu et. al. [29], is used to model the temperature dependence

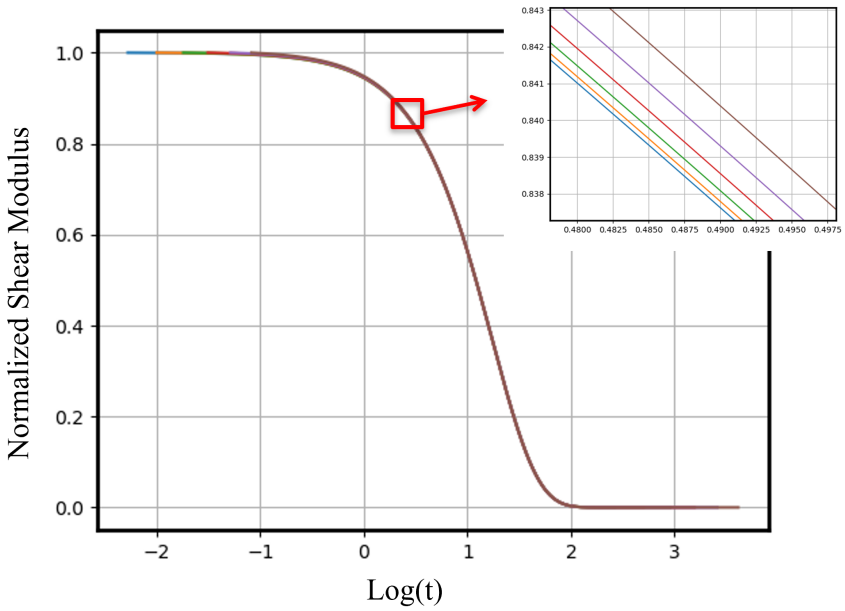

Figure 3.15: The master curve and the shifted functions at different temperatures.

of the viscoelastic material properties without assuming the TRS behavior.

3.6.2 Temperature dependent Burgers parameters

As demonstrated in Section 3.5, the Burgers model is completely adequate for simulating the viscoelastic behavior of glass at any given temperature. This suggests that, if a relationship between the Burgers parameters and the corresponding temperature can be established, the temperature-dependent viscoelastic parameters can be derived without using the relaxation moduli and the shift factor. As shown before, the relaxation parameters, weights w_i, and the relaxation times τ_i, can be directly calculated from the Burgers parameters. Hence if a temperature-dependent function is established for each Burgers parameter, the relaxation parameters can be obtained at any temperature without making any assumptions regarding the shift factor [29].

To obtain the temperature-dependent functions, the compression test data from the five experimental temperatures, shown in Fig. 3.8, is used to obtain the four Burgers parameters (E_1, η_1, E_2, and η_2) at each temperature by curve fitting. As mentioned

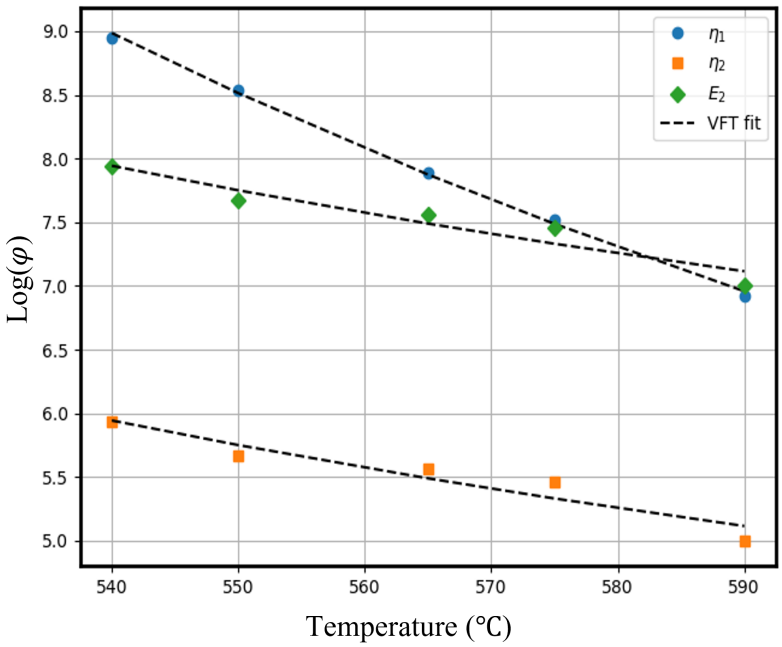

Figure 3.16: Temperature dependent Burgers model parameters, P-SK57.

in Section 3.4, the parameter E_1 represents the instantaneous elastic response and is assumed to be equal to Young's modulus of the material at room temperature, hence temperature independent. The relations of the other parameters, i.e., E_2, η_1, and η_2, with temperature as plotted in Fig. 3.16, show that the values of these properties decrease with increasing temperature.

The next step is to identify a mathematical model to describe the temperature dependence of the Burgers parameters. From Fig. 3.16 it is observed that the parameters show a trend that is similar to that of the glass viscosity [40]. In fact, as shown in Eq. 3.14, the parameter η_1 of the Burgers model represents the bulk viscosity of the glass material. And in the literature [17, 29], the Vogel-Fulcher-Tammann (VFT) equation is commonly used to describe the temperature dependence of the equilibrium glass viscosity. As such, the VFT equation is chosen in this study to model the temperature dependence of the Burgers parameters. The VFT equation is given as follows,

$$\log(\varphi) = A(\varphi) + \frac{B(\varphi)}{T - T_o(\varphi)} \tag{3.19}$$

where φ is each of the three parameters of the Burgers model, T is the temperature, and A, B, and T_o are the fit parameters. To reduce the number of fit parameters, T_o which corresponds to the Kauzmann temperature [29], is considered to be the same for all three parameters, i.e., $T_o(\eta_1) = T_o(E_2) = T_o(\eta_2)$. Also, as observed in Fig. 3.16, the temperature dependence of the parameter E_2 is similar to that of the parameter η_2 (the Kelvin component parameters of the Burger model), this shows that both the parameters have similar B coefficients, i.e., $B(E_2) = B(\eta_2)$.

As shown in Fig. 3.16, the VFT model using a set of six fitting coefficients, i.e., $A(\eta_1)$, $B(\eta_1)$, $A(E_2)$, $B(E_2)$, $A(\eta_2)$, T_o, is able to describe the temperature dependence of the Burger parameters. Using the determined coefficients, the Burgers parameters can be determined at any given temperature eventually obtaining the relaxation parameters without the need for the relaxation moduli or the shift factor.

Table 3.3: Temperature dependent viscoelastic parameters.

VFT coefficients	P-SK57	D-ZK3
$A(\eta_1)$	-2.5	-6.71
$B(\eta_1)$	2677.37	4653.02
$A(E_2)$	3.25	-0.8
$B(E_2)$	1094.30	2605.78
$A(\eta_2)$	1.25	-2.8
T_o	306.79	244.5

3.7 Numerical Validation

In order to validate the proposed viscoelastic characterization method developed in this study, the numerical model shown in Fig. 3.10 is used to perform the compression tests at different temperatures. To include the thermal dependency in the

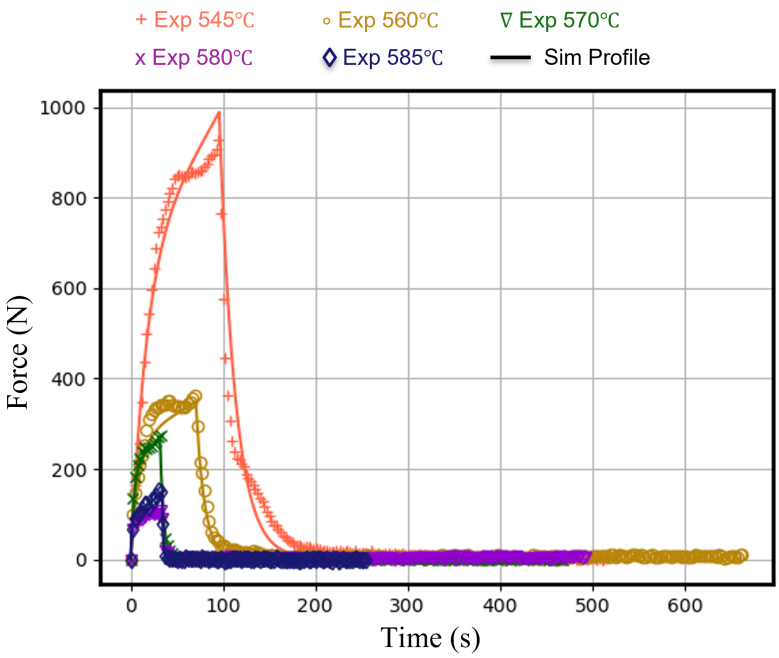

Figure 3.17: Validation of the temperature dependency of the Burgers model.

viscoelastic model, a UMAT sub-routine is programmed in ABAQUS. The viscoelastic parameters that are used as input to the UMAT are as given in Table 3.3. To validate the viscoelastic model as well as the temperature dependency, the simulations are performed at different temperatures that are not used in the VFT fitting function. Figure 3.17 shows the simulation results as well as the experimental data at five different temperatures. As shown, the simulation results obtained by using the VFT function are in good agreement with the experimental data over the temperature range used in this study.

To further validate the model, compression tests are carried out on other types of glass that are commonly used in glass press molding. For this purpose, a dense barium crown optical glass D-ZK3 (CDGM) is chosen. The thermomechanical properties of the glass material are given in Table 3.1. To obtain the viscoelastic parameters, the compression tests are performed at different temperatures. Figure 3.18 shows the Burgers model fit to the experimental data at five different temperatures. It shows good fitting accuracy over the entire temperature range. To verify the obtained

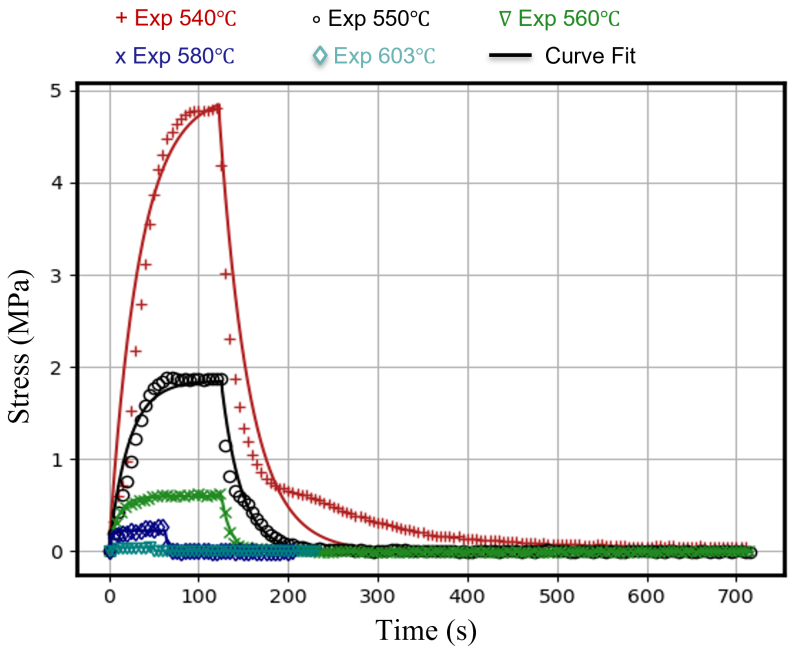

Figure 3.18: Stress profiles of D-ZK3 at different temperatures and the corresponding curve fit of Burgers model.

viscoelastic parameters, the FE simulations are performed at different temperatures. Figure 3.19 compares the experimental force profiles to the simulated results at five different temperatures.

Figure 3.20 shows the Burgers parameters of the D-ZK3 glass at different temperatures. The VFT function, as described in Section 3.6.2, is used to obtain the temperature-dependent viscoelastic parameters. The corresponding values are as provided in Table 3.3. Figure 3.21 shows the experimental force profiles compared to simulated results at four different temperatures that are not used in the fitting functions. These data show that the numerical calculations are accurate at other temperatures within the glass molding range. The validation results of two different glass categories reinforce the proposed method's validity in describing and modeling the thermo-viscoelastic nature of glass for FEM simulation in the glass molding process.

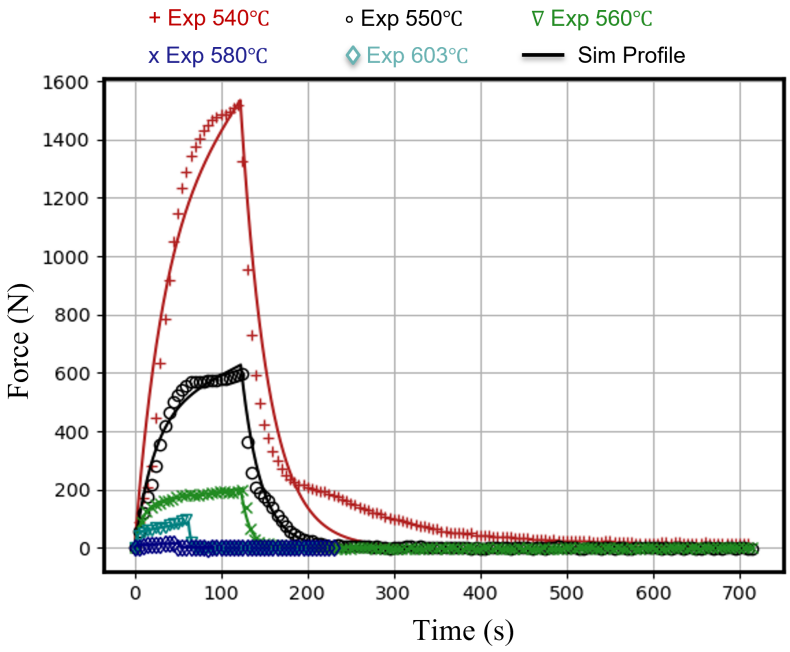

Figure 3.19: Numerical verification of the force profiles at different temperatures, D-ZK3.

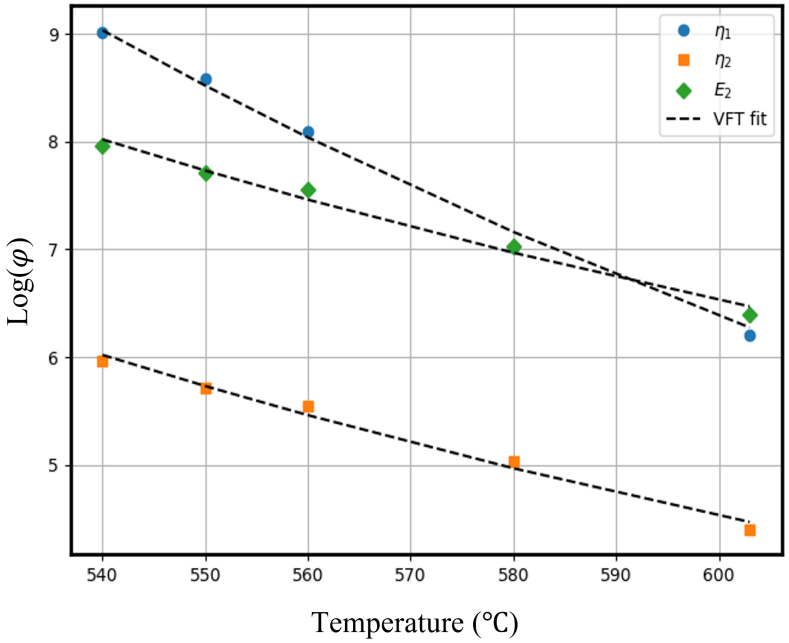

Figure 3.20: Temperature dependent Burgers model parameters, D-ZK3.

3.8 Conclusions

Utilizing a constant strain rate and stress relaxation test, this chapter overcomes the current limitations of modeling viscoelastic materials. The Burgers model is used

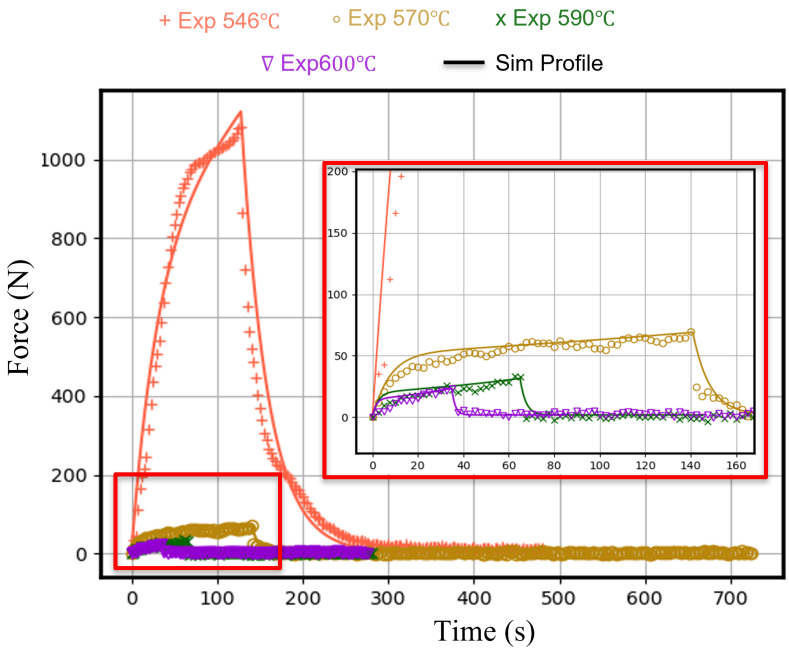

Figure 3.21: Validation of the temperature dependency of the Burgers model, D-ZK3.

to simulate the viscoelastic response under conditions of constant strain rate and constant strain. It is demonstrated that the obtained model parameters accurately depict the viscoelastic response of the glass material over a broad range of molding temperatures. In addition, the parameter η_1 of the Burgers model is correlated with the material's bulk viscosity. The obtained viscosity values at various temperatures are in close agreement with the viscosity data provided by the manufacturer. In this investigation, temperature-dependent Burgers parameters based on the VFT function are used to model the temperature-dependent viscoelasticity. The temperature dependence is incorporated into the numerical model using the ABAQUS user subroutine UMAT. Excellent agreement between the experimental and simulated results of two distinct glass types at differing molding temperatures enhances the validity of the proposed model.

CHAPTER 4: EVALUATION OF STRUCTURAL RELAXATION PARAMETERS USING IMPULSE EXCITATION TEST

As stated in Chapter 1, when a glass within the transition range is subjected to a sudden change in temperature, it shows a time-dependent change in property. This time-dependent behavior is known as structural relaxation. The TNM model that explained the changes in the fictive temperature T_f, (as discussed in Chapter 2 and represented by Eqs. 2.19 - 2.21) with respect to time and temperature has been successfully used in literature to describe the structural relaxation behavior of glass [7, 11]. Typically, the structural relaxation of a material is characterized by observing the change in the physical property of the glass when subjected to a sudden temperature jump. Ideally, one can use to thermal expansion of the glass to define the structural relaxation behavior. But due to difficulties associated with accurately and precisely obtaining the expansion behavior of the glass in the transition region, researchers have used properties such as the refractive index, density, heat capacity, etc, to identify the structural relaxation parameters [41–43]. But in the aforementioned studies, the relaxation-induced property changes were generally very small, leading to insufficient experimental data on the structural relaxation of the glass.

Compared to other properties, the Young's modulus is utilized considerably less as an observable parameter for studying structural relaxation. It has been shown, however, to be an outstanding indicator of relaxation behavior [44, 45]. Also, contrary to the density or refractive index, the variation of the elastic modulus in the glass transition range is much higher, allowing for a more accurate characterization of the structural relaxation parameters [46]. Typically, to measure the elastic modulus at

high temperatures, experimental methods such as ultrasonic echography, Brillouin light scattering technique, or direct mechanical vibration methods are commonly used [7, 45]. As such, in this study, the structural relaxation parameters of an optical glass D-ZK3 are obtained by measuring the variation of the Youngs modulus above the glass transition temperature. The change in the elastic modulus was obtained from the impulse excitation test (IET) performed on a precision glass molding machine, according to the American Society for Testing and Materials (ASTM) standard E1876 [47]. The TNM model is used to describe the variation of modulus with time and temperature.

4.1 Theory

4.1.1 Impulse excitation test

The impulse excitation test is a non-destructive testing method used to determine the mechanical properties of a material. It is commonly used for characterizing the elastic modulus, shear modulus, and Poisson's ratio. During the IET experiment, the sample is excited by applying a small mechanical impulse using a striker, and the resulting fundamental resonant frequency of the sample is measured. From these measurements, the elastic properties of the material being tested are determined.

In order to determine Young's modulus of the glass sample using the excitation test, a rectangular sample is supported at a distance of 0.224 $\times$ L (L is the length of the sample) from each end, as depicted in Fig. 4.4. The specimen is then gently tapped in the center, and the resulting vibrations are recorded by a microphone placed close to the specimen. The acquired vibration signal is then converted to the frequency domain using the fast Fourier transformations, and the resulting resonant frequency is determined. Utilizing the classical beam theory [47], the measured resonant frequency is used to calculate the Youngs modulus of the material, which is given by the Eq. 4.1 [47].

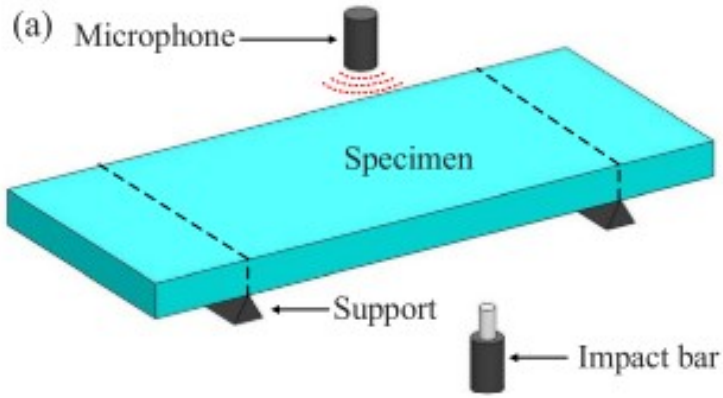

Figure 4.1: IET specimen setup for measuring Young's modulus [30].

$$E = 0.9465 \left(\frac{m f_f^2}{b} \right) \left(\frac{L^3}{t^3} \right) T_1 \tag{4.1}$$

where m is the mass, b is the width, L is the length, and t is the thickness of the glass sample. f_f is the fundamental resonant frequency in Hz, and T_1 is the correction factor given by Eq. 4.2.

$$T_1 = 1 + 6.585 \left(\frac{t}{L} \right)^2 \tag{4.2}$$

4.1.2 TNM model

The TNM model, described in Chapter 2, utilizes the fictive temperature T_f to describe the unique characteristics of the change in glass properties with respect to temperature through the glass transition region. As such, once the fictive temperature is known, any property that obeys the structural relaxation can be determined, or vice-versa. In fact, as shown in Schere [11], when a glass sample equilibrated at temperature T_1 is suddenly subjected to a different temperature T_2, the changes in the glass properties and the fictive temperature with time satisfy the proportionality

given in Eq. 4.3

$$M_p(t) = \frac{p(t) - p_2}{p_1 - p_2} = \frac{T_f(t) - T_2}{T_1 - T_2} \tag{4.3}$$

where p is the measured property of the glass sample, p_1, and p_2 are the equilibrium values of the property at the temperatures T_1 and T_2, respectively. T_f is the fictive temperature and M_p is the structural response function. According to the TNM model, the structural response function is given by the below equations,

$$M_p(t) = exp\left[-\left(\frac{t}{\tau_p}\right)^b\right] \tag{4.4}$$

where b is a constant, and τ_p is the relaxation time given by Eq. 4.5.

$$\tau_p = \tau_0 \left(\frac{x\Delta h}{RT} + \frac{(1-x)\Delta h}{RT_f}\right) \tag{4.5}$$

where τ_o is a constant, Δh is the activation energy, R is the ideal gas constant, and x is a non-linearity constant reflecting the influence of temperature and structure on the relaxation time [15]. According to Eq. 4.4, to model the structural relaxation function a total of four parameters, which are τ_o, Δh, b, and x, are to be determined experimentally.

4.2 Experimental setup

The structural relaxation function is determined experimentally by using the impulse excitation technique. The relaxation parameters of D-ZK3 (CDGM) glass, a commonly used glass type in precision glass molding with a transition temperature of 511°C are determined. The thermal and mechanical properties of the glass material are as given in Table 3.1. A rectangular glass sample of dimensions 60 mm × 2.5 mm × 2 mm is used in the IET tests. The surface of the samples is highly polished to reduce any surface roughness effects. The glass samples are freely supported at the

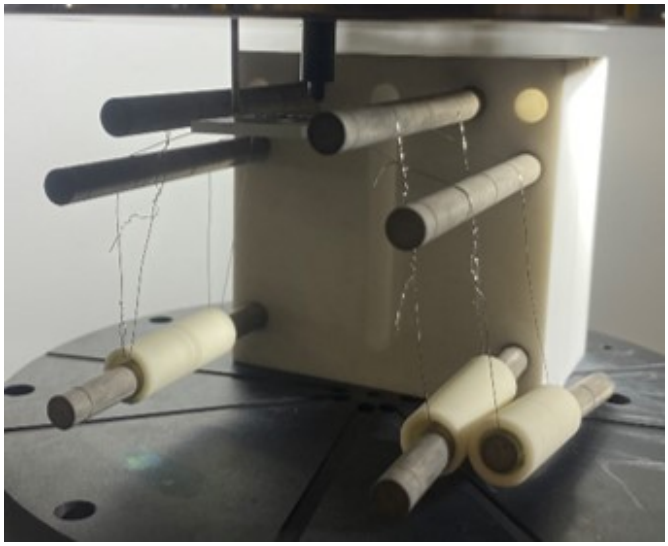

Figure 4.2: Glass sample suspended at the two nodes of their first vibration mode.

nodes corresponding to their first mode of vibration using a ceramic support structure as shown in Fig. 4.2.

A precision glass molding machine (Moore Nanotech GPM170) was used for the impulse excitation tests. The test setup inside the molding machine is as shown in Fig. 4.3. The glass sample was excited by applying an impulse load at the mid-section of the glass beam. To impart an impulse load on the glass sample, a striker at the top of the setup is actuated in regular intervals, which then hits a spring-loaded hammer that gently taps the suspended glass sample. The resulting audio was recorded using a high temperature-resistant microphone placed at a certain distance from the glass sample. Figure 4.4 shows the audio signal and calculated the resonant frequency of the sample, which can be used to calculate Young's modulus according to ASTM-E1876 [47]. A thermocouple is placed close to the glass sample to record the temperature during the experiments.

Initially, the IET setup was used to do a crawl test, where the glass samples are heated from room temperature to 550°C with a heating rate of 5°C/min. During the test, the glass sample is excited at regular intervals to measure the change in Young's modulus with respect to temperature. The results from the crawl test are

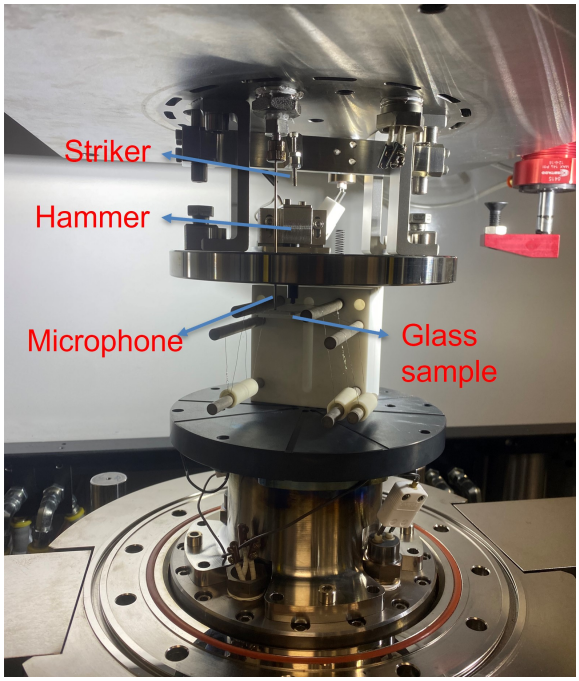

Figure 4.3: Impulse excitation test setup in Moore Nanotech GPM170.

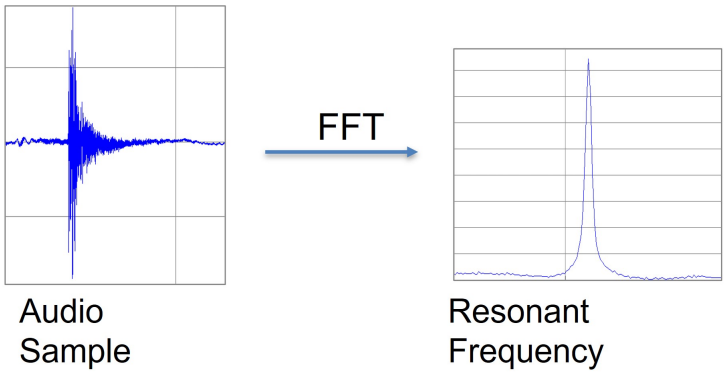

Figure 4.4: Audio sample and the resulting resonant frequency obtained using IET.

used to calibrate the thermocouple used for feedback control during the excitation testing. Once the thermocouple is calibrated, the temperature step tests were carried out at four different temperature ranges to characterize the structural relaxation parameters. The temperature jumps were from 480°C, 510°C, 525°C, and 540°C to 525°C, 525°C, 540°C, and 525°C, respectively. During the step test, the glass samples are slowly heated to the initial temperature at 2°C/min and soaked until the modulus is equilibrated. Then by using full power heating or cooling (about 20°C/min), a

temperature jump is applied to the glass sample, and the corresponding change in the Young's modulus is recorded till equilibrium is achieved.

4.3 Estimation of structural relaxation parameters

Figure 4.5 shows the results from the crawl test where the sample is heated from room temperature to 550°C at a rate of 5°C/min. Initially, the modulus tends to decrease progressively as the temperature increases. This is due to the fact that the viscosity of the glass material is high at low temperatures preventing any atomic rearrangements on the experimental time scale [11]. As observed from Fig. 4.5, the change in modulus is gradual below a temperature of 510°C. However, when heated above this temperature, the rate of change of the elastic modulus increases suddenly, indicating the glass transition, i.e., 510°C is the transition temperature. In fact, the transition temperature obtained from the IET test closely matches to the transition temperature reported in the manufacturer's data sheet [48] and shown in Table 3.1.

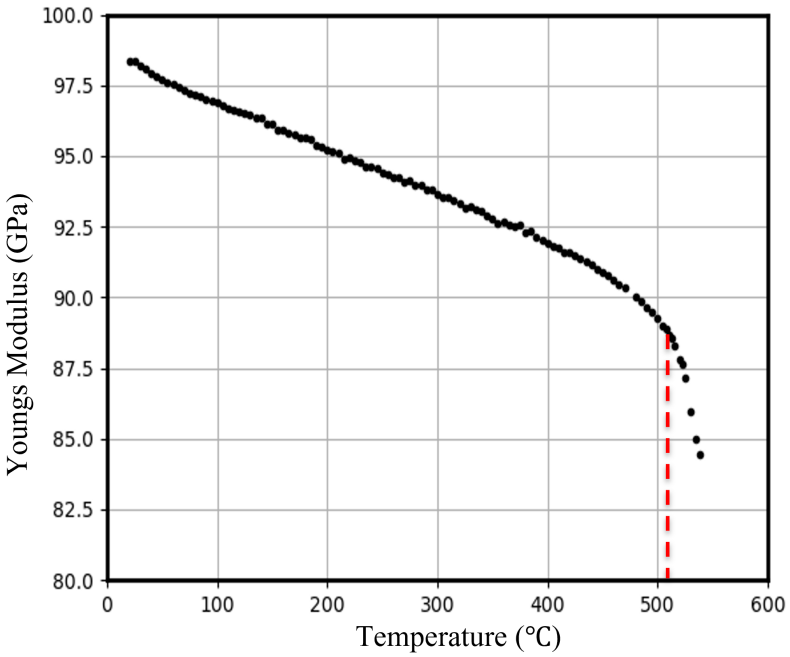

Figure 4.5: Change in Young's modulus with respect to temperature during the crawl test.

Figure 4.6 shows the change in Young's modulus with a change in temperature

from 480°C to 525°C. During the crawl test, Young's modulus at 480°C is observed to be about 91 GPa. Even when the glass sample is held at this temperature for hours, Young's modulus did not change any further. However, this is not the case at higher temperatures. When the sample temperature is increased from 480°C to 525°C using full power heating, the change in temperature takes about 2 min. However, the variation in Young's modulus does not synchronize with the temperature change, as shown in Fig. 4.6. After about 50 min, the modulus levels off at 84.5 GPa. The time needed to equilibrate the material reduces with the increase of either the starting temperature or the ending temperature. For the case of the temperature jump from 510°C to 525°C, the equilibration takes about 25 min, and the modulus changes from 87.5 to 84.5 GPa, as shown in Fig. 4.7. From 525°C to 540°C, the modulus reduces from 84.5 to 81 GPa in only 15 min, as shown in Fig. 4.8. If the specimen is cooled from 540°C to 525°C by flowing nitrogen, the modulus increases again from 81 to 84.5 GPa, as shown in Fig. 4.9. However, the relaxation process takes a shorter time as the initial temperature is high. As explained in Chapter 2, even with the same target temperature, the thermal history of the sample affects the relaxation process [11]. For comparison, the approach curve from 510°C to 525°C has also been added to Fig. 4.9. Even though both tests have the same target temperature and magnitude of temperature variation, the relaxation rate in the case of cooling is faster than that in heating.

To determine the structural relaxation parameters, the TNM model (Eq. 4.4) is fit to the experimental data obtained from the initial temperature step tests simultaneously. A non-linear curve fitting algorithm is used to obtain the fit parameters. The TNM model parameters for D-ZK3 glass are as follows: τ_o = 8.07e-09 , Δh = 24975.89, b = 0.66, and x = 0.34. The resulting theoretical curves for the different tests are as shown in Figs. 4.6 - 4.8, respectively, showing an excellent agreement. Further, to verify the fit parameters, the theoretically obtained is compared to the

experimental data obtained from 540°C to 525°C temperature jump test. Figure 4.9 shows a good agreement between the TNM model and the experimental data.

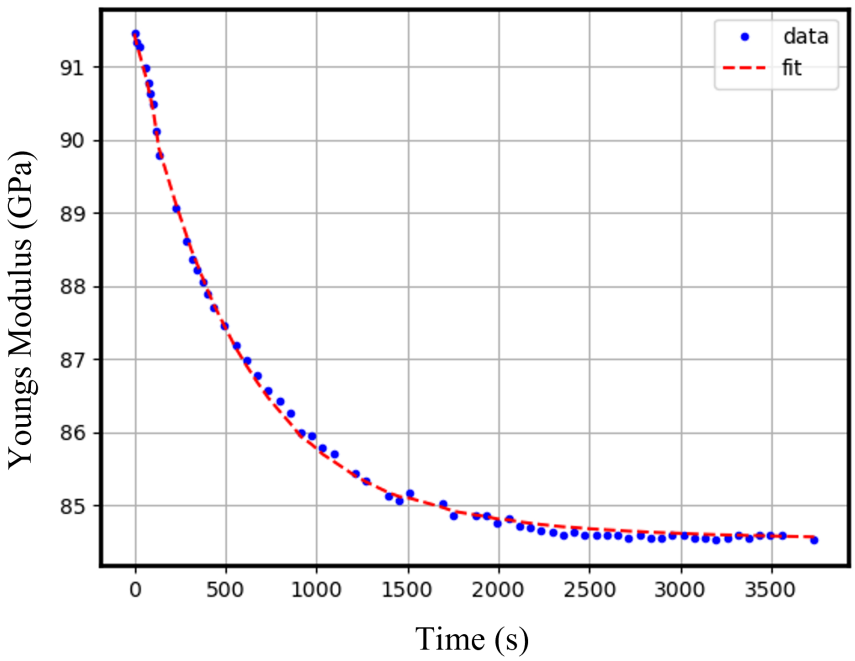

Figure 4.6: Change in Young's modulus with respect to time and the corresponding TNM model fit at a temperature jump from 480°C to 525°C.

4.4 Implementation of structural relaxation behavior in FE model

The structural relaxation of glass is implemented in the FE model by adding a time dependency to the thermal expansion coefficient. The coefficient of thermal expansion of a glass cooled through the transition region follows the path shown in Fig. 4.10. The expansion coefficient is constant when the glass is above or below the transition range. However, in between the transition region, when cooled, the expansion coefficient changes non-linearly depending on the cooling rate and the structural relaxation parameters. When the glass is above the transition region, the resulting thermal strain is given by Eq. 4.6

$$d\varepsilon_v = \alpha_L dT \tag{4.6}$$

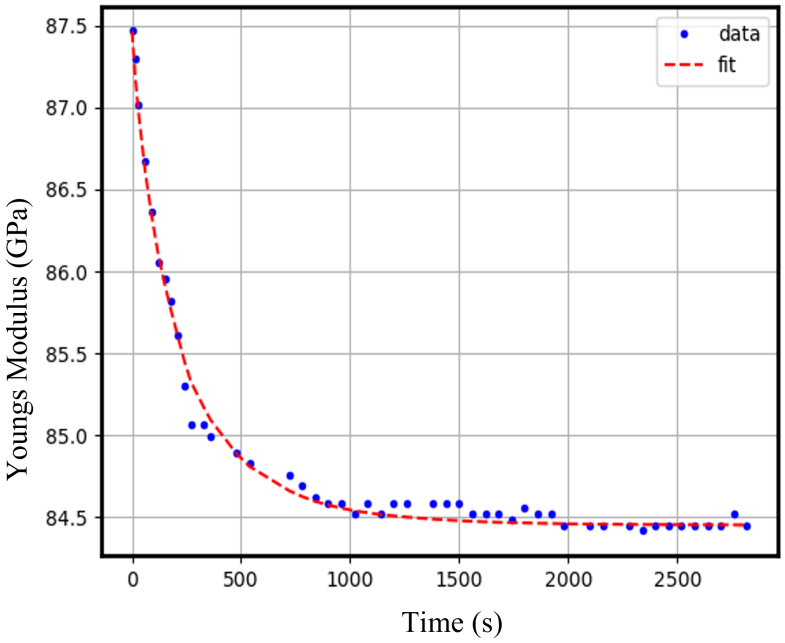

Figure 4.7: Change in Young's modulus with respect to time and the corresponding TNM model fit at a temperature jump from 510°C to 525°C.

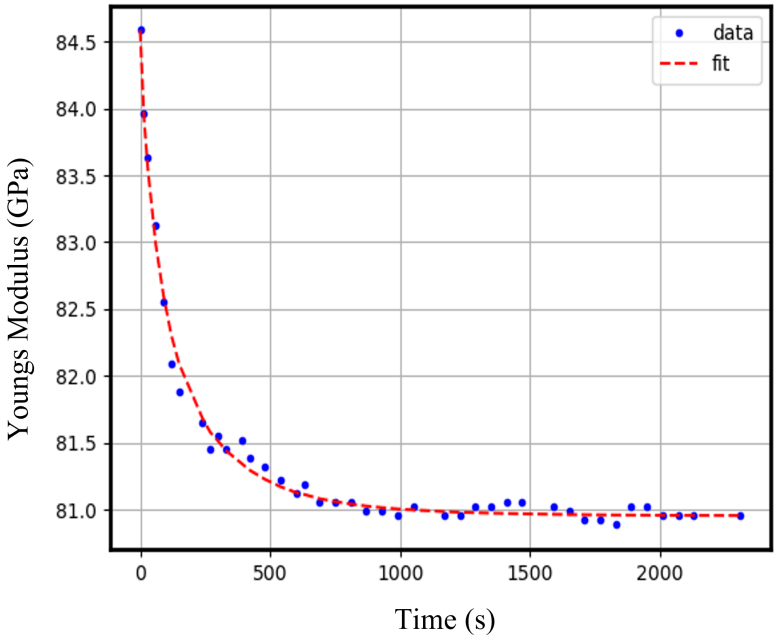

Figure 4.8: Change in Young's modulus with respect to time and the corresponding TNM model fit at a temperature jump from 525°C to 525°C.

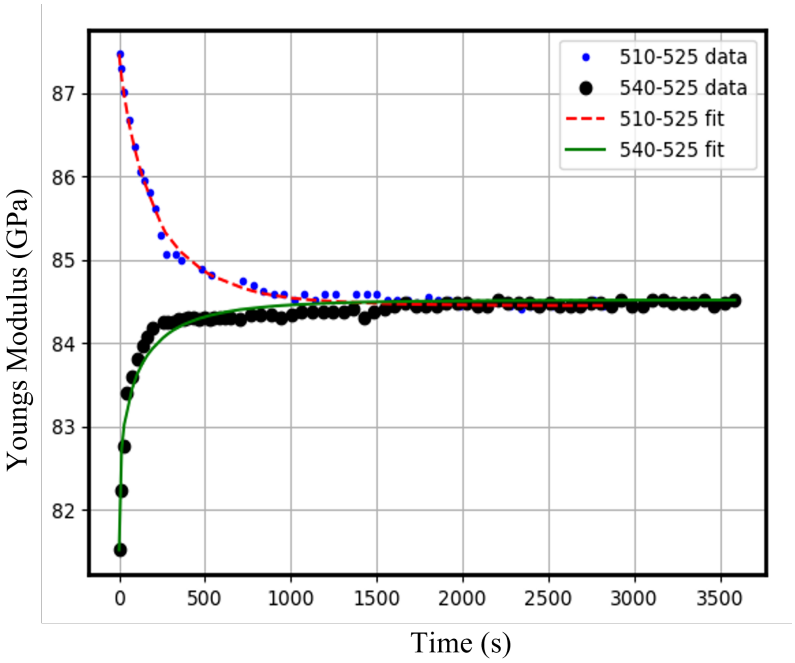

Figure 4.9: Change in Young's modulus with respect to time and the corresponding TNM model fit at a temperature jump from 510 °C and 540°C to 525°C.

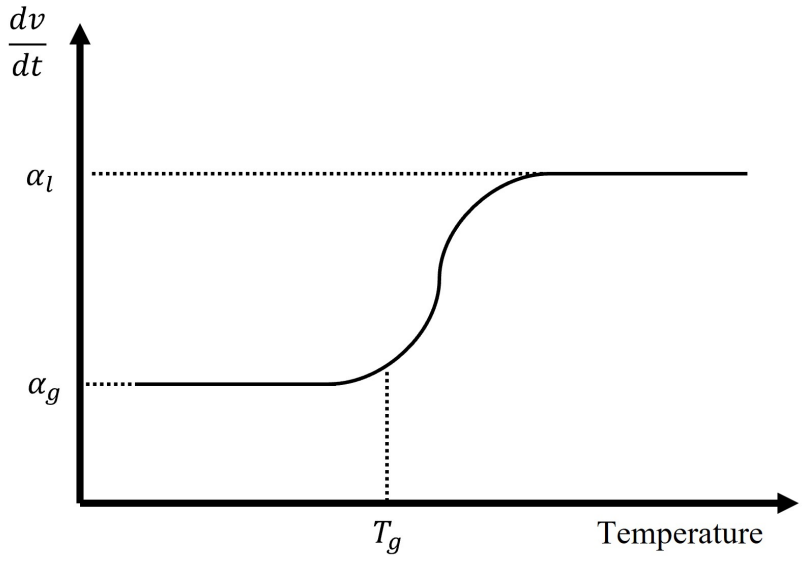

Figure 4.10: Coefficient of thermal expansion of glass cooled through transition region.

where α_L is the liquid thermal expansion coefficient. When the glass is below the transition region, i.e., solid or glassy state, the strain is given by Eq. 4.7

$$d\varepsilon_v = \alpha_G dT \tag{4.7}$$

where α_G is the solid thermal expansion coefficient. However, when the glass is the transition region, the strain is dependent on both the temperature and the fictive temperature, as shown below:

$$d\varepsilon_v = \alpha_G dT + (\alpha_L - \alpha_G) dT_f \tag{4.8}$$

where T_f is the fictive temperature given by the TNM model as described in Chapter 2.

A semi-implicit finite difference scheme provided by Moarvosky et al [49] is used to solve the TNM model (Eqs. 2.19-2.21) numerically to evaluate the fictive temperature, which is given by,

$$T_f(t) = \sum_{i=1}^{n} \frac{w_i \left(\tau_{p_i} * T_{f_i}(t - dt) + T(t)\Delta t\right)}{\tau_{p_i} + \Delta t} \tag{4.9}$$

$$\tau_{p_i} = \tau_{p_i ref} exp\left[-\frac{\Delta h}{R}\left(\frac{1}{T_r} - \frac{x}{T(t)} - \frac{1-x}{T_f(t-dt)}\right)\right] \tag{4.10}$$

where Δh, and x are the relaxation parameters, w_i, and $\tau_{p_i ref}$ are the weights and the relaxation times of the Prony series, respectively, obtained at a reference temperature T_r. The Prony series coefficients are obtained from the stretched exponential function form of the relaxation function calculated at the reference temperature, as given below:

$$M_p = exp\left[-\left(\frac{t}{\tau_p(T_r)}\right)^b\right] = \sum_{i=1}^{n} w_i exp\left(-\frac{t}{\tau_{p_i}}\right) \tag{4.11}$$

where w_i are the weights whose sum is equal to 1, and $\tau_p(T_r)$ is the structural relaxation time, given by Eq. 4.5, evaluated at the reference temperature T_r. The reference temperature is selected to be 50-100°C higher than the transition temperature of the glass. As at higher temperatures, the structural relaxation process is faster, and the

difference between the actual and fictive temperatures will be negligible [7,50]. Hence, by substituting $T_f = T_r$, Eq. 4.5 reduces to,

$$\tau_p(T_r) = \tau_o exp\left(\frac{\Delta h}{R * T_r}\right) \tag{4.12}$$

The structural relaxation behavior, given by Eqs. 4.6 - 4.12, is implemented in ABAQUS by using a user subroutine UEXPAN. A six-term Prony series is used to define the relaxation behavior by choosing a reference temperature of 600°C, which is well above the transition temperature of the glass (511°C) used in this study. The relaxation parameters and the Prony series coefficients used in this study are given in Table 4.1

4.5 Conclusions

In this study, the impulse excitation test is used to characterize the structural relaxation parameters of the glass material. The structural relaxation of the glass is modeled using the TNM model. Four different temperature jump tests are used to obtain and verify the TNM model parameters in this study. It was shown that the obtained model parameters accurately depict the structural relaxation response of the glass material. Finally, in this study, the material testing required for characterizing the glass material is designed to be implemented on the glass molding machine. This helps to streamline the development and testing of new glass materials that can be used in precision glass molding.

Table 4.1: Structural relaxation parameters used in the numerical model.

Solid expansion coefficient, α_G (10^{-6}/K)		9.3	
Liquid expansion coefficient, α_L (10^{-5}/K) [51]		3.3	
Activation energy, Δh		24975.89	
Nonlinearity parameter, x		0.34	
Relaxation function			
Stretched exponential		Prony series (T=600°C)	
b	τ_o	w_i	τ_i
0.66	$8.07e^{-09}$	0.0055	0.042
		0.279	30.562
		0.459	10.033
		0.001	1.006
		0.202	1.924
		0.003	0.631

CHAPTER 5: FINITE ELEMENT MODEL OF PRECISION GLASS MOLDING PROCESS AND MOLD COMPENSATION

5.1 Introduction

As stated previously, one of the major drawbacks of the precision glass molding process is the deviation of the lens profile at the end of the molding process. Generally, during the cooling cycle of the glass molding process, the mold tooling and the lens undergo thermal shrinkage. However, due to different thermal properties (typically, glass has a higher thermal expansion coefficient than molds), the profile of the glass lens tends to deviate from the mold shape, affecting the optical quality. To compensate for the deviations empirically, the mold surface profile is modified iteratively by trial and error until the desired lens profile is achieved. Often, this requires a few weeks to months of design iterations to manufacture the molds to meet the product specifications. On the other hand, numerical simulations provide a faster and more viable option to compensate the molds.

A review article by Brown [52] shows the research done in developing numerical models for glass pressing operations. The initial numerical models assumed the glass to be Newtonian viscous fluid and ignored the viscoelastic and structural relaxation characteristics [53–55]. Jain et al. [8, 17] used a finite element model with a standard linear solid (SLS) material model to represent the loading conditions and a single Maxwell model to represent the relaxation part of the molding process. They showed that the material model used in their study needs to be revised to model the molding process accurately. Later studies [7, 50, 56] used the generalized Maxwell model, a more accurate material model, to simulate the precision glass molding process. However, as stated previously, due to the complexity of the model and a high number

of fitting parameters, the models used in these studies are accurate only at the testing temperatures used in these studies.

As such, this chapter develops a finite element model to simulate the glass molding process by incorporating the material model developed in this study. The material properties obtained in previous chapters are used in the developed model to analyze the lens curve deviation. The experimentally obtained profile deviations are compared to the numerical simulation of a biconvex lens. Finally, a double-sided aspherical lens is numerically molded to analyze the profile deviations, and the molds are compensated accordingly.

5.2 Molding Process details and the molding machine

The Moore Nanotech precision glass molding machine (GPM170), as shown in Fig. 3.2, is used in this study to mold a biconvex lens made of D-ZK3 (CDGM) and P-SK57 (Schott) type glass. The process steps, the corresponding thermal profile, and the mold displacement during the molding process are shown in Fig. 5.1. It shows the different stages used in the precision glass molding process. Initially, the entire molding assembly is heated from 250°C to the molding temperature at 25°C/min. Typically, IR lamps heat the molding assembly in precision molding machines. However, the amount of heating power available is limited by the exposure of the molds to IR radiation during the molding process. Especially when the molds are close together during the pressing stage of the molding process, the lamps are turned off to prevent any damage to the mold tooling. This leads to temperature non-uniformity during the pressing stage. In this study, to maintain isothermal temperature conditions during molding, conductive-based platen heaters are used along with the lamps for molding the glass lens [37]. As shown in Fig. 5.2, the platen heaters are placed directly below the molds and constantly heat the molds throughout the molding cycle.

After isothermal conditions are achieved in the heating cycle, the glass preform is pressed into the final lens shape by applying a constant velocity to the top mold until

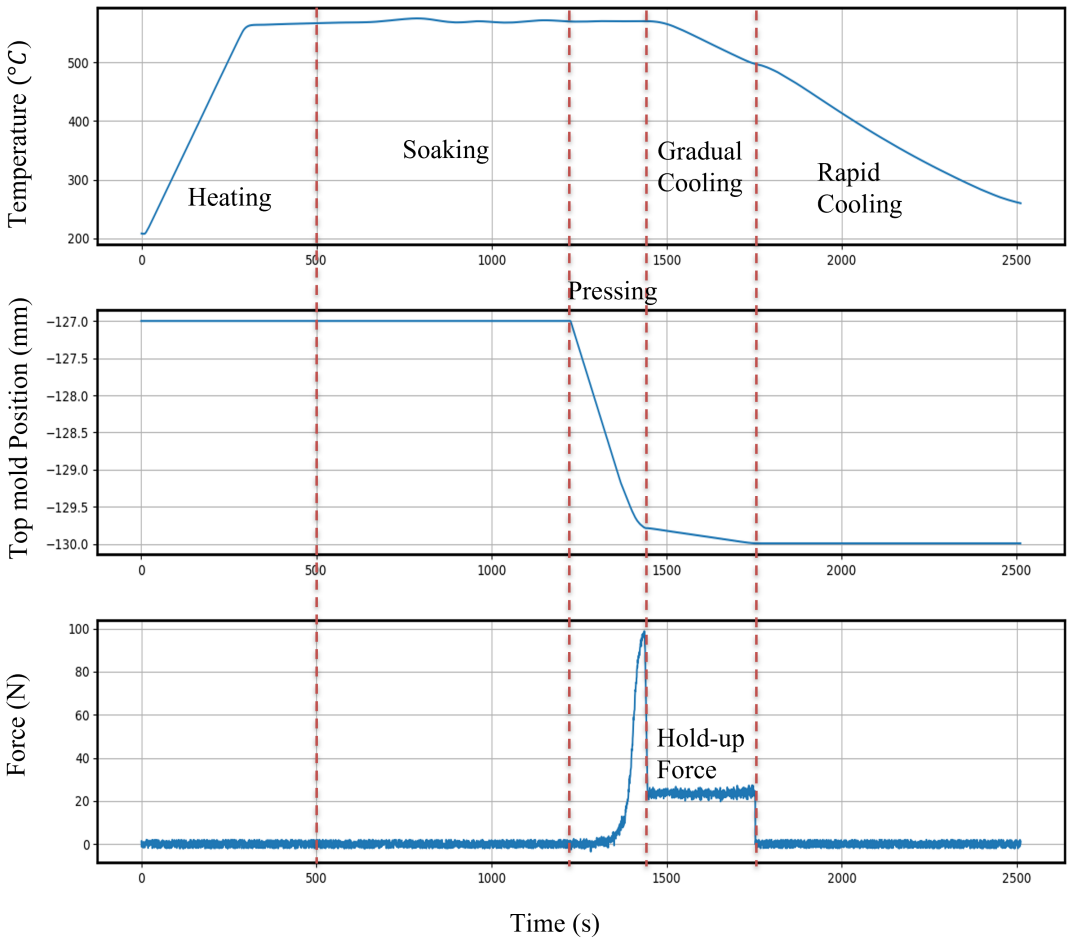

Figure 5.1: Process data from GPM170 molding machine (Nanotech), for a lens made of D-ZK3 at 570°C.

the desired center thickness is achieved. Then, the molding setup is gradually cooled by pumping nitrogen into the molding chamber. The nitrogen flow rate is controlled to achieve the desired cooling rate (25°C/min). During the gradual cooling step, the loading is switched from displacement controlled to force-controlled to apply a hold-up force of 30 N. The hold-up force helps to prevent any gross changes in the shape of the lens, as the glass is still above the transition temperature during the gradual cooling step. Finally, the top mold is displaced by about 0.15 mm from its current position, and the mold assembly is cooled to the release temperature at 75°C/min.

Typically, both the spherical and aspherical lens profiles are defined using the sag equation, given below

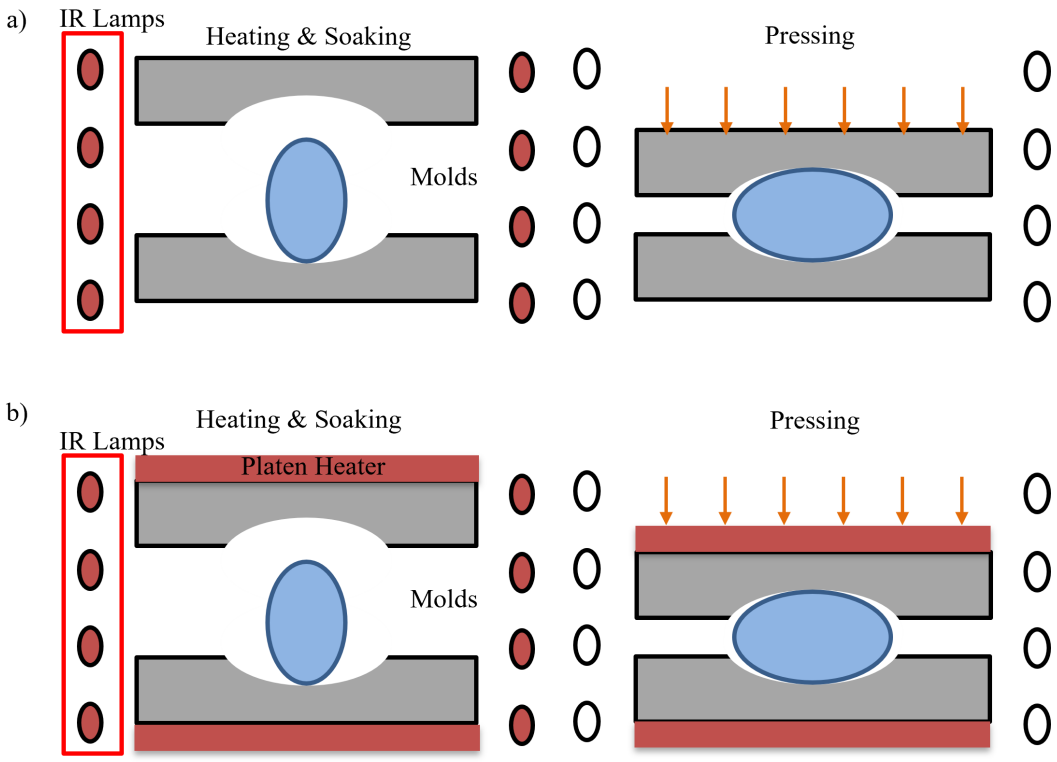

Figure 5.2: Molding process with a) only IR lamps, and b) IR lamps and platen heaters

$$z = \frac{x^2}{R\left(1+\sqrt{1-(1+k)\frac{x^2}{R^2}}\right)} + \sum_{i=1}^{n} A_{2i}x^{2i} \tag{5.1}$$

where x is the radial distance from the central axis, Z is the sag height, k is the conic constant, R is the radius of curvature, and A_{2i} are the aspheric coefficients. The first term on the right-hand side of Eq. 5.1 is the spherical term used to define the spherical surfaces. The aspherical surfaces are defined by adding the aspheric coefficients A_{2i}, to the spherical term. Initially, to compare the experimental and numerical results, spherical molds with an aperture diameter of 3.01 mm and a radius of curvature of 3 mm is used. The molds are as shown in Fig. 5.3.

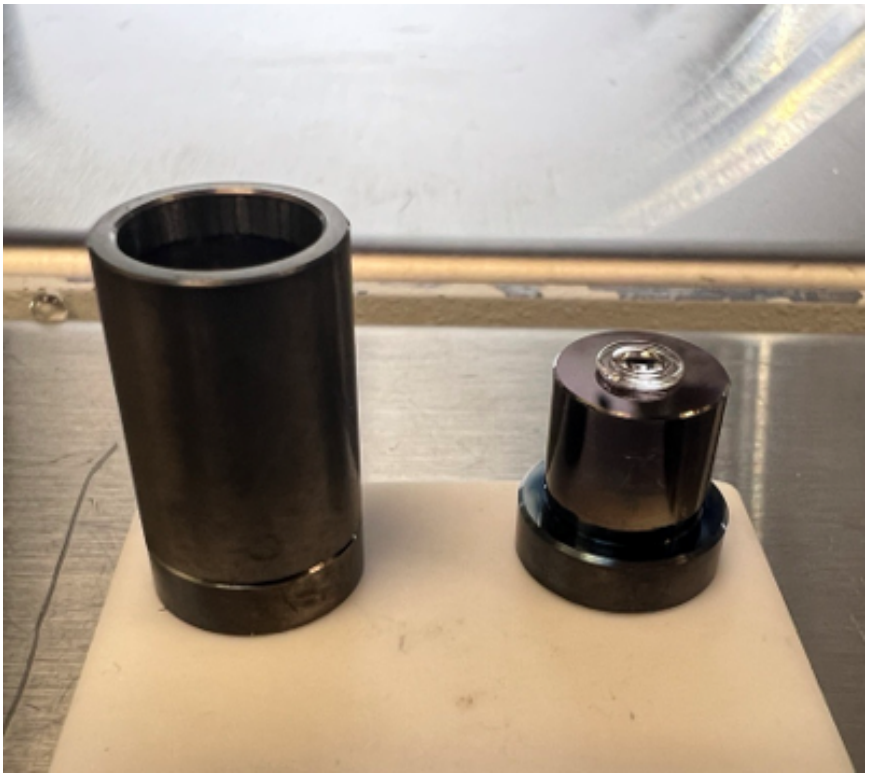

Figure 5.3: The biconvex molds used in the experiment.

5.3 Finite Element Model

Numerical simulations of the precision glass molding process are carried out using the commercially available finite element software ABAQUS/Standard [57]. Considering the geometry of the molds and the ball preform used in this study and the symmetry of the loading conditions, the process is simulated using an axisymmetric model. The molds are modeled as elastic components, while the glass is modeled as a viscoelastic material. The elastic and thermal properties used in the simulation are given in Table 3.1. The viscoelastic properties of the glass are incorporated into the model by defining a user-subroutine UMAT to include temperature-dependent viscoelasticity. Moreover, finally, the structural relaxation parameters are defined using a UEXPAN user subroutine in ABAQUS.

The different stages of the molding process are modeled as fully coupled temperature displacement analysis to simulate the thermal and mechanical aspects of the

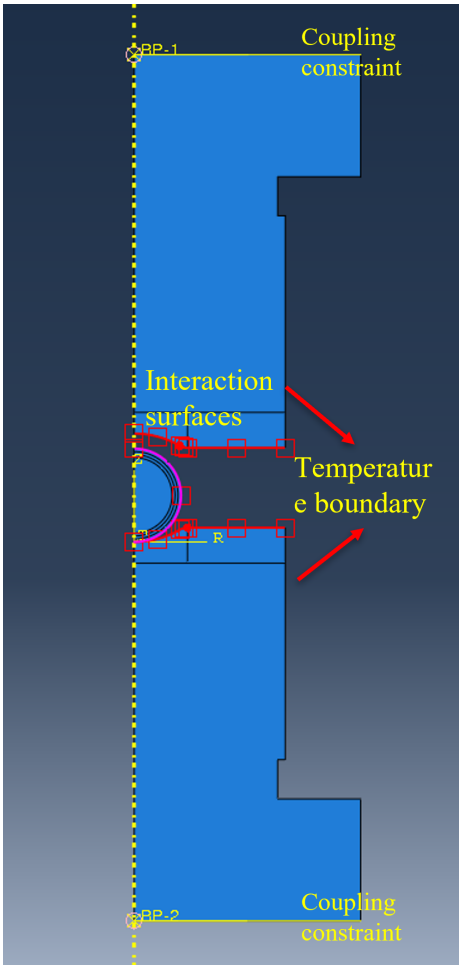

Figure 5.4: Finite element model

molding process. Assuming isothermal conditions during the molding process, the heating step is modeled as a steady-state analysis (time-independent), while the rest of the process steps (pressing, gradual cooling, and rapid cooling) are modeled as transient analysis to simulate the time-dependent material response. The initial geometry of the molds and the glass are as shown in Fig. 5.4. The upper and lower molds are meshed with 4600 and 4583 linear quadrilateral elements of type CAX4T, respectively, and the ball preform is discretized with 25,251 CAX4T elements. A refined mesh is used at the interface between the glass and the molds to better define the geometry of the mold surface (the spherical and radius segments of the mold surface) and the pressed lens, as shown in Fig. 5.5.

The interaction between the glass and the molds is defined using a surface-to-surface contact algorithm in ABAQUS. The mold surfaces are chosen as the main surface, and the outer edge of the ball preform is defined as the secondary surface in the contact definition, shown in Fig. 5.4. The normal behavior of the contact interface is defined using the hard contact formulation, and the tangential behavior is defined using the penalty contact algorithm with a friction coefficient of 0.05 in ABAQUS. Based on the model developed by Anathasam [7], heat transfer across the contact interface is also included. Finally, the mechanical boundary conditions are defined in the model by using two kinematic coupling constraints, one between a reference point (RF-1) and the top surface of the top mold and the other between a reference point (RF-2) and the bottom surface of the bottom mold, as shown in Fig. 5.4. However, in the definition of the coupling constraints, only the vertical degree of freedom of the mold surfaces is restricted to move along with that of their respective reference points. Gravity is also included in the model.

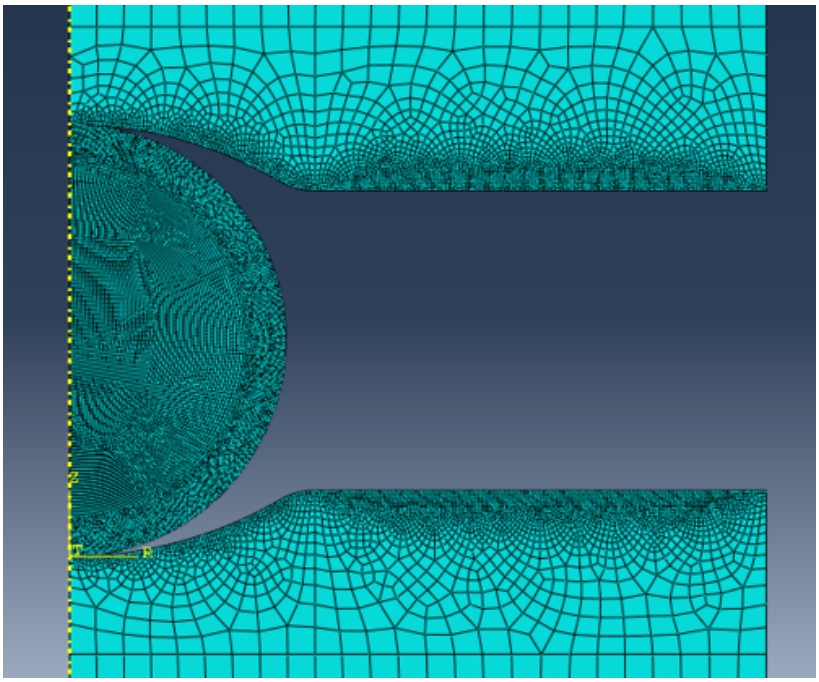

Figure 5.5: Finite element mesh

During the initial heating stage of the model, both the top and bottom molds

are fixed in their positions. In fact, the bottom mold is fixed at its initial position throughout the simulation. In the pressing step of the model, a constant velocity is applied on the top mold to deform the glass preform until the desired center thickness. During the gradual cooling cycle, the velocity boundary condition is switched to the force boundary condition, and a concentrated load (hold-up force) is applied to the top mold. Finally, the top mold is displaced by 0.15 mm in the opposite direction to simulate the release of the lens from the molds in the final step of the simulation. The temperature boundary conditions are defined on the outer edges of the mold, and the duration of the different stages is adjusted based on the cooling and loading rates used in the simulation.

5.4 Experimental vs. Numerical lens profile

A D-ZK3 glass gob of diameter 3.1 mm is molded into a biconvex lens at a molding temperature of 570°C on a GPM170 using the mold set shown in Fig. 5.3. The process data from the machine is shown in Fig. 5.1. A molding velocity of 1 mm/min is used during the pressing stage, and a hold-up force of 25N is applied during the gradual cooling cycle. The mold tooling, along with the pressed lens, is cooled from 570°C to 490°C at a cooling rate of 25°C/min during the gradual cooling cycle, and finally, the lens is cooled to the release temperature of 250°C at 50°C/min during the rapid cooling cycle. The temperature and force profiles from the experiment are defined as boundary conditions in the FEM model.

The experimental lens profile is measured using a profilometer, whereas the numerical lens profile is determined using the coordinates of the deformed FE mesh nodes at the end of the simulation. The deviation of the lens profile is calculated by subtracting the measured lens profiles from the surface of the original mold. The deviations measured numerically and experimentally with respect to the radius of the lens are depicted in Fig. 5.6. While the experimental and numerical deviations are comparable at the lens's center, the difference nears 0.15 μm at the lens's outer edge.

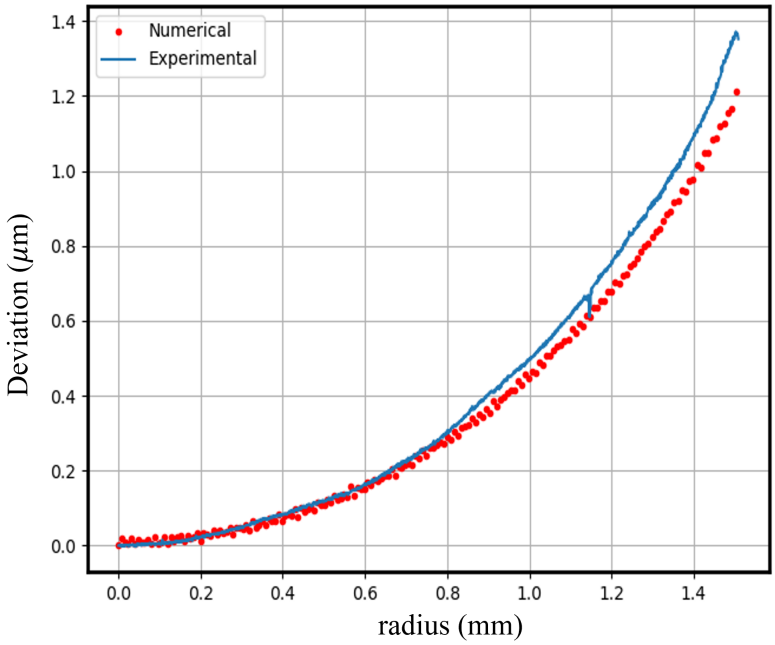

Figure 5.6: Experimental vs Numerical profile deviation.

The misalignment of the top and bottom molds in the experiments is the primary cause of the discrepancy between the simulation and the experimental data. It was observed that, in the molding experiments the decentration between the top and bottom mold is around 0.2 mm. The experimental mold misalignment contradicts the axisymmetric assumptions used in the simulation and also results in a lens of poor quality. Therefore, the mold tooling must be correctly aligned before any additional experiments can be conducted.

5.5 Double Aspheric Lens

The numerical model developed in this chapter is utilized to simulate the molding process for a D-ZK3 glass double aspheric lens. The sag equation (Eq. 5.1) is used to define the mold profiles. The spherical term of the sag equation contains the following constants: for the bottom mold, a radius of curvature of 5.9 and a conic constant of -10; and for the top mold, a radius of curvature of -8.895 and a conic constant of -1.420. The aspherical coefficients of the upper and lower molds are shown in the

Table 5.1. The required center thickness of the lens is set to 0.8 mm. The glass is formed with a molding velocity of 1 mm/min, a progressive cooling rate of 25°C/min, and a hold-up force of approximately 4 N, 10 N, and 22 N at a molding temperature of 570°C, 560°C, and 570°C, respectively. To minimize additional lens deformation during the gradual cooling phase and to meet center thickness requirements, it was necessary to vary the hold-up force at the different temperatures.

Table 5.1: Asphere lens profile parameters.

Aspheric Coefficients	Bottom Profile	Top Profile
A_2	0.06718649	-0.0137811255
A_4	-0.011428	0.0419097220
A_6	-0.05311931	-0.1069610314
A_8	0.06260547	0.1301152752
A_{10}	-0.05230059	-0.0768102593
A_{12}	0.03178715	0.0248841417
A_{14}	-0.01241399	-0.0042105655
A_{16}	0.002695199	0.0002883259
A_{18}	-0.000242262	-

Figures 5.7a and 5.7b depict the deviation of the bottom and top profiles of the molded lens at various molding temperatures, respectively. The maximum profile deviation of the bottom and upper surfaces is observed at a molding temperature of 550°C. In addition, irrespective of the molding temperature, the magnitude of the deviation increased as the distance from the lens center increased.

5.6 Mold compensation

In order to compensate the molds for the form deviation, the lens profile at a molding temperature of 550°C is considered. The deformed lens profile obtained by molding on the original molds is initially fitted to the sag equation given by Eq. 5.1.

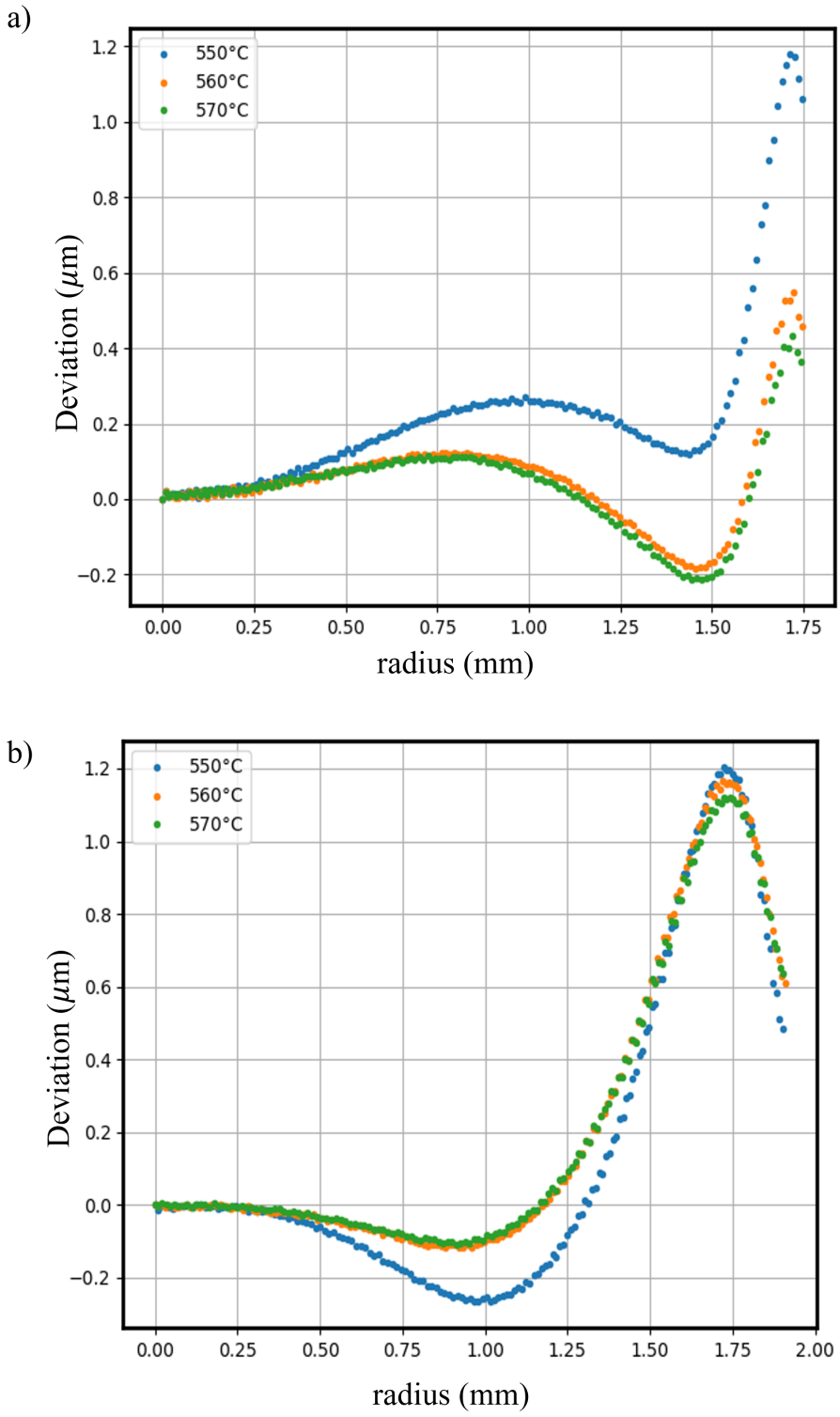

Figure 5.7: Double aspheric lens profile deviation a) Bottom profile, and b) Top profile.

In the curve fitting process, it is presumed that the spherical terms of the sag equation are equivalent to those of the mold profile, and only the aspherical coefficients are used in the curve fit. The aspherical coefficients (A_{cm}) of the compensated mold are given by Eq. 5.2.

$$A_{cm} = A_{om} + (A_{om} - A_d) \tag{5.2}$$

where A_{om} are the aspherical coefficients of the original mold, and A_d, are the curve fit aspherical coefficients of the deformed lens. The aspherical coefficients of the original mold, the deformed lens, and the compensated mold, for the bottom and top profiles are as given in Table 5.2 and Table 5.3, respectively.

Table 5.2: Aspherical coefficients of compensated bottom mold.

Aspheric Coefficients	Original Mold	Deformed Lens	Compensated Mold
A_2	0.06718649	0.06785004	0.06652293
A_4	-0.011428	-0.01249589	-0.01036010
A_6	-0.05311931	-0.05073405	-0.05550457
A_8	0.06260547	0.05882566	0.06638528
A_{10}	-0.05230059	-0.04909461	-0.05550657
A_{12}	0.03178715	0.03037483	0.03319947
A_{14}	-0.01241399	-0.01214345	-0.01268452
A_{16}	0.002695199	0.00269505	0.00269535
A_{18}	-0.000242262	-0.00024681	-0.00023770

Figures 5.8a and 5.8b show the deviation in the bottom and top profile, respectively, before and after molding compensation. The form error (peak-to-valley) of the deviations in the molded lens has been reduced from 1.2 μm to 0.13 μm in the bottom lens surface and from 1.43 μm to 0.11 μm in the top surface.

Table 5.3: Aspherical coefficients of compensated top mold.

Aspheric Coefficients	Original Mold	Deformed Lens	Compensated Mold
A_2	-0.0137811255	-0.01393081	-0.01363144
A_4	0.0419097220	0.04162174	0.042197700
A_6	-0.1069610314	-0.10785713	-0.10606493
A_8	0.1301152752	0.13259938	0.12763117
A_{10}	-0.0768102593	-0.07895323	-0.07466728
A_{12}	0.0248841417	0.02578786	0.02398042
A_{14}	-0.0042105655	-0.00439848	-0.00402265
A_{16}	0.0002883259	0.00030358	0.00027306

5.7 Conclusions

This study simulates the precision glass manufacturing process using an axisymmetric finite element model. Using the D-ZK3 glass material, a bi-convex lens is formed, and the derived lens profile deviations are compared to the experimentally formed lens. The numerical profile resembles the experimental lens profile in the center but deviates toward the lens periphery. In the experimental arrangement, the misalignment of the molds is the cause of the error. In addition, the model is used to simulate the molding process of a double aspheric lens at various molding temperatures. Using a mold compensation technique, the mold surfaces are modified to account for deviations in the lens profile. The profile deviations of the lenses produced with the modified molds were significantly reduced. However, it is observed that as the molding temperature decreased, the deviation between the top and bottom lens profiles increased. This demonstrates that appropriate molding parameters must be determined before mold compensation techniques can be implemented.

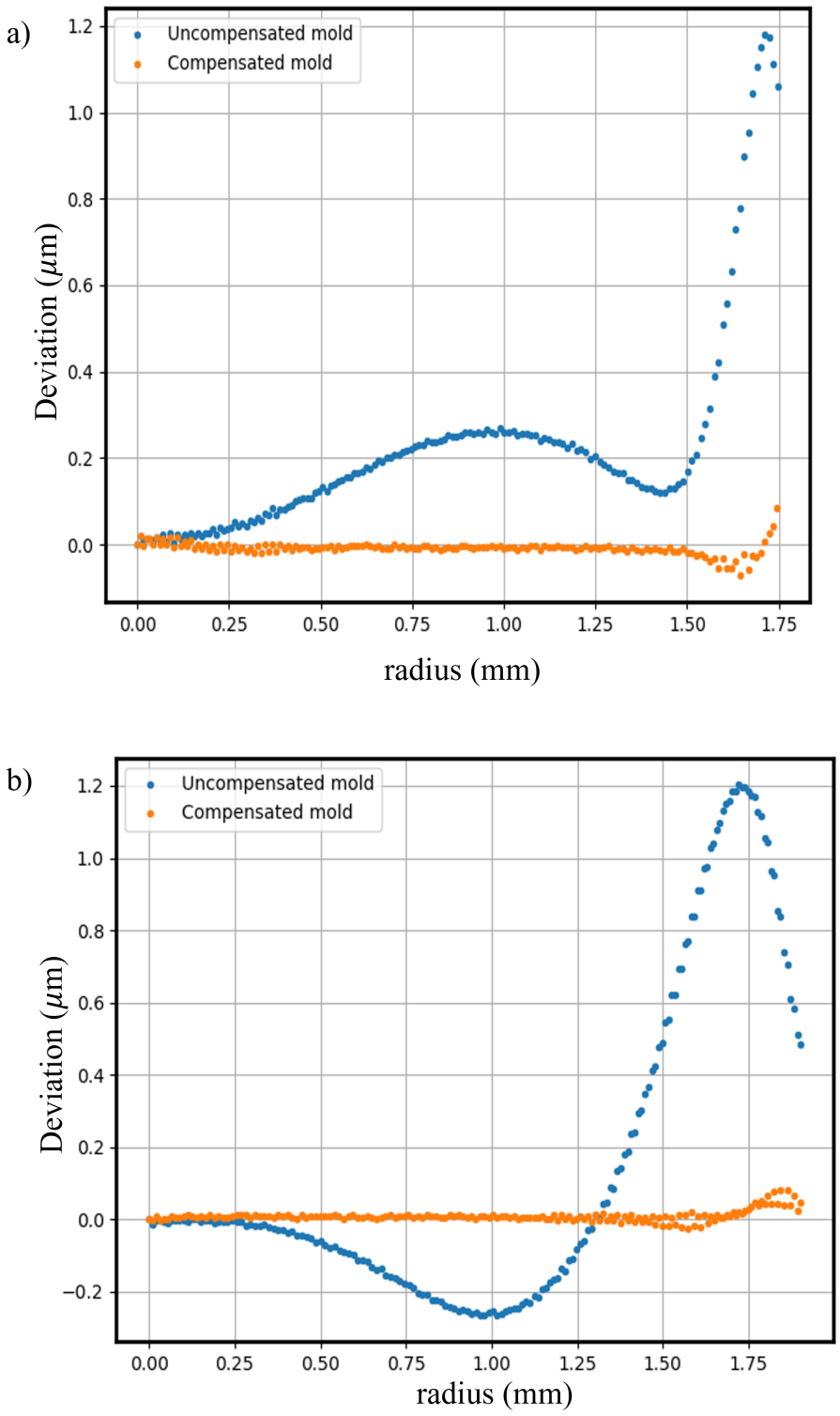

Figure 5.8: Profile deviations before and after mold compensation a) Bottom profile, and b) Top profile.

CHAPTER 6: SELECTION OF PROCESS PARAMETERS IN PRECISION GLASS MOLDING PROCESS

6.1 Introduction

The precision glass molding process involves several process parameters, and the proper selection of these parameters plays a vital role in achieving the required profile accuracy as well as the optical quality of the molded lens. Empirically, the parameters of the molding process are altered by trial and error until the desired center of the thickness (CT) of the glass lens is achieved. However, due to the complex and obscure nature of the molding process, it often takes weeks or months of process development to meet the dimensional requirements. Nevertheless, fulfilling the required dimensional specifications does not necessarily equate to high optical quality. As seen in the previous chapter, various parameter sets used for molding the lens may provide the required center thickness but will result in lenses with varying optical quality. Hence it is imperative to study the mechanism of different process parameters and develop a sustainable technique to realize Industry 4.0 of the precision glass molding process.

A few empirical evaluations of the effect of process parameters on the glass molding process have been published in the literature. The early studies were limited to analyzing the influence of molding temperature on the molding process [58,59]. Waqas [60] was the first to use the design of experiments using a three-level approach to obtain a parameter set with minimum cycle time and better repeatability. Cha et al. [61] investigated the influence of a few molding process parameters on aspheric glass lenses experimentally. The influence of the parameters on the peak-to-valley form error was investigated using a two-level strategy. Gleason et al. [62] analyzed

the effect of various process parameters on the center thickness of the molded lens using the design of experiments. They had to reduce the number of process parameters from seven to four in order to better interpret the results of the DOE. In their initial DOE, they utilized two glass types, N-BK7 and L-BAL35, and concluded that the influence of glass type (within a glass family) on the final thickness of molded optic is negligible. Although the experimental studies provided some useful insights into the effects of glass molding parameters, their scope and interpretation of the effects of individual molding process parameters were limited.

In contrast, precise numerical simulations provide a cost-effective, in-depth analysis of the molding process and aid in minimizing issues throughout the precision glass molding manufacturing process. Zhou et al. [63] used a finite element model to analyze the sensitivity of various process parameters on the profile deviation of the molded lens. The results indicated that the cooling rate has no effect on the profile deviation, whereas increasing the hold-up force decreased the magnitude of the deviation. A similar analysis was used by Kejun et al. [64] to examine the effect of process parameters on the curve deviation of a double aspheric lens. Contrary to the findings of Zhou et al. [63], Tao et al. [65] analyzed the residual stresses in the molded lens at various cooling rates and demonstrated that the residual stresses increased as the cooling rate increased, while the profile deviations decreased. Although numerical models are shown to be able to predict the deviations of the molded lens in the precision glass molding process, the lack of proper material characterization at different molding temperatures and a proper understanding of the influence of various process steps and their parameters has led to contradictory conclusions in the literature.

In this chapter, the finite element model and the material parameters derived in this study are used to conduct an in-depth analysis of the effect of various process parameters on the curve deviation and residual stresses for two distinct glass materials. On the basis of the observations, a novel molding process is proposed to reduce the

influence of molding parameters on the curve deviation and residual stresses in the molded lens. In addition, the molding process devised in this chapter significantly reduces the total cycle time of the molding process.

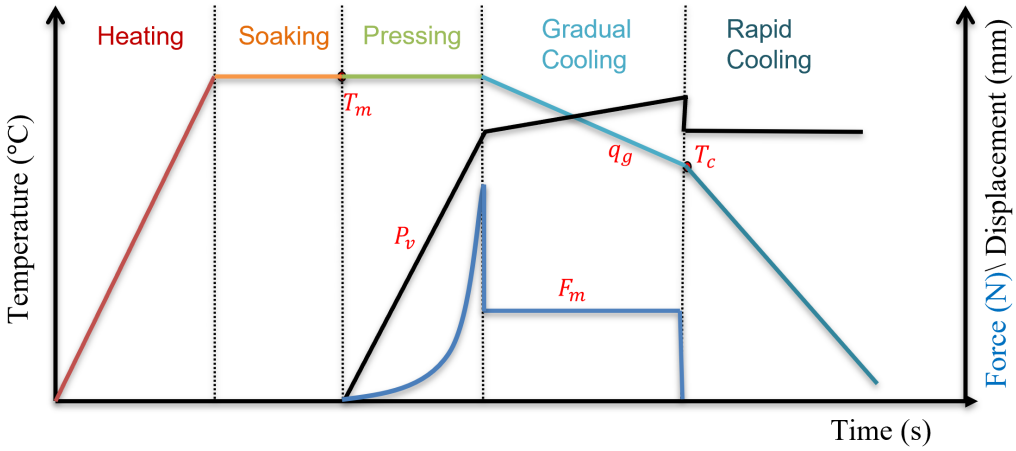

Figure 6.1: Process parameters in precision glass molding process.

6.2 Overview of the Molding Process

Historically, the molding process consisted of five stages, as depicted in Fig. 6.1: Heating, soaking, pressing, Gradual cooling, and rapid cooling. During the heating and soaking phase, the glass sample is heated from room temperature to molding temperature and held at that temperature for a predetermined amount of time. Proper selection of heating and soaking periods is essential for achieving a uniform sample temperature. However, once the isothermal conditions are established and maintained throughout the molding cycle, the heating and soaking parameters will have no effect on the lens's deviations or residual stresses. Therefore, once the effect of other process parameters has been determined, it is simple to empirically optimize the heating and soaking cycles. As such, the heating and soaking stages of the molding process are not considered for parameter optimization. Similarly, during the rapid cooling stage of the molding process, the pressed lens is cooled from the annealing temperature to the release temperature or room temperature. Below the annealing temperature,

glass can be regarded as an elastic solid [11], and the cooling rates employed during this step have no influence on the deviation or residual stresses. And therefore, the rapid cooling rate is considered to be constant in this study.

Figure 6.1 identifies the process parameters in the pressing and the gradual cooling stages of the molding process. The parameters are as follows: molding temperature (T_m), molding velocity (P_v), gradual cooling rate (q_g), and the hold-up force (F_m). Zhou et al. [63] demonstrated that the annealing temperature (T_c) has a negligible influence on the curve deviation if it is set below the transition point of the glass. Typically, the annealing point can be optimized to reduce the gradual cooling step time. However, in this study, the temperature at the end of the gradual cooling phase is set to the annealing temperature of the glass (viscosity of 14 Pa-s), which is approximately 470°C for both the glasses analyzed.

6.3 Issues with Hold-up Force

A force is applied to the molded lens in the annealing stage of the molding process to help to maintain the shape of the lens as it is cooled below the annealing point. The magnitude of the force required is highly dependent on the molding temperature and the gradual cooling rate used during the molding process. As illustrated in Fig. 6.2, if the magnitude is too large, the lens is further deformed during the annealing step, and if it is too small, the molded lens shrinks significantly. Typically, if the molding temperatures are close to the transition point of the glass [21, 63], a higher magnitude force can be applied without further deforming the molded lens. However, if molding temperatures well above the transition temperature are used, the force required might be on the order of a few Newtons to milliNewtons depending on the size of the optic. And applying forces of such low magnitude on a typical glass press molding machine is unrealistic.

Due to the aforementioned limitations, the hold-up force is substituted by displacement-controlled unloading during the annealing phase in this study. To release the lens

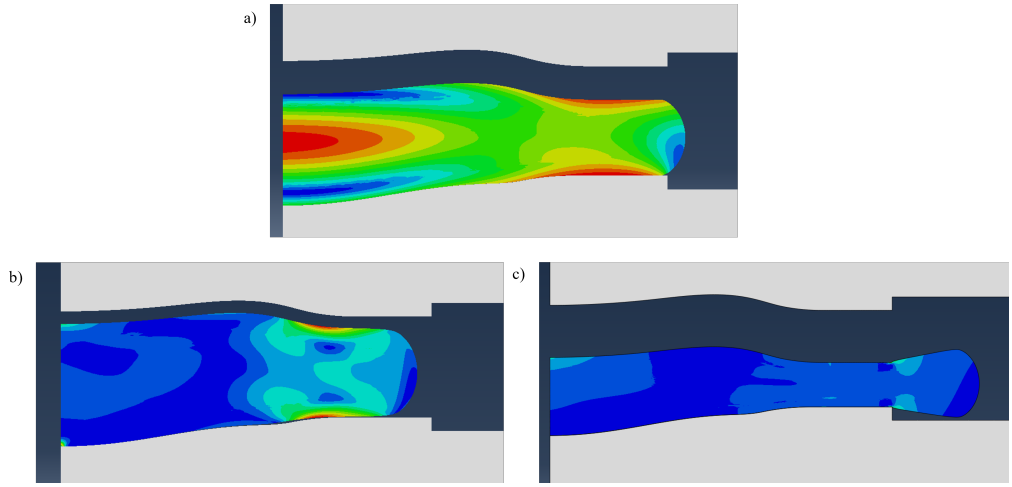

Figure 6.2: The final profile of the lens when molded with a) appropriate hold-up force, b) low hold-up force, and c) excessive hold-up force.

during the annealing phase, the top mold is retracted from the molded lens at a predetermined speed, designated as the release velocity in this study. The effect of the release velocity on the curve deviation and the residual stresses will be addressed during the course of this chapter.

6.4 Influence of Molding Step Parameters

The double aspheric lens described in the preceding chapter is used in this section to analyze the influence of the compression stage parameters on the curve deviation and the residual stresses. For this purpose, the cooling rate during the annealing phase is set to 25°C/min, and the top mold release velocity is set to 0.2 mm/min. It should be noted that the center thickness of the molded lens is maintained at 0.8 mm in all the simulations in this study.

6.4.1 Effect of viscoelastic material properties

In order to compare the influence of viscoelastic properties of the two glass materials used in this study, the viscosity of the glass is chosen as the control parameter as opposed to the molding temperature. As observed in Chapter 3, the viscosity-temperature curve of each glass material is distinct. Therefore, selecting a molding

viscosity rather than a molding temperature normalizes the impact of the glass material. [62]. Typically, in precision glass molding, a molding viscosity between $10^{8.0}$ - $10^{6.8}$ Pa.s is recommended to reduce the forces required during the molding process [66]. As such, in this investigation the viscosity range of $10^{8.0}$ - $10^{6.8}$ Pa.s is utilized. The molding viscosity and the corresponding molding temperature of D-ZK3 and P-SK57 glass are as given in Table 6.1.

Table 6.1: Temperature of different materials at similar viscosity.

Log(η) Pa.s	8.0	7.8	7.6	7.4	7.2	7.0	6.8
D-ZK3 (°C)	560.814	565.188	569.686	574.311	579.07	583.012	589.012
P-SK57 (°C)	561.904	566.86	572.012	577.373	582.954	588.771	594.838

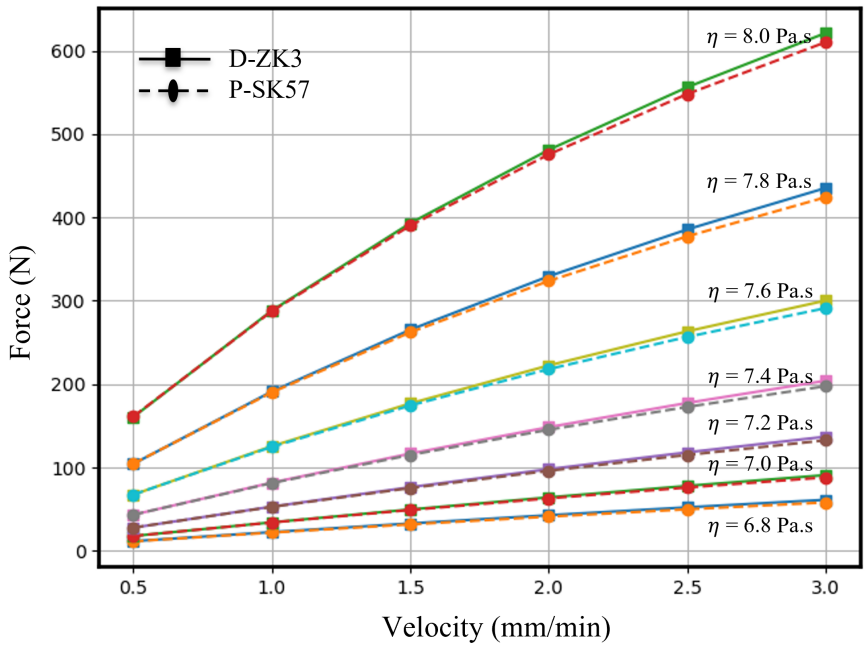

Figure 6.3: Maximum force at the end of the pressing cycle.

The double aspherical lens is molded using the two materials at each molding viscosity given in Table 6.1. At each viscosity, molding velocities ranging from 0.5 mm/min to 3.0 mm/min are used to form the final shape of the lens. Figure 6.3 shows the maximum reaction force at the end of the pressing step for both the materials

at different viscosity and molding velocities. It is observed that when subjected to similar molding conditions, the viscoelastic response of both materials is similar. In fact, looking back at Chapter 3, despite the distinct temperature response of the two glasses, their Burgers parameters at similar viscosity are identical. A similar observation was made by Gleason et al. [62] in their initial design of experiments between L-BAL35 and N-BK7 glass. The materials used in this study and by Gleason et al. [62] are members of the same family of oxide glasses, with only minor variations in modifier concentrations. As such, using viscosity as a control parameter in the molding process normalizes the effect of glass material (for oxide glasses). And thus, the optimized molding process parameters will be similar between different materials. Hence, for further analysis of different parameters, only P-SK57 glass is considered.

6.4.2 Effect of molding viscosity

The pressing velocity is set to 1.5 mm/min in order to examine the influence of molding viscosity on the curve deviation of the lens. Figures 6.4a and 6.4b illustrate the deviation in the bottom and top profile of the double aspheric lens for various viscosities. The maximal deviation of the bottom and top profiles tends to increase as the viscosity increases from $10^{6.8}$ Pa.s to $10^{8.0}$ Pa.s (i.e. as the molding temperature decreases). Figure 6.5 illustrates the form error (peak-to-valley, PV) of the deviations at various viscosities. The form error increased from approximately one micron to 7.8 μm for the bottom profile and from 1.5 μm to 4.7 μm for the top profile. Although the results indicate that selecting a lower viscosity is advantageous, this can often contribute to high molding temperatures depending on the type of glass (e.g., for BK7, around 700°C), resulting in a longer process time and glass-to-mold sticking issues [67].

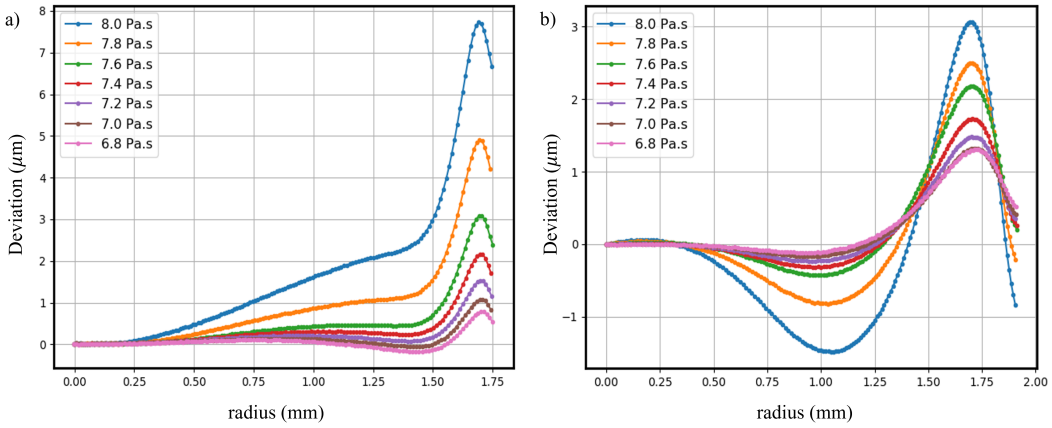

Figure 6.4: Effect of molding viscosity on profile deviation a) Bottom profile, and b) Top profile.

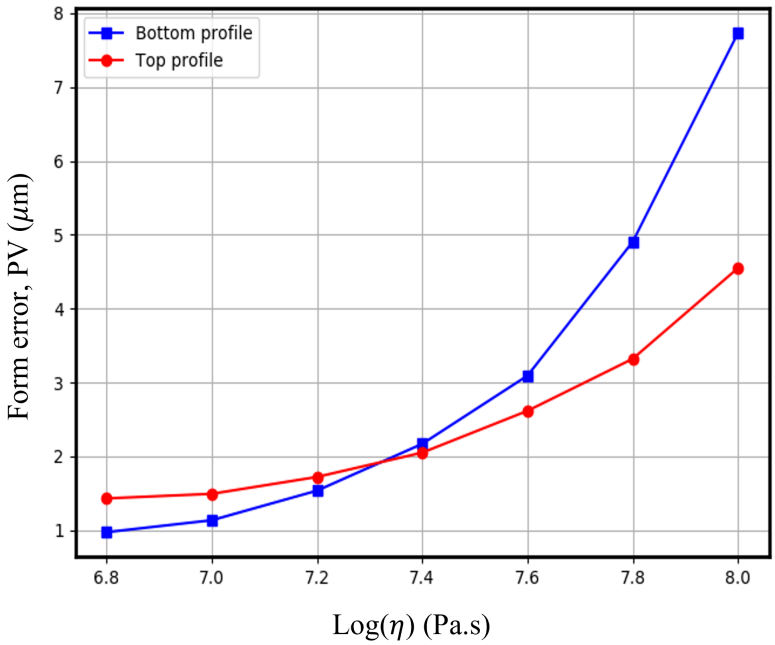

Figure 6.5: Form error of the molded lens at different viscosities.

6.4.3 Effect of molding velocity

To analyze the effect of molding velocity on the curve deviation of the molded lens, the molding viscosity is set to $10^{7.6}$ Pa.s. Figure 6.6a and 6.6b depict, respectively, the deviation in the bottom and upper profiles of the molded lens at various velocities. As the molding velocity was increased from 0.5 mm/min to 3.0 mm/min, the deviation

of the bottom and upper profiles increased. Figure 6.7 shows the form error (PV) of the deviations at different velocities. The form error increased from 1.3 μm to 5.4 μm on the bottom profile, and it increased from 1.57 μm to 3.57μm on the top profile as the molding velocities increased.

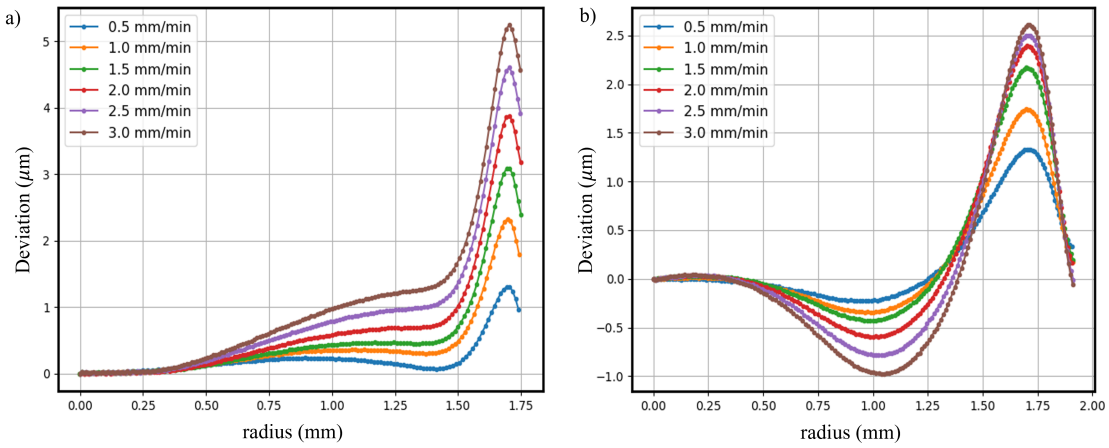

Figure 6.6: Effect of molding velocity on profile deviation a) Bottom profile, and b) Top profile.

6.5 Stress Relaxation in Molded Lens

As demonstrated in Section 6.3, employing a lower molding viscosity and molding velocity will reduce profile deviation and improve the lens' optical quality. However, as previously mentioned, using a reduced viscosity may result in higher molding temperatures (depending on the type of glass; for BK7 glass, around 700°C) and longer molding process times (increased heating and soaking time). Similarly, choosing a slower molding speed will also prolong the pressing step time required to achieve the specified center thickness of the molded lens. Therefore, in order to attain optimal lens quality and reduce manufacturing cycle time, it is essential to comprehend the lens deviation mechanism in the molded lens.

Generally, in the glass molding process, the lens tends to deviate from the mold profile during the gradual cooling step of the manufacturing process due to thermal shrinkage and the relaxation of the residual stresses induced during the pressing stage.

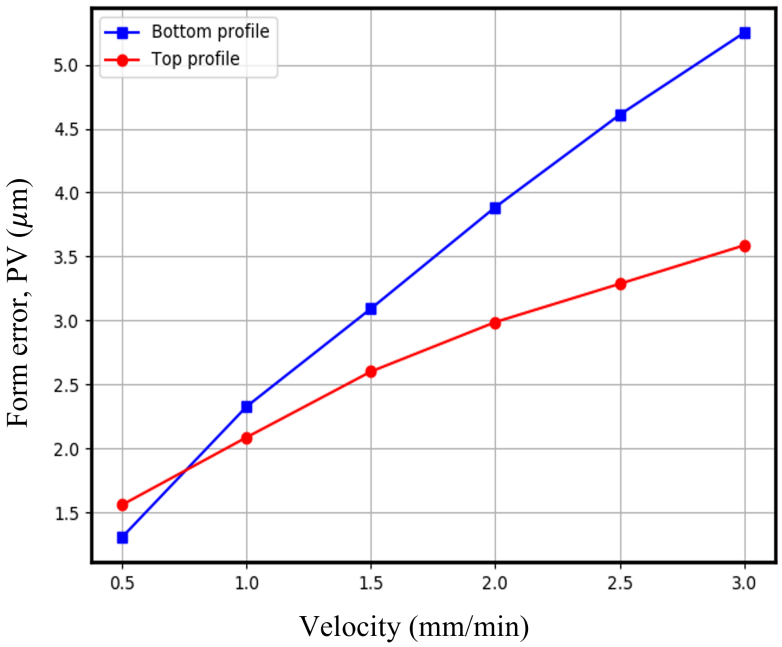

Figure 6.7: Form error of the molded lens at different molding velocities.

The deviation of the lens profile due to thermal shrinkage is a material characteristic that can only be eliminated through mold compensation. However, the deviation due to the relaxation of residual stresses is a property of the process parameters and can be minimized or even avoided by the proper selection of the molding parameters. As such, analyzing the stress profiles in the molded lens during the pressing and gradual cooling step will help to optimize the molding process.

Figures 6.8a and 6.8b shows the Mises stress distribution in the molded lens at a molding viscosity of $10^{8.0}$ Pa.s and $10^{6.8}$ Pa.s, respectively, at the end of the pressing stage and the gradual cooling stage. During the pressing stage, in both instances, the stresses that are induced into the lens by the end of the pressing stage are completely relaxed by the end of the gradual cooling stage. A similar stress distribution is observed at varied molding viscosities and velocities used in this study. However, the magnitude of the stresses increased as the molding viscosity or the molding velocity increased. Figures 6.9 and 6.10 depict the change in the maximum Mises stress in the lens during the pressing and gradual cooling steps with different viscosities and

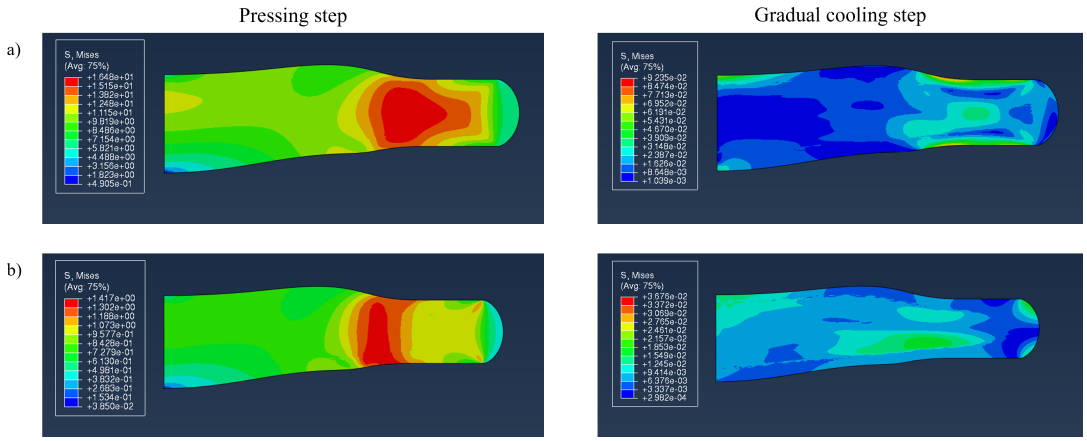

Figure 6.8: Stress distribution in the molded lens at the end of pressing and gradual cooling step a) at a viscosity of 10^8 Pa.s and b) at a viscosity of $10^{6.8}$ Pa.s.

velocities, respectively. It is observed that the magnitude of deviation in the lens profile is directly proportional to the magnitude of the stress at the commencement of the gradual cooling phase. For example, the test case with a viscosity of $10^{7.4}$ Pa.s and velocity of 1.5 mm/min has a maximum stress of 4.92 MPa with a form error of 2.16 μm and 2.04 μm in the bottom and top profiles respectively. Similarly, in the test case with a viscosity of $10^{7.6}$ Pa.s and velocity of 1 mm/min has a maximum stress of 5.33 MPa with a form error of 2.32 μm and 2.08 μm in the bottom and top profiles respectively. This indicates that minimizing the stresses at the end of the pressing phase will minimize the deviation in the molded lens.

As seen in Chapter 3, the stresses in the glass can be minimized by using the constant strain approach. To that extent, a relaxation step is incorporated between the pressing and gradual cooling stages of the molding process. During the relaxation phase, the molding temperature is held constant. It is evident from stress relaxation experimental data that the stresses relax quicker at higher temperatures. As such, relaxing the glass at the molding temperature rather than during the gradual cooling phase should take a reduced period of time. However, adding a relaxation step to the process might increase the total manufacturing time, it might enable the use of faster cooling rates during the gradual cooling phase without any adverse effects on the

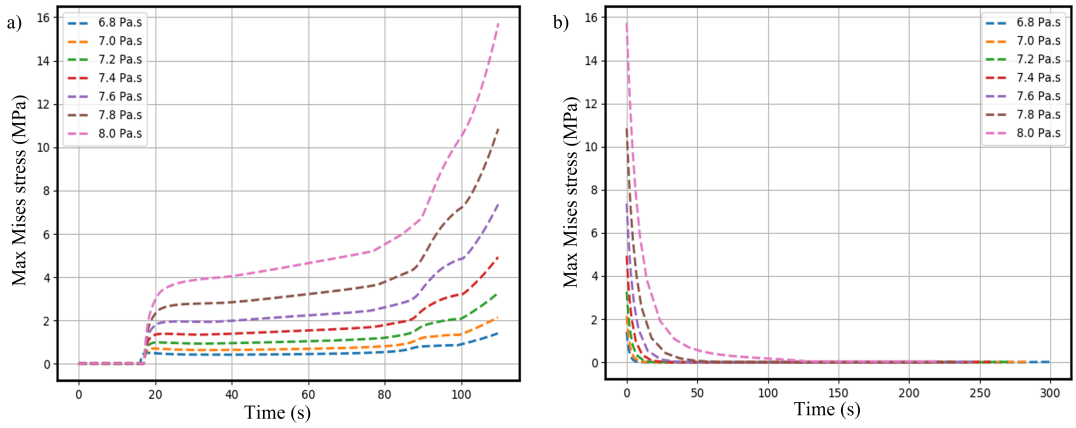

Figure 6.9: Maximum Mises stress in the molded lens at different viscosities a) Pressing step b) Gradual cooling step.

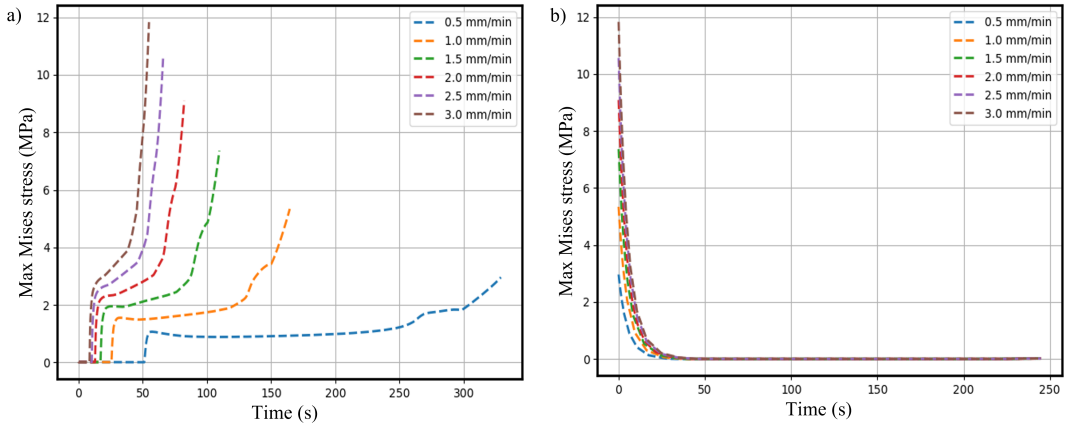

Figure 6.10: Maximum Mises stress in the molded lens at different velocities a) Pressing step b) Gradual cooling step.

optical quality. To implement the constant strain conditions during the relaxation phase, the top mold is held in position for a specific duration depending on the molding viscosity.

The simulations used in Section 6.3.2 and Section 6.3.3 are repeated by adding a relaxation phase to the molding process. Figure 6.11 shows the form error in the profile deviation at various viscosities with and without the relaxation step. It is observed that with the modified molding process, the molding viscosity has no influence on the profile deviation. The form error on the bottom profile is around 0.6 μm and 1.2 μm on the top profile at different molding viscosities used in this

investigation. Similarly, Fig. 6.12 depicts the form error in the profile deviation of the molded lens at different molding velocities before and after modifying the molding process. Similar to viscosity, molding velocity has no influence on the profile deviation with the modified molding process. As such, by adding a relaxation phase to the molding process, any influence of the pressing step parameters is eliminated.

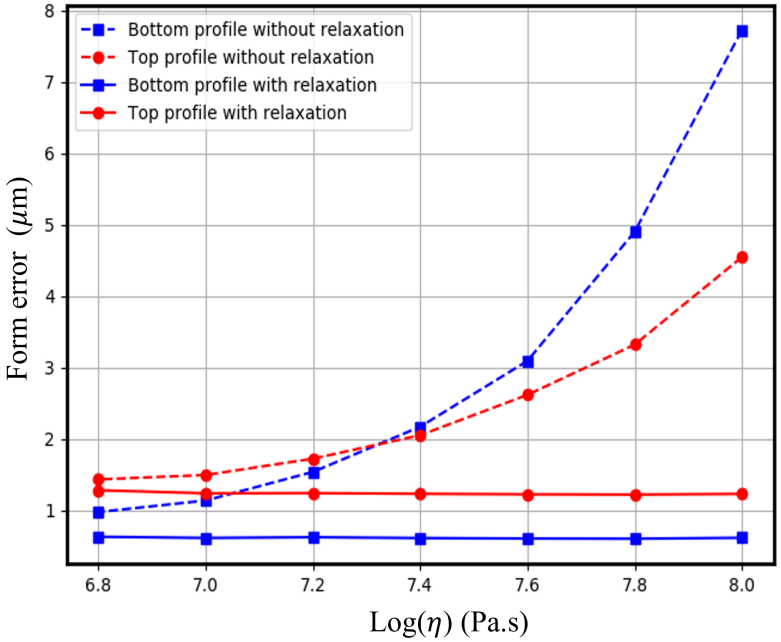

Figure 6.11: Form error (PV) vs molding viscosity in the top and bottom lens profile with and without relaxation.

6.6 Influence of Gradual Cooling Parameters

The modified molding process, i.e., with the relaxation step, is used to analyze the influence of the release velocity and the cooling rate applied during the gradual cooling stage of the molding process. Since the pressing step parameters have no effect, a molding viscosity of $10^{7.6}$ Pa.s and a molding velocity of 3.0 mm/min are used in the simulations. The rapid cooling rate is set to 70°C/min

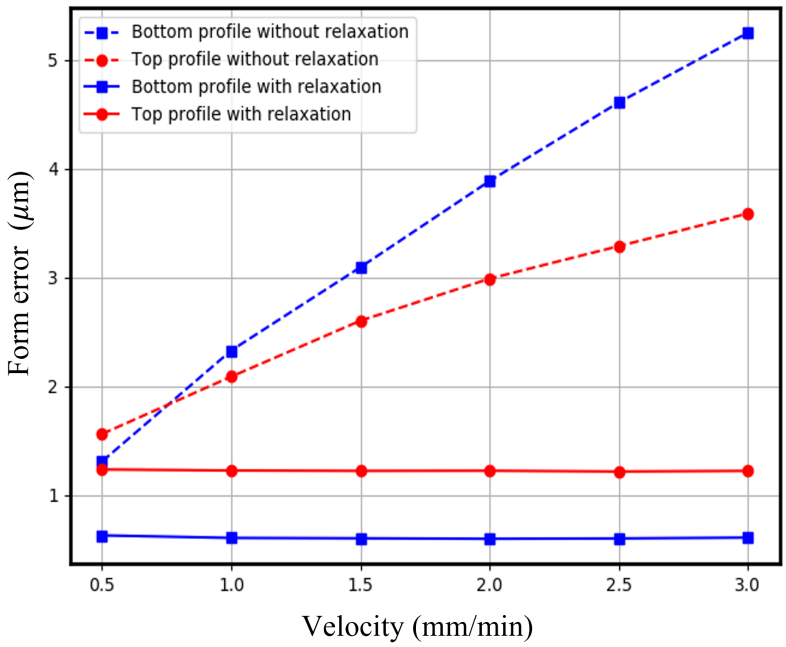

Figure 6.12: Form error (PV) vs molding velocity in the top and bottom lens profile with and without relaxation.

6.6.1 Effect of Release Velocity

To investigate the effect of release velocity on the profile deviation, the gradual cooling rate is set to 25°C/min. The release velocities used are as follows, 0.2, 0.5, 1.0, 1.5, 2.0, 2.5, and 3.0 mm/min. Figure 6.13 shows the form error remained the same in both the bottom and top profiles of the molded lens at various release velocities. It should be noted that the center thickness of the molded lens is approximately 0.8 mm (the required CT), even when the top mold is removed swiftly from the lens. This shows that the commonly used hold-up force during the gradual cooling stage is not necessary if the stresses in the molded lens are relaxed prior to the cooling phase.

6.6.2 Effect of Gradual Cooling rate

To study the influence of gradual cooling rate on the profile deviation on the profile deviation, a release velocity of 3 mm/min is used in the simulations. Cooling rates of 5, 10, 20, 40, 70, and 100°C/min are used in the analysis. Figure 6.14 shows the form

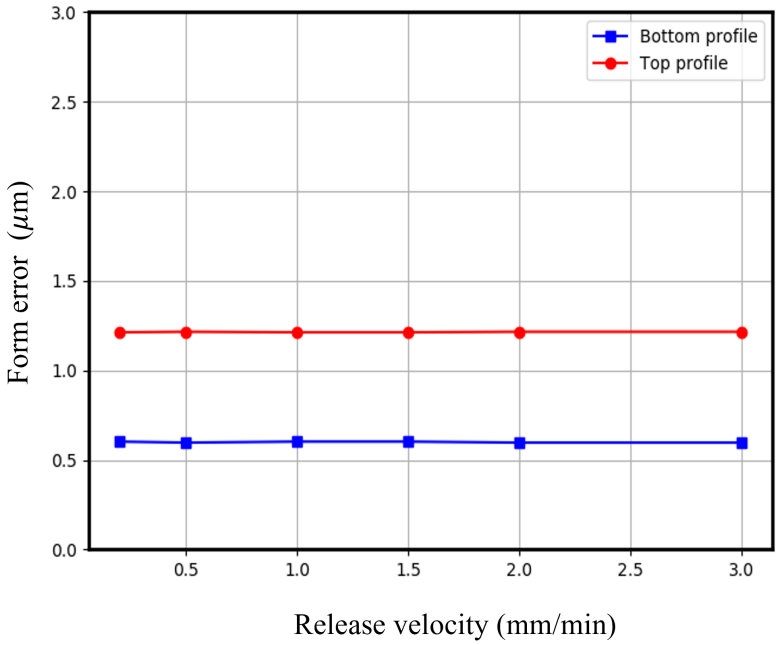

Figure 6.13: Form error (PV) of the molded lens at different release velocities.

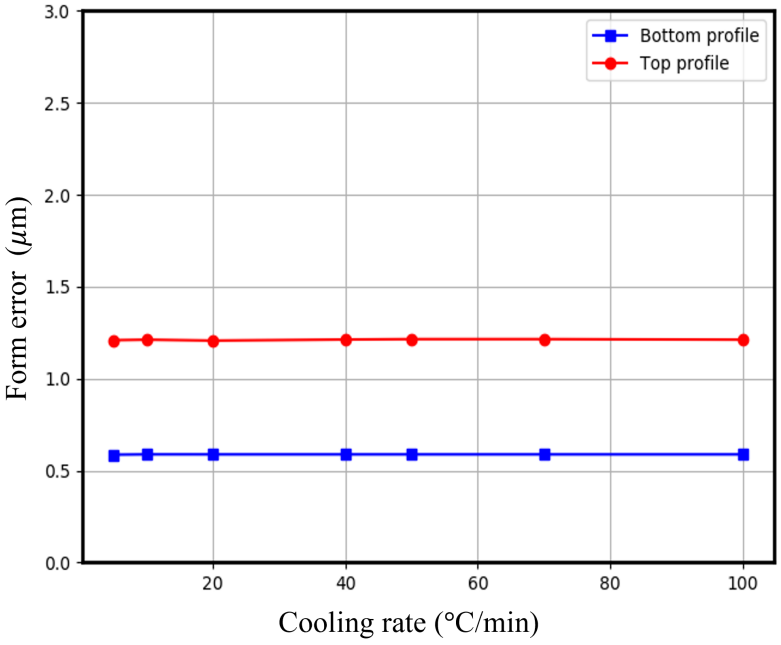

Figure 6.14: Form error (PV) of the molded lens at different gradual cooling rates.

error in the top and bottom profiles at various gradual cooling rates. It is observed that the cooling rate had no effect on the profile deviation with the inclusion of a relaxation phase in the molding process.

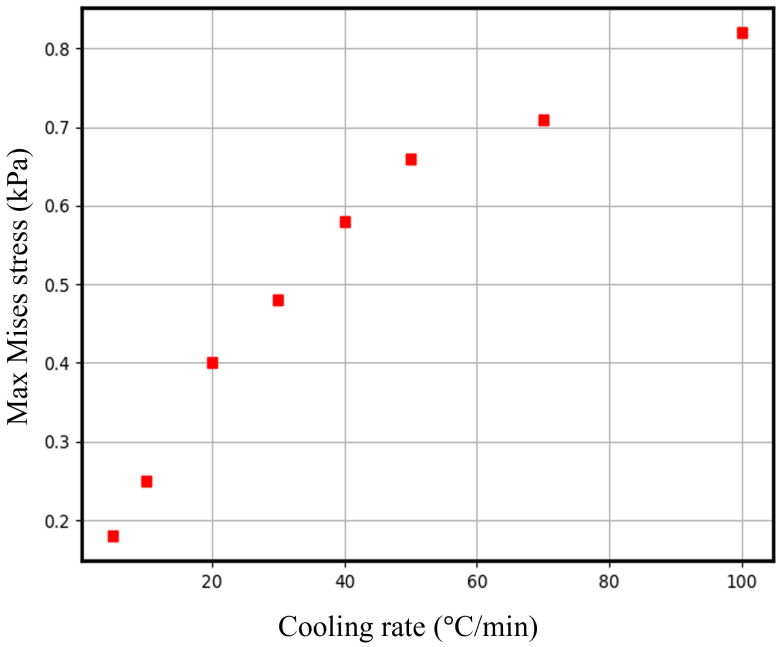

Figure 6.15: Maximum residual stress in the molded lens at different gradual cooling rates.

Figure 6.15 shows the maximum Mises stress in the molded lens at the end of the molding process. As observed, the magnitude of the stress increased with an increase in the cooling rate. However, even with a higher cooling rate of 100°C/min, the residual stress in the molded glass is below 1 kPa, considered to be negligible to affect the optical quality of the molded lens [68].

6.7 Effect of Friction Coefficient

Finally, the modified molding process is used to analyze the effect of the friction coefficient between the glass and the mold interface. The molding viscosity is set to $10^{7.6}$ Pa.s, molding velocity of 3 mm/min, release velocity of 3 mm/min, and gradual cooling rate of 25°C/min are used in the analysis. Figure 6.16 shows the effect of friction coefficient on the form error of the molded lens. As the friction coefficient increased, the stresses in the molded lens increased during the pressing step, increasing the relaxation time. But similar to the response of molding viscosity or the molding velocity, if the stresses are relaxed completely before cooling the molded lens, the

friction coefficient has no effect on the lens quality.

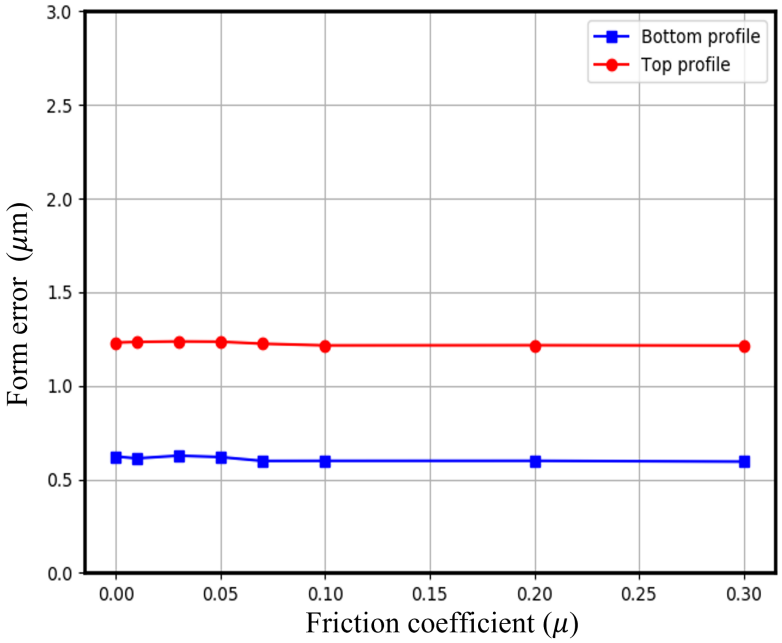

Figure 6.16: Form error (PV) vs friction coefficient in the top and bottom lens profile with and without relaxation.

6.8 Conventional vs Modified Molding Process

Based on the observations in this study, it is evident that by using a distinct relaxation phase in the molding process, both the pressing and gradual cooling steps have no adverse effects on the molded lens. As such, to shorten the total molding cycle time, the conventionally used two-step cooling process is consolidated into a single rapid cooling step. Figure 6.17 shows the temperature profile with respect to time using the conventional versus the proposed molding process. The parameters in both simulations are selected such that the deviations and residual stresses in the molded lens profile are comparable. In both cases, a P-SK57 glass sample is molded into a double aspheric lens at a molding viscosity of $10^{8.0}$ Pa.s, with a molding velocity of 3.0 mm/min. In the conventional process, the pressing step is followed by a gradual cooling step with a cooling rate of 10°C/min and a hold-up force of 20N. In the modified process, the glass is relaxed for a minute and then rapidly cooled with a

cooling rate of 70°C/min. The rapid cooling rate is the same in both cases. As observed, in both cases, the heating and pressing time remained but by eliminating the gradual cooling phase, the total process time was reduced significantly, thereby decreasing the production cost of a single molded lens.

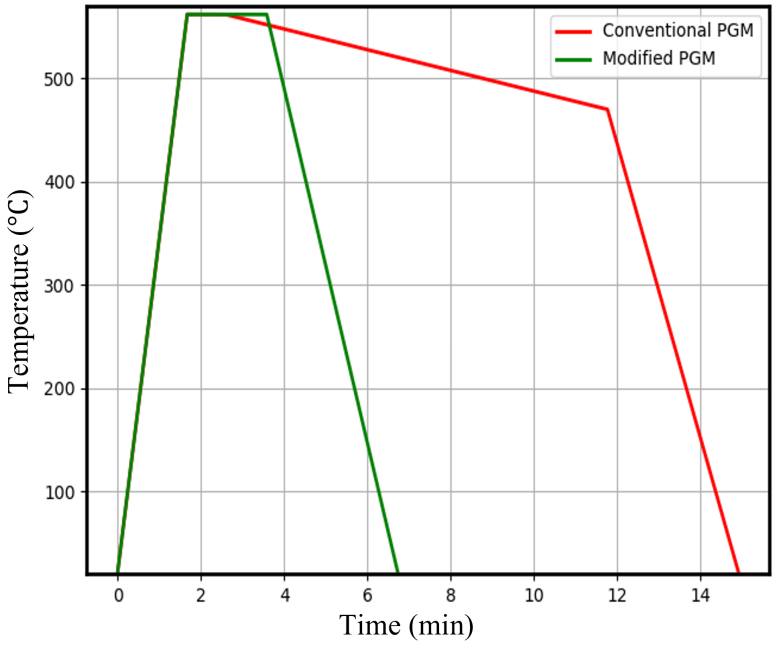

Figure 6.17: Temperature profile with respect to cycle time in a conventional vs modified molding process.

Figure 6.18 shows the profile deviation in P-SK57 and D-ZK3 double aspherical lens. It is observed that deviations in D-ZK3 are slightly higher than that of the P-SK57 glass type under similar molding conditions. While the stress relaxation parameters are similar for both materials at similar molding viscosity, the structural relaxation parameters (i.e., the volume expansion) differ for both materials. As such, the deviations observed in the lens profile using the modified molding process are solely dependent on the volume expansion of the glass material.

6.9 Conclusion

The selection of process parameters in precision glass manufacturing has a significant impact on the optical quality and profile deviation of the molded lens. In this

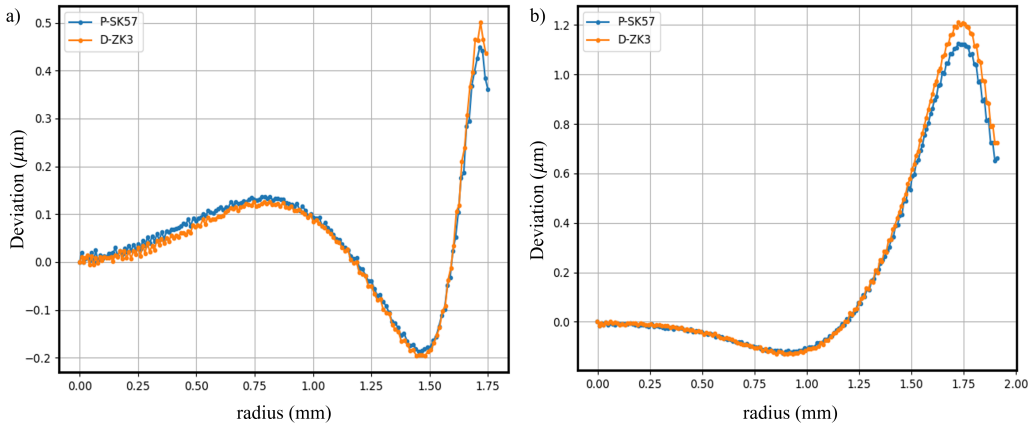

Figure 6.18: Profile deviation in different glass materials under similar molding conditions a) bottom profile and b) top profile

study, the developed numerical model is utilized to examine the effect of molding parameters on profile deviation and residual stresses. It was observed that using molding viscosity as a control parameter instead of molding temperature normalizes the influence of viscoelastic material properties on the molding process. Based on the observations in this study, a modified molding process is proposed to minimize the influence of various process parameters on the lens's profile deviation and residual stresses. This study demonstrates that the modified molding process reduces molding cycle time by more than 50% compared to the conventional molding process.

CHAPTER 7: CONCLUSIONS AND FUTURE WORK

7.1 Conclusions

The precision glass molding process provides several advantages over conventional glass manufacturing techniques by enabling the production of intricate and precise glass components with close tolerances. It has been demonstrated to be a cost-effective method for producing glass components, as it eliminates the need for post-processing stages such as grinding and polishing. Despite its numerous benefits, the technique's application is constrained by a few drawbacks, such as lens profile deviations and the lack of clarity regarding the impact of the involved process parameters on the optical quality of the molded lens. Typically, manufacturing a new lens design or producing a lens with a different glass material can require several months of process development in order to achieve the required optical quality. As such, the development of a reliable numerical model to simulate the precision glass molding process will contribute to the realization of Industry 4.0 for the glass molding process.

The accurate characterization of the thermo-viscoelastic properties of the glass material is one of the essential factors for simulating the precision glass molding process. As a result, a novel material testing procedure is devised in this study, which is shown to accurately model the viscoelastic response of the glass material over a broad range of molding temperatures. The creep compression tests that are typically used in the literature are replaced with constant strain rate and stress relaxation tests. The viscoelastic parameters at various temperatures are determined using the Burgers model under constant strain rate conditions. In addition, the Burgers parameter η_1 is shown to be correlated to the bulk viscosity of the glass material and to accurately predict the viscosity of the material over the temperature

range used in this investigation. The TRS assumption commonly used in the literature to model temperature-dependent viscoelasticity is shown to be deficient over the temperature range used in this study. Instead, the temperature dependence is modeled using the VFT function's temperature-dependent Burgers parameters. Using an ABAQUS UMAT subroutine, the temperature-dependent viscoelastic parameters are implemented in the numerical model. It is demonstrated that the proposed model accurately predicts the thermo-viscoelastic response of two distinct glass types across a wide range of molding temperatures.

The structural relaxation parameters are obtained from the impulse excitation test based on ASTM standard E1876. In this investigation, the Tool-Narayanaswamy-Moynihan model is used to model the structural relaxation response of glass. The parameters of the TNM model are obtained from the relaxation response of Young's modulus of the glass to a sudden change in temperature. The particle swarm optimization algorithm is used to fit the experimental data. The obtained TNM model parameters are shown to accurately characterize the relaxation phenomenon over the entire temperature range tested. Finally, in this study, the material testing required for characterizing the glass material is designed to be implemented on the glass molding machine. This helps to streamline the development and testing of new glass materials that can be used in precision glass molding.

This study establishes a coupled thermo-mechanical axisymmetric finite element model to simulate the precision glass molding process on two distinct glass types. ABAQUS UMAT and UEXPAN subroutines are developed to incorporate the derived stress relaxation and structural relaxation parameters into the FE model. The developed numerical model is used to simulate the molding process of the biconvex lens, and the obtained deviations in the lens profile are compared to experimental data. The results demonstrated a fair agreement with minor deviations toward the lens's periphery. A thorough analysis revealed that the experimentally shaped lens

has a significant decentration error that deviates from the numerical model's axisymmetric postulate. In addition, the developed model is utilized to perform a numerical analysis of the profile deviation of a double aspheric lens. A mold compensation technique is implemented to modify the mold profiles for deviations. The profile deviations of lenses molded on compensated molds are shown to be within the design parameters. However, the magnitude of the deviation of the molded lens depends on the molding parameters, implying that the molds' compensation depends on the chosen process parameters.

Finally, to address the dependency of the optical quality of the molded lens on the process parameters, the developed numerical model is used in this study to analyze the influence of different process steps and the corresponding process parameters on the profile deviations and residual stresses. Rather than the molding temperature, the molding viscosity is used as the control parameter to normalize the influence of various glass materials. This demonstrated that the viscoelastic response of the two distinct glass types utilized in this study is comparable at similar molding viscosities. This shows that the influence of the viscoelastic material on the optical quality is negligible under similar molding conditions. The evolution of the stresses in the lens during the various molding stages is analyzed, and it is demonstrated that the influence of the molding parameters on the profile deviation is eliminated by relaxing the stresses in the lens at the molding temperature rather than during the gradual cooling phase. With the modified molding process, it was observed that during the gradual cooling phase, the residual stresses in the molded lens increased as the cooling rate increased. However, the maximal stress is less than 1 kPa, which is negligible, even when cooled at 100°C/min. Based on the observation, the conventional molding process is modified by adding a relaxation phase prior to lens cooling, and the two-step lens cooling process is replaced with a single rapid cooling step. It is demonstrated that the modified precision glass molding process reduces the total process time by

more than 50 percent compared to the conventional process for producing an optical lens of comparable quality. The proposed molding process substantially reduces the cost of producing a molded lens.

7.2 Future Work

Future work could potentially focus on the following topics:

1. Viscoelastic material properties are known to be a key factor in developing a reliable numerical model. While this study establishes a novel testing technique to obtain the unique set of material parameters, the uncertainty associated with each parameter needs to be further evaluated to improve confidence in the predicted results.

2. The accuracy of the developed model in this study can be further evaluated by scaling the numerical model. Although scaling the model to micrometers might be advantageous, it might introduce numerical errors into the simulation by inadvertently scaling the material properties. A tradeoff between the scaling factor and the numerical accuracy should be analyzed to accurately predict the deviations that are in microns and sub-microns.

3. The material testing developed in this study can be extended to analyze chalcogenide glass materials used in IR optics.

4. The developed model can be extended to simulate glass molding of diffractive and freeform optics.

REFERENCES

[1] A. Jain, *Experimental study and numerical analysis of compression molding process for manufacturing precision aspherical glass lenses.* PhD thesis, The Ohio State University, 2006.

[2] "Glass aspherical lens demand." https://bisresearch.com/news/glass-aspherical-lens-generating-the-highest-demand-among-high-precision-asphere-products.

[3] S. D. Jacobs, "International progress on advanced optics and sensors," pp. 3–14, 2003.

[4] B. G. Angle, M. and C. Maier, "Method for molding glass lenses.," *U.S. Patent 3,833,347.*, 1974.

[5] C. K. Wu, "Optical articles prepared from hydrated glasses.," *U.S. Patent 4,073,654.*, 1978.

[6] G. A. Meden-Piesslinger and J. H. Van de Heuvel, "Precision pressed optical components made of glass and glass suitable therefor.," *U.S. Patent 4,391,915.*, 1983.

[7] B. Ananthasayanam, *Computational modeling of precision molding of aspheric glass optics.* PhD thesis, Clemson University, 2008.

[8] A. Jain and A. Y. Yi, "Finite element modeling of structural relaxation during annealing of a precision-molded glass lens.," *Journal of Manufacturing Science and Engineering*, vol. 128, no. 3, pp. 683–690, 2006.

[9] D. Joshi, M. Peiman, M. J. David, R. Kathleen, C., and J. Paul, F., "Thermo-mechanical characterization of glass at high temperature using the cylinder compression test. part ii: No-slip experiments, viscoelastic constants, and sensitivity.," *Journal of Rheology*, vol. 57, no. 5, pp. 1391–1410, 2013.

[10] L. Su, P. He, and Y. Y. Allen, "Investigation of glass thickness effect on thermal slumping by experimental and numerical methods.," *Journal of Materials Processing Technology*, vol. 221, no. 12, pp. 1995–2003, 2011.

[11] G. W. Scherer, *Relaxation in glass and composites.* John Wiley & Sons, 1986.

[12] M. Garcia-Valles, H. S. Hafez, I. Cruz-Matias, and etc., "Calculation of viscosity-temperature curves for glass obtained from four wastewater treatment plants in egypt.," *Journal of Thermal Analysis and Calorimetry*, vol. 111, no. 1, pp. 107–114, 2013.

[13] T. Zhou, J. Yan, and T. Kuriyagawa, "Evaluating the viscoelastic properties of glass above transition temperature for numerical modeling of lens molding process.," in *International Symposium on Photoelectronic Detection and Imaging 2007: Optoelectronic System Design, Manufacturing, and Testing*, vol. 6624.

[14] A. Q. Tool, "Relation between inelastic deformability and thermal expansion of glass in its annealing range.," *Journal of the American Ceramic Society*, vol. 29, no. 9, pp. 240–253, 1946.

[15] O. S. Narayanaswamy, "A model of structural relaxation in glass.," *Journal of the American Ceramic Society*, vol. 54, no. 10, pp. 491–498, 1971.

[16] C. T. Moynihan, A. J. Easteal, and a. T. J. De Bolt, M. A., "Dependence of the fictive temperature of glass on cooling rate.," *Journal of the American Ceramic Society*, vol. 59, no. 1-2, pp. 12–16, 1976.

[17] A. Jain and A. Y. Yi, "Numerical modeling of viscoelastic stress relaxation during glass lens forming process.," *Journal of the American Ceramic Society*, vol. 88, no. 3, pp. 530–535, 2005.

[18] D. Joshi, P. Mosaddegh, J. David Musgraves, K. C. Richardson, and P. F. Joseph, "Thermo-mechanical characterization of glass at high temperature using the cylinder compression test. part i: Viscoelasticity, friction, and ppv.," *Journal of Rheology*, vol. 57, no. 5, pp. 1367–1389, 2013.

[19] Y. Jiwang, T. Zhou, N. Yoshihara, and T. Kuriyagawa, "Shape transferability and microscopic deformation of molding dies in aspherical glass lens molding press.," *Journal of Manufacturing Technology Research*, vol. 1, no. 1-2, pp. 85–102, 2009.

[20] T. Zhou, J. Yan, J. Masuda, and T. Kuriyagawa, "Investigation on the viscoelasticity of optical glass in ultraprecision lens molding process.," *Journal of Materials Processing Technology*, vol. 209, no. 9, pp. 4484–4489, 2009.

[21] B. Ananthasayanam, P. F. Joseph, D. Joshi, S. Gaylord, L. Petit, V. Y. Blouin, K. C. Richardson, D. L. Cler, M. Stairiker, and M. Tardiff, "Final shape of precision molded optics: Part iâcomputational approach, material definitions and the effect of lens shape.," *Journal of Thermal stresses*, vol. 35, no. 6, pp. 550–578, 2012.

[22] M. Arai, Y. Kato, and T. Kodera, "Characterization of the thermo-viscoelastic property of glass and numerical simulation of the press molding of glass lens.," *Journal of Thermal Stresses*, vol. 32, no. 12, pp. 1235–1255, 2009.

[23] J. De Bast and P. Gilard, "Variation of the viscosity of glass and the relaxation of stresses during stabilization.," *Physics Chemistry Glasses*, vol. 4, no. 4, pp. 117–128, 1963.

[24] S. M. Rekhson, "Viscosity and stress relaxation in commercial glasses in the glass transition region.," *Journal of non-crystalline solids*, vol. 38, pp. 457–462, 1980.

[25] A. Jain, F. Gregory, C., and Y. Allen, Y., "Viscosity measurement by cylindrical compression for numerical modeling of precision lens molding process.," *Journal of the American Ceramic Society*, vol. 88, no. 9, pp. 2409–2414, 2005.

[26] D. Joshi, M. Peiman, M. J. David, R. Kathleen, C., and J. Paul, F., "Thermo-mechanical characterization of glass at high temperature using the cylinder compression test. part i: Viscoelasticity, friction, and ppv.," *Journal of Rheology*, vol. 57, no. 5, pp. 1367–1389, 2013.

[27] J. Zhou, Y. Jianfeng, L. L., James, S. Lianguan, and Y. Allen, "Stress relaxation and refractive index change of as2s3 in compression molding.," *International Journal of Applied Glass Science*, vol. 8, no. 3, pp. 255–265, 2017.

[28] J. Yu, L. Hong, Z. Yingying, N. Thai, V., J. Xiaomo, and H. Junzhi, "Stress relaxation and refractive index change of as2s3 in compression molding.," *Journal of the American Ceramic Society*, vol. 102, no. 11, pp. 6606–6617, 2019.

[29] T. Vu, Anh, V. Anh, Ngoc, G. Tim, and B. Thomas, "Modeling of thermoâviscoelastic material behavior of glass over a wide temperature range in glass compression molding.," *Journal of the American Ceramic Society*, vol. 103, no. 4, pp. 2791–2807, 2020.

[30] Y. Zhang, Y. Shaohui, L. Rongguang, L. Hong, X. Huapan, and Y. Ningxiao, "New testing and calculation method for determination viscoelasticity of optical glass.," *Optics Express*, vol. 28, no. 1, pp. 626–640, 2020.

[31] ASTM:C1351M-96, "Standard test method for measurement of viscosity of glass between 10^4 pa.s and 10^8 pa.s by viscous compression of a solid right cylinder [metric].," *ASTM International, West Conshohocken, PA*, vol. 15.02, 2022.

[32] H. Meinhard, F. Wolfgang, and G. Peter, "Viscosity of glass below the transformation temperature.," in *Glass Science and Technology (Frankfurt)*, vol. 74, 2001.

[33] R. Bruckner, Y. Yue, and A. Habeck, "Determination of the rheological properties of high-viscous melts by the cylinder compression method.," *Glass Science and Technology*, vol. 67, no. 5, pp. 114–29, 1994.

[34] L. Zhang, Z. Wenchen, and A. Y. Yi, "Investigation of thermoforming mechanism and optical propertiesâ change of chalcogenide glass in precision glass molding.," *Applied Optics*, vol. 57, no. 22, pp. 6358–6368, 2018.

[35] N. Findley, W, S. Lai, J, and K. Onaran, *Creep and relaxation of nonlinear viscoelastic materials, with an introduction to linear viscoelasticity.* North-Holland Publishing, 1976.

[36] *Schott P-SK57 datasheet.* United States: SCHOTT, 2014.

[37] B. Dhanooj and M. Christopher, "Reduction of cycle time during press molding of glass lenses.," *In Society of Photo-Optical Instrumentation Engineers (SPIE) Conference Series*, vol. 12219, p. 1221904, 2022.

[38] J. M. Caruthers and R. E. Cohen, "Consequences of thermorheological complexity in viscoelastic materials.," *Rheologica Acta*, vol. 19, pp. 606–613, 1980.

[39] E. R. Pierik, W. J. B. Grouve, M. van Drongelen, and R. Akkerman, "The influence of physical ageing on the in-plane shear creep compliance of 5hs c/pps.," *Mechanics of Time-Dependent Materials*, vol. 24, pp. 197–220, 2020.

[40] A. Fluegel, "Glass viscosity calculation based on a global statistical modelling approach.," *Journal of Glass Science and Technology Part A*, vol. 48, no. 1, pp. 13–30, 2007.

[41] M. Hara and S. Suetoshi, "Density change of glass in transformation range.," *Rep. Res. Lab. Asahi Glass Co*, vol. 5, p. 126, 1955.

[42] A. Sipp and R. Pascal, "Equivalence of volume, enthalpy and viscosity relaxation kinetics in glass-forming silicate liquids.," *Journal of Non-Crystalline Solids*, vol. 298, no. 2-3, pp. 202–212, 2002.

[43] P. B. Macedo and N. Albert, "Effects of a distribution of volume relaxation times in the annealing of bsc glass.," *Journal of Research of the National Bureau of Standards. Section A, Physics and Chemistry*, vol. 71, no. 3, p. 231, 1967.

[44] B. Olsen, Niels, C. D. Jeppe, and C. Tage, "Structural relaxation monitored by instantaneous shear modulus.," *Physical review letters*, vol. 81, no. 5, pp. 1031–1033, 1998.

[45] H. R. Liu, Weidong and Z. Liangchi, "Revealing structural relaxation of optical glass through the temperature dependence of young's modulus.," *Journal of the American Ceramic Society*, vol. 97, no. 11, pp. 3475–3482, 2014.

[46] H. S. Chen, "The influence of structural relaxation on the density and youngâs modulus of metallic glasses.," *Journal of Applied Physics*, vol. 49, no. 6, pp. 3289–3291, 1978.

[47] ASTM:E1876-15, "Standard test method for dynamic youngâs modulus, shear modulus, and poissonâs ratio by impulse excitation of vibration.," *ASTM International, West Conshohocken, PA*, 2015.

[48] *CDGM D-ZK3 datasheet*. United States: Universal Photonics incorporated, 2013.

[49] A. Markovsky, F. S. Thomas, and D. C. Boyd, "An efficient and stable algorithm for calculating fictive temperatures.," *Journal of the American Ceramic society*, vol. 67, no. 4, pp. c56–c57, 1984.

[50] D. Pallicity, Tarkes, V. AnhâTuan, P. M. Krishnamurthi, Ramesh, L. Gang, and D. Olaf, "An efficient and stable algorithm for calculating fictive temperatures.," *Journal of the American Ceramic society*, vol. 100, no. 10, pp. 4680–4698, 2017.

[51] Y. Zhang, Y. Kaiyuan, and F. Fengzhou, "Pre-compensation of mold in precision glass molding based on mathematical analysis.," *Micromachines*, vol. 11, no. 12, p. 1069, 2020.

[52] M. Brown, "A review of research in numerical simulation for the glass-pressing process.," *Proceedings of the Institution of Mechanical Engineers, Part B: Journal of Engineering Manufacture*, vol. 221, no. 9, pp. 1377–1386, 2007.

[53] G. Weidmann, K. Holtberg, and H. Eisermann, "Pressing of drinking glass stems," *Mathematical Simulation in Glass Technology*, pp. 307–317, 2002.

[54] M. Hyre, "Numerical simulation of glass forming and conditioning.," *Journal of the American Ceramic Society*, vol. 85, no. 5, pp. 1047–1056, 2002.

[55] M. Hyre, "Numerical modeling of glass container forming.," in *American Institute of Physics Conference Proceedings, Materials Processing and Design: Modeling, Simulation and Applications; NUMIFORM 2004*, pp. 245–250.

[56] T. F. Soules, R. F. Busbey, S. M. Rekhson, A. Markovsky, and M. A. Burke., "Finite element calculation of stresses in glass parts undergoing viscous relaxation.," *Journal of the American Ceramic Society*, vol. 70, no. 2, pp. 90–95, 1987.

[57] *ABAQUS/Standard User's Manual, Version 2021.* United States: Dassault Systèmes Simulia Corp, 2021.

[58] G. C. Firestone, J. Anurag, and Y. Y. Allen, "Precision laboratory apparatus for high temperature compression molding of glass lenses.," *Review of scientific instruments*, vol. 76, no. 6, 2005.

[59] Y.-C. Tsai, H. Chinghua, and H. Jung-Chung, "Glass material model for the forming stage of the glass molding process.," *Journal of Materials Processing Technology*, vol. 201, no. 1-3, pp. 751–754, 2008.

[60] W. Iqbal, *Identifying the optimum process parameters of precision glass molding for aspherical lenses.* PhD thesis, Clemson University, 2009.

[61] D. H. Cha, H. S. Park, Y. Hwang, J.-H. Kim, and H.-J. Kim, "Experimental study of glass molding process and transcription characteristics of mold surface in molding of aspheric glass lenses.," *Optical review*, vol. 18, no. 2, pp. 241–246, 2011.

[62] B. Gleason, W. Peter, M. J. David, and R. Kathleen, "Using design of experiments to improve precision glass moulding.," *International Journal of Experimental Design and Process Optimisation*, vol. 3, no. 3, pp. 263–275, 2013.

[63] J. Zhou, L. Mujun, H. Yang, S. Tianyi, J. Yueliang, and S. Lianguan, "Numerical evaluation on the curve deviation of the molded glass lens.," *Journal of Manufacturing Science and Engineering*, vol. 136, no. 5, pp. 1–11, 2014.

[64] Z. Kejun, S. Shi, Z. Chen, Z. Liu, and Y. Zhang, "Prediction of profile deviation during glass molding of double-aspheric lens.," *Journal of Engineering Science Technology Review*, vol. 13, no. 2, pp. 50–56, 2020.

[65] B. Tao, H. Peng, S. Lianguan, and Y. Allen, "Quantitatively measurement and analysis of residual stresses in molded aspherical glass lenses.," *The International Journal of Advanced Manufacturing Technology*, vol. 74, pp. 1167–1174, 2014.

[66] S. Gaylord, A. Balajee, T. Benjamin, P. Laeticia, C. Chris, F. Ulrich, J. Paul, and R. Kathleen, "Thermal and structural property characterization of commercially moldable glasses.," *Journal of the American Ceramic Society*, vol. 93, no. 8, pp. 2207–2214, 2010.

[67] D. Rieser, S. Gerd, and M. Peter, "Investigations on glass-to-mold sticking in the hot forming process.," *Journal of Non-Crystalline Solids*, vol. 354, no. 12-13, pp. 1393–1397, 2008.

[68] H. Aben and C. Guillemet, *Photoelasticity ofglass.* New York, United States: Springer, 1993.

APPENDIX A: Equivalency between the Burgers model and the two-term generalized Maxwell model

The constitutive equation of the Burgers model in the differential form is given in Eq. A.1 [35].

$$\sigma + p_1\dot{\sigma} + p_2\ddot{\sigma} = q_1\dot{\epsilon} + q_2\ddot{\epsilon} \tag{A.1}$$

where

$$\begin{gathered} p_1 = \frac{\eta_1}{E_1} + \frac{\eta_1}{E_2} + \frac{\eta_2}{E_2}; p_2 = \frac{\eta_1\eta_2}{E_1E_2} \\ q_1 = \eta_1; q_2 = \frac{\eta_1\eta_2}{E_2} \end{gathered} \tag{A.2}$$

The stress relaxation response of the Burgers model obtained by Laplace transform is as follows,

$$\sigma(t) = \frac{\epsilon}{\bar{A}}\left[\left(q_1 - \frac{q_2}{\tau_2}\right)e^{-t/\tau_2} - \left(q_1 - \frac{q2}{\tau_1}\right)e^{-t/\tau_1}\right] \tag{A.3}$$

where τ_1 and τ_2 are the relaxation times given by,

$$\tau_1 = \frac{2p_2}{p_1 + \bar{A}}; \quad \tau_2 = \frac{2p_2}{p_1 - \bar{A}} \tag{A.4}$$

The shear parameters of the Burgers model are calculated using the Burgers parameters obtained from the experimental data,

$$\begin{aligned} G_1 &= \frac{E_1}{2(1+\nu)}, \ \mu_1 = \frac{\eta_1}{2(1+\nu)} \\ G_2 &= \frac{E_2}{2(1+\nu)}, \ \mu_2 = \frac{\eta_2}{2(1+\nu)} \end{aligned} \tag{A.5}$$

Substituting equation A.5 into equation A.3, the shear relaxation modulus is obtained

$$G(t) = \frac{G_1 \tau_1 \tau_2}{\tau_2 - \tau_1} \left[\left(\frac{G_2}{\mu_2} - \frac{1}{\tau_2} \right) e^{-t/\tau_2} + \left(\frac{1}{\tau_1} - \frac{G_2}{\mu_2} \right) e^{-t/\tau_1} \right] \tag{A.6}$$

Equation A.6 can also be written as,

$$G(t) = G_1 \left[w_1 e^{-t/\tau_2} + w_2 e^{-t/\tau_1} \right] \tag{A.7}$$

where w_1 and w_2 are the weights of the shear function given by equations A.8 and their sum is always equal to one.

$$w_1 = \frac{\tau_1 \tau_2}{\tau_2 - \tau_1} \left(\frac{G_2}{\mu_2} - \frac{1}{\tau_2} \right) \tag{A.8}$$

$$w_2 = \frac{\tau_1 \tau_2}{\tau_2 - \tau_1} \left(\frac{1}{\tau_1} - \frac{G_2}{\mu_2} \right) \tag{A.9}$$